UCRL-18433

cy. 2

π^0 ENERGY SPECTRUM IN $K^+ \rightarrow \pi^0 \mu^+ \nu$. SEARCH FOR DIRECT RADIATION IN $K^+ \rightarrow \pi^+ \pi^0 \gamma$

Peter Klaus Kijewski
(Ph.D. Thesis)

June 1969

AEC Contract No. W-7405-eng-48

TWO-WEEK LOAN COPY

This is a Library Circulating Copy which may be borrowed for two weeks. For a personal retention copy, call Tech. Info. Division, Ext. 5545

5718

LRL

LAWRENCE RADIATION LABORATORY

UNIVERSITY of CALIFORNIA BERKELEY

UCRL-18433

34 la

DISCLAIMER

This document was prepared as an account of work sponsored by the United States Government. While this document is believed to contain correct information, neither the United States Government nor any agency thereof, nor the Regents of the University of California, nor any of their employees, makes any warranty, express or implied, or assumes any legal responsibility for the accuracy, completeness, or usefulness of any information, apparatus, product, or process disclosed, or represents that its use would not infringe privately owned rights. Reference herein to any specific commercial product, process, or service by its trade name, trademark, manufacturer, or otherwise, does not necessarily constitute or imply its endorsement, recommendation, or favoring by the United States Government or any agency thereof, or the Regents of the University of California. The views and opinions of authors expressed herein do not necessarily state or reflect those of the United States Government or any agency thereof or the Regents of the University of California.

π^o ENERGY SPECTRUM IN $K^+ \to \pi^o \mu^+ \nu$.

SEARCH FOR DIRECT RADIATION IN $K^+ \to \pi^+ \pi^o \gamma$.

Table of Contents

Abstract v

Part I. $K^+ \to \pi^o \mu^+ \nu$

I. Introduction 1

II. Theory 6

III. Experiment 11

IV. Analysis

A. Reconstruction of events 17

B. Kinematic Reconstruction 24

C. Detection Efficiency 36

D. Background 41

E. Selection of Events 47

F. Calculation of Parameters 51

V. Conclusions 58

Appendices 62

References 65

Part II. $K^+ \to \pi^+ \pi^o \gamma$

I. Introduction 67

II. Theory 72

III. Scanning and Selection of Events 75

IV. Analysis

A. Kinematic Reconstruction 80

B. Background 86

C. Calculation of Parameters 89

V. Summary and Conclusions 95

Appendices 97

References 99

Acknowledgments 100

π^o ENERGY SPECTRUM IN $K^+ \to \pi^o \mu^+ \nu$

SEARCH FOR DIRECT RADIATION IN $K^+ \to \pi^+ \pi^o \gamma$ *

Peter Klaus Kijewski

Lawrence Radiation Laboratory
University of California
Berkeley, California

June 1969

ABSTRACT

We have analyzed 2041 events of the type $K^+ \to \pi^o \mu^+ \nu$ to gain some understanding about the matrix element of the strangeness changing hadron current. In our experiment this current describes the transition $K^+ \to \pi^o$. The most general matrix element can be written in terms of two Lorentz scalars called form factors:

$$< K^+ | J_\lambda^{h,\Delta S=1} | \pi^o > = f_+(q^2)(P_K+P_\pi) + f_-(q^2)(P_K-P_\pi)$$

f_+ and f_- are the form factors; P_K and P_π are the four momenta of the kaon and pion respectively; q^2 is the four momentum transfer to the lepton pair.

The events for this analysis were obtained from a spark chamber experiment at the Berkeley Bevatron. We observe both converted γ-rays from the π^o and are able to reconstruct the kinematics of each event completely. This allows us to determine the π^o energy distribution which we use to get information about f_+ and f_-. The slope of the π^o energy spectrum is sensitive to the ratio $\xi(0) = f_-(0)/f_+(0)$. If we assume that f_+ and f_- are independent of q^2, we obtain from a measurement of the slope the result $\xi(0) = -0.3 \pm 0.3$. We can introduce a q^2 dependence of f by means of a linear approximation:

$$f_{\pm}(q^2) = f_{\pm}(0)(1 + \lambda_{\pm} \frac{q^2}{m\pi^{o2}})$$

If we take $\lambda_- = 0$ and fit our data to $\xi(0)$ and λ_+ we find that:

$$\xi(0) = -0.5 \qquad \lambda_+ = 0.009$$

In a separate experiment we have searched through our data for events of the type $K^+ \rightarrow \pi^+ \pi^o \gamma$. These events are distinguished by the fact that they produce three showers in our spark chambers. The decay $K^+ \rightarrow \pi^+ \pi^o \gamma$ would be of interest in studying time reversal invariance if one could observe decays produced by direct radiation rather than inner bremsstrahlung. The two types of events can be told apart by the fact that for inner bremsstrahlung the γ-ray is mostly emitted in the same direction as the π^+, while for direct radiation the γ-ray is emitted in the opposite direction to the π^+. Hence we are interested in the distribution of events as a function of $\hat{\pi}^+ \cdot \hat{\gamma}$ to distinguish the two types of radiation.

We have found 27 events which satisfy a two constraint fit to the kinematics of $K^+ \rightarrow \pi^+ \pi^o \gamma$. We analyze them in terms of the decay rate:

$$\frac{d\Gamma}{dT_{\pi^+} d\cos\theta} = |X_B g + X_E \, \ell^{i(\delta_1 - \delta_0)} h|^2 + |X_M|^2 \, h^2$$

Here it is assumed that direct radiation is dominated by dipole radiation. X_B, X_E, X_M are parameters which describe the contributions of inner bremstrahlung, electric dipole radiation and magnetic dipole radiation respectively. g and h are functions of the kinematic variables. We

have made a likelihood fit of our events to this decay rate and find:

$X_E = 0.8 \begin{smallmatrix} +1.2 \\ -0.9 \end{smallmatrix}$ $\qquad$ X_M assumed 0

$X_M = 2.1 \pm 1.5$ $\qquad$ X_E assumed 0

What this result says is that our events are distributed in the variable $\hat{\pi}^+ \cdot \hat{\gamma}$ as would be expected from inner bremsstrahlung without the presence of direct radiation.

---

* Work performed under the auspices of the U. S. Atomic Energy Commission.

I. INTRODUCTION

Many weak interaction processes have been successfully described by using a Hamiltonian of the form:

$$H_W = \frac{G}{\sqrt{2}} J_\lambda J_\lambda^\dagger + \text{h.c.} \qquad \text{I-1}$$

G is the weak coupling constant. J_λ is a current in analogy with electromagnetic interactions. We can write J_λ as a sum of currents:

$$J_\lambda = J_\lambda^\ell + J_\lambda^{h,\Delta S=0} + J_\lambda^{h,\Delta S=1} \qquad \text{I-2}$$

J_λ^ℓ is the lepton current; $J_\lambda^{\ell,\Delta S=0}$ is the hadron current of strangeness conserving transitions; $J_\lambda^{h,\Delta S=1}$ is the hadron current of strangeness violating transitions. The form of the matrix element $< B|J_\lambda^\ell|A >$ is well understood in the case that $|A>$ and $|B>$ are the state vectors of leptons. For example, the purely leptonic decay $\mu \to e\nu\bar{\nu}$ and the strangeness conserving decay $n \to pe\nu$ have yielded information about the matrix elements $< e|J_\lambda^\ell|\nu >$ and $< \mu|J_\lambda^\ell|\nu >$.

If we use Eq. I-2 in Eq. I-1 we get a sum of terms:

$$H_W = \frac{G}{\sqrt{2}} \Big[J_\lambda^\ell J_\lambda^{\ell\dagger} + J_\lambda^{h,\Delta S=0} J_\lambda^{\ell\dagger} + J_\lambda^{h,\Delta S=1} J_\lambda^{\ell\dagger} + J_\lambda^{h,\Delta S=0}\left(J_\lambda^{h,\Delta S=0}\right)^\dagger + J_\lambda^{h,\Delta S=1}\left(J_\lambda^{h,\Delta S=1}\right)^\dagger + J_\lambda^{h,\Delta S=1}\left(J_\lambda^{h,\Delta S=0}\right)^\dagger + \text{h.c.}\Big]$$

The first term applies to the transition $\mu \to e\nu\bar{\nu}$; the second term applies to $n \to pe\nu$. In our experiment we are interested in the third term to study the matrix elements of the current $J_\lambda^{h,\Delta S=1}$. We have looked at the decay mode $K^+ \to \pi^0\mu^+\nu$ whose decay rate is proportional to the square of the matrix element:

$$< K^+|H_W|\pi^o\mu\nu > = \frac{G}{\sqrt{2}} < K^+|J_\lambda^{h,\Delta S=1}|\pi^o > < \mu|J_\lambda^{\ell^\dagger}|\nu > \qquad \text{I-3}$$

The part of the matrix element involving hadrons is unknown. Hence we write its most general form in terms of parameters to be measured:

$$< K^+|J_\lambda^{h,\Delta S=1}|\pi^o > = f_+(q^2)(P_K+P_\pi) + f_-(q^2)(P_K-P_\pi) \qquad \text{I-4}$$

P_K, P_π are the K^+, π^o four momenta respectively; $q^2 = (P_K-P_\pi)^2$ is the four momentum transfer to the lepton pair. f_+ and f_- are parameters.

A knowledge of f_+ and f_- is interesting for two reasons. First, an equation similar to I-3 can be written for K_{e3} decay ($K^+ \to \pi^o e^+\nu$). The principle of μ-e universality assumes that $f_-^e = f_-^\mu$ and $f_+^e = f_+^\mu$. So we can use the form factors found from the $K_{\mu 3}$ decay mode ($K^+ \to \pi^o\mu^+\nu$) to calculate the ratio $\Gamma(K_{\mu 3})/\Gamma(K_{e3})$. If this prediction disagrees with a direct measurement of the ratio $\Gamma(K_{\mu 3})/\Gamma(K_{e3})$ then a violation of μ-e universality is the only explanation within the framework of the current-current interaction hypothesis. Second, predictions can be made about f_+ and f_- using the algebra of currents. The results of such calculations are discussed below in Section II.

There are several methods which can be used to measure f_+ and f_-:

1) μ^+ total polarization in $K^+ \to \pi^o\mu^+\nu$ gives f_-/f_+.[1,2]
2) $K^+ \to \pi^o e^+\nu$ Dalitz plot and branching ratio gives f_+.[3,4]
3) Branching ratio $\Gamma(K_{\mu 3})/\Gamma(K_{e3})$ gives f_-/f_+.[5,6]
4) $K^+ \to \pi^o\mu^+\nu$ Dalitz plot gives f_- and f_+.[7,8]

Many measurements of ξ have been made. μ^+ polarization experiments usually give a value for $\xi = f_-/f_+$ in the neighborhood of -1. For example D. Cutts[2] using the same events as this analysis found $\xi = -0.95 \pm 0.3$.

Taking an average of measurements for $R = \Gamma(K_{\mu 3})/\Gamma(K_{e3}) = 0.68$[5] we can calculate $\xi(0) = 0.25 \pm 0.14$. The European X-2 collaboration[6] find a lower value for R than the above and they quote $\xi(0) = -0.6 \pm 0.2$ (evaluated at $\lambda_+ = 0.023$). An older $K_{\mu 3}$ Dalitz plot analysis by Callahan[7] found $\xi = 0.72 \pm 0.37$. A more recent measurement by Eisler et al.[8] using the Dalitz plot method gives $\xi(0) = -0.5 \pm 0.9$.

The disagreement between ξ as obtained from $\Gamma(K_{\mu 3})/\Gamma(K_{e3})$ and μ^+ polarization indicates a violation of μ-e universality. We have repeated a Dalitz plot measurment to get a measurement of ξ independent of any assumption about μ-e universality. One of the two existing experiments has a rather large error; the other experiment is in complete disagreement with the μ^+ polarization results. The confirmation of a positive value for ξ measured by the Dalitz plot method raises the possibility that we have to go beyond the current-current hypothesis to describe weak decays.

Appendix I gives a formula for the Dalitz plot density as a function of E_{π^o}, E_μ, f_+, and f_-. A very simple equation can be written for the decay rate if we assume that the form factors are independent of q^2:

$$\frac{d\Gamma}{dE_\mu dE_{\pi^o}} = N(E_\mu)\left[1 + \alpha(E_\mu, \xi)y\right]$$

$$y = 2\left(\frac{E_{\pi^o}-E_{\pi^o}(\text{MINIMUM})}{E_{\pi^o}(\text{MAXIMUM})-E_{\pi^o}(\text{MINIMUM})}\right) - 1 \qquad \text{I-5}$$

$$-1 \leq y \leq 1$$

We have looked at the change of the Dalitz plot density as a function of the π^o energy. It is apparent from Eq. I-5 that the π^o energy spectrum is a straight line with slope α. The slope of the spectrum constitutes

then a direct measurement of ξ. Figure 1 shows the relation between α and ξ. Note there are two values of ξ for each value of α.

We have fitted our π^o spectrum to the rate given in I-5 and find that $\xi = -0.3 \pm 0.3$. This result assumes that the form factors f_+ and f_- are independent of q^2. We have extended our analysis to search for the dependence of the form factors on q^2. For this purpose we write:

$$f_+(q^2) = f_+(0)\left[1 + \lambda_+ \frac{q^2}{m_{\pi^o}^2}\right]$$
$$f_-(q^2) = f_-(0)\left[1 + \lambda_- \frac{q^2}{m_{\pi^o}^2}\right] \qquad \text{I-6}$$

λ_+ and λ_- are parameters which determine the q^2 dependence of f_+ and f_- to first order in q^2. q^2 does not depend on the muon energy but only on the pion energy. Hence a value of λ different from zero adds terms to Eq. I-5 which are non-linear in E_{π^o}. Our results are presented in terms of contour plots of a likelihood function. Figure 17 assumes $\lambda_- = 0$; Figure 18 assumes $\lambda_+ = 0$.

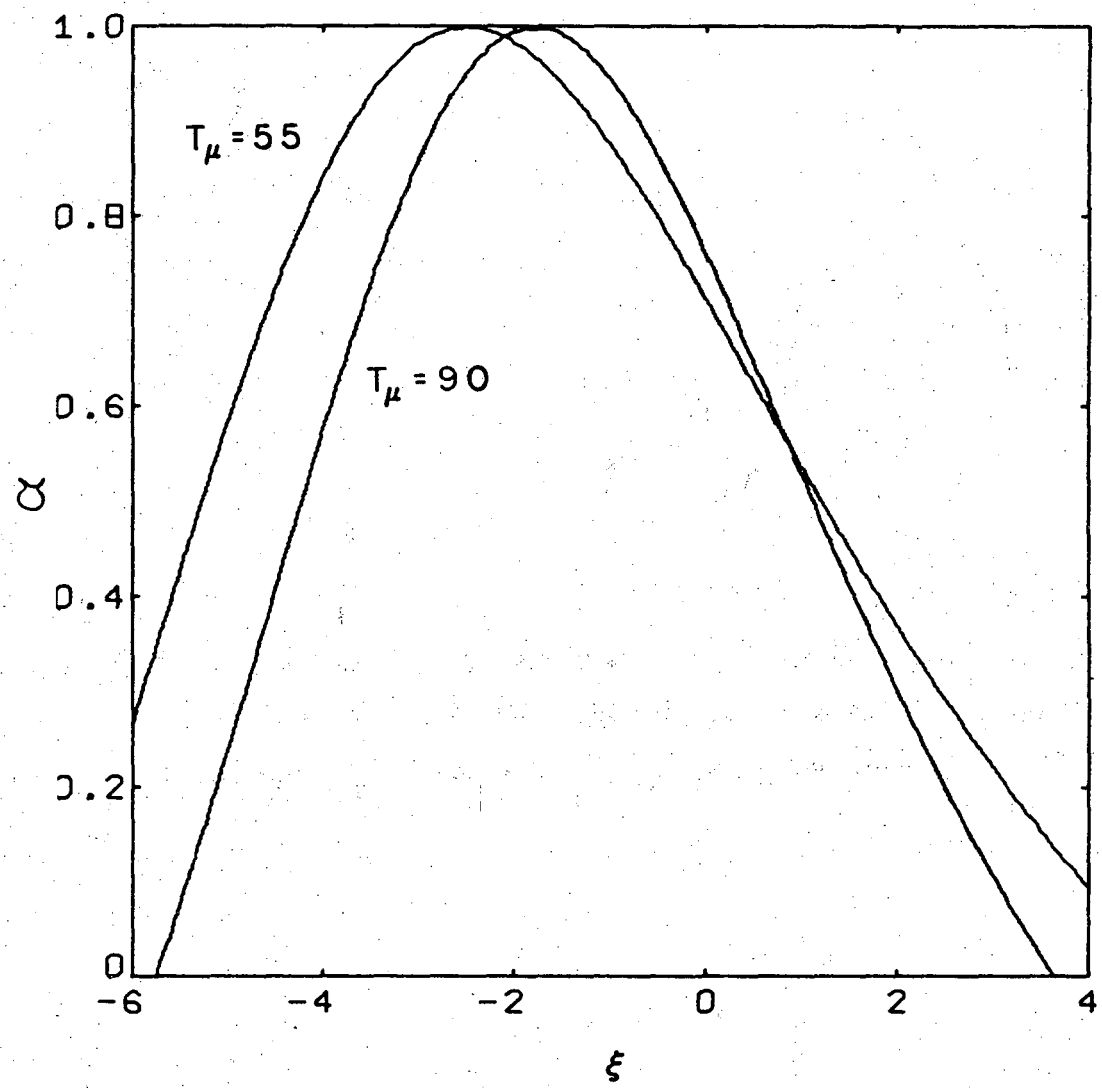

XBL 6812-6374

Fig. 1. α is the slope of the π^0 energy spectrum as shown in Eq. I-5. ξ is the ratio of the form factor f_- and f_+. T_μ is the kinetic energy of the muon.

II. THEORY

The study of hadron currents in the weak interactions is complicated by the strong interactions of the hadrons. A convenient way to parametrize the modifications due to strong interactions is through form factors. Equation I-4 is the most general Lorentz invariant form we can write for the matrix element of the hadron current between the physical states K^+ and π^0. f_+ and f_- are empirical factors containing the effect of strong interactions.

Current algebra allows us to relate the matrix element in I-4 to other matrix elements of the hadron currents. These in turn can be calculated from the masses and decay rates of various hadrons. If these masses and decay rates are known, we can use them to calculate f_+ and f_- with the help of current algebra relations. Many such calculations have been made.[9,10] The earliest attempts used a straight forward application of current algebra in conjunction with PCAC. The most serious drawback of this approach is that form factors are calculated with unphysical values for the variables. For example Callan and Treiman[9] found the value of ξ at the point $q^2 = m_K^2$, $P_\pi^2 = 0$. They assumed that the form factors do not change much when extrapolated to the physical region. Their result is $\xi = 0.3$. More recent calculations[10] invoke dispersion relations and superconvergent sum rules. With their help extrapolations in the variables P_K^2 and P_π^2 to the physical region can be computed. However, more parameters are necessary to make a prediction. Particles such as the κ (~ 700, 0^+) and K_A(1320, 1^+) are assumed to exist. Theoretical estimates of their masses, and in some cases their widths, have to be made. The resulting formulas for f_- and

and f_+ depend on a host of constants whose values are not well known.

Table I lists some of the representative theoretical predictions that have been made for ξ. The bibliography lists many other papers which attempt to calculate ξ. The ranges of the physical variables in our experiment are limited to:

$$P_K^{\ 2} = m_K^{\ 2}$$
$$P_\pi^{\ 2} = m_\pi^{\ 2}$$
$$m_\mu^{\ 2} \leq q^2 \leq (m_K - m_\pi)^2$$

Several of the results in the table depend on λ_+ as an unknown parameter. Answers are quoted for $\lambda_+ = 0$ and $\lambda_+ = 0.02$. The latter value is a natural one to take if we assume the decay is dominated by an intermediate K*. In this case f_+ takes the form:

$$f_+(q^2) = \frac{\text{CONSTANT}}{m_{K*}^{\ 2} - q^2} \qquad \text{II-1}$$

Comparing this equation with I-6 we get:

$$\lambda_+ \simeq \left(\frac{m_{\pi^o}}{m_{K*}}\right)^2 = 0.023$$

This value is confirmed by K_{e3} decay experiments.[3]

The above discussion concerned only vector form factors. If we assume that scalar and tensor couplings are also present we have to make the substitutions:

$$f_+ \rightarrow f_+ + \frac{m_\mu}{m_K} f_T$$
$$f_- \rightarrow f_- + \frac{m_K}{m_\mu} f_S + \frac{(P_K + P_\pi)\cdot(P_\mu - P_\nu)}{m_K m_\mu} f_T \qquad \text{II-2}$$

Table I. Theoretical Predictions for $\xi(0) = f_-(0)/f_+(0)$, λ_+, λ_-.

Reference	$\xi(0)$	λ_+	λ_-	Comments
Callan Treiman	0.3			$P_\pi \to 0$; ξ is evaluated at $q^2 = m_K^2$
Berman, Roy	-1.0	<0.05		Adler consistency condition; K_{e4} form factors approximately constant.
Pati, Sebastian	-0.22	0.022	0.028	Once subtracted dispersion relations; K*, $\mathcal{K}$ intermediate states, $f_K/f_\pi = 1.28$, $m(\mathcal{K}) = 1.6$ BeV
	small negative		~0.24	No $\mathcal{K}$ meson, $f_+(0) \sim 1$
Mathur, Pandit, Marshak	-0.2			K*, $\mathcal{K}$ meson (width, mass); dispersion relations
Hsu	-1.54	0	0.024	Spectral function sum rules;
	-1.05	0.02	0.01	K*, $\mathcal{K}$, KA(1280), A_1, ρ; superconvergence relations; λ_+ is a parameter.
	-0.52	0	-0.035	KA(1320)
	-0.024	0.02	-0.05	
Matsuda, Oneda	<-0.026			Unsubtracted dispersion relations; $\mathcal{K}$, K* intermediate states.
	>-0.28			
Biswas, Smith	0.43	-0.37		Spectral function sum rules; superconvergence relations; λ_- set equal 0; K*, A_1, intermediate states.
Majumdar	-7.88	0.02	.07	Spectral function sum rules; K*, A_1, KA(1320), $\mathcal{K}$; λ_+ is a parameter.

(continued on next page)

Table I. (continued)

Reference	$\xi(0)$	λ_+	λ_-	Comments
	-0.37	0.02	-0.14	No K
B. W. Lee				Chiral dynamics; field-current identity; δ is a free parameter.
	0.026	0.018	-0.2	$\delta = -1/3$ (from A, ρ widths)
	0.054	0.016	-0.083	$\delta=0$

$$\xi \rightarrow \frac{\xi + \frac{m_K}{m_\mu}\frac{f_S}{f_+} + \frac{(P_K+P_{\pi^o})(P_\mu-P_\nu)}{m_K m_\mu}\frac{f_T}{f_+}}{1 + \frac{m_\mu}{m_K}\frac{f_T}{f_+}}$$

Assuming that $f_T = 0$, it is apparent that this experiment can measure only the sum:

$$\xi' = \xi + \frac{m_K}{m_\mu}\frac{f_S}{f_+}$$

Our fits are made taking $f_S = 0$. We cannot separate the effect of ξ and f_S/f_+ on our π^o spectrum. On the other hand, f_T/f_+ introduces a dependence on E_{π^o}. Comparing with Eq. I-6 we see that the parameter λ_- also gives a dependence of the form factor on E_{π^o}. So in fitting for λ_- we have to assume that $f_T = 0$. Clearly these parameters can be used to reconcile conflicting results from different experimental methods.

If we believe in μ-e universality, results from K_{e3} experiments can be used to show that f_S and f_T are small. Because of the smallness of the electron mass, the form factor f_- does not affect the K_{e3} Dalitz plot. So a direct measurement of f_S and f_T is possible. Imlay et al.[4] find that the contribution from scalar coupling to the total K_{e3} decay rate is less than 5%; in a later analysis[4] they find that the contribution from tensor coupling is less than 4%.

III. EXPERIMENT

The K^+ mesons observed in our experiment were produced in a copper or uranium target in the 5.3 BeV external proton beam of the Berkeley Bevatron. Figure 2 shows the beam transport system used to momentum and mass analyze the K^+ beam. An electrostatic separator was used to separate K^+ mesons from π^+ mesons. About one in twenty charged particles in the vicinity of the K-stopper were kaons. The 500 MeV/c kaons were degraded to rest in a carbon dust stopper of dimension 2" × 2-1/3"× 3" and density 0.85 g/cm^2. We stopped on the average 700 kaons per Bevatron pulse. The beam was on for 700 milliseconds every six seconds. Figure 3 shows the counter telescope used to select stopping K^+ mesons followed by a charged decay particle. S_1, S_2, S_3, S_4 define the incoming beam. S_5 surrounds the stopping material except on the faces toward the incoming K^+ beam and the counter T_4. A stopping K^+ is signalled by the logic:

$$R_1 = S_1 S_2 S_3 S_4 \overline{C_B} \overline{S_5}$$

The Cerenkov counter vetoes pions and electrons. $\overline{S_5}$ rejects pions which pass through the stopper. R_1 opens a gate of 38 ns duration 6 ns after the K-stop. The gate is in coincidence with the signal:

$$R_2 = T_2 T_3 T_4 \overline{C_\mu} \overline{T_5}$$

R_2 requires a charged particle of $\beta < 0.75$ to stop between T_4 and T_5. The Cerenkov counter was used mainly to reject events of the type $K^+ \rightarrow \pi^0 e^+ \nu$. The 6 ns delay was chosen to reject particles that come from K^+ decays in flight or from the scattering of incoming charged particles toward T_4. T_4 eliminates short range pions from τ' decay

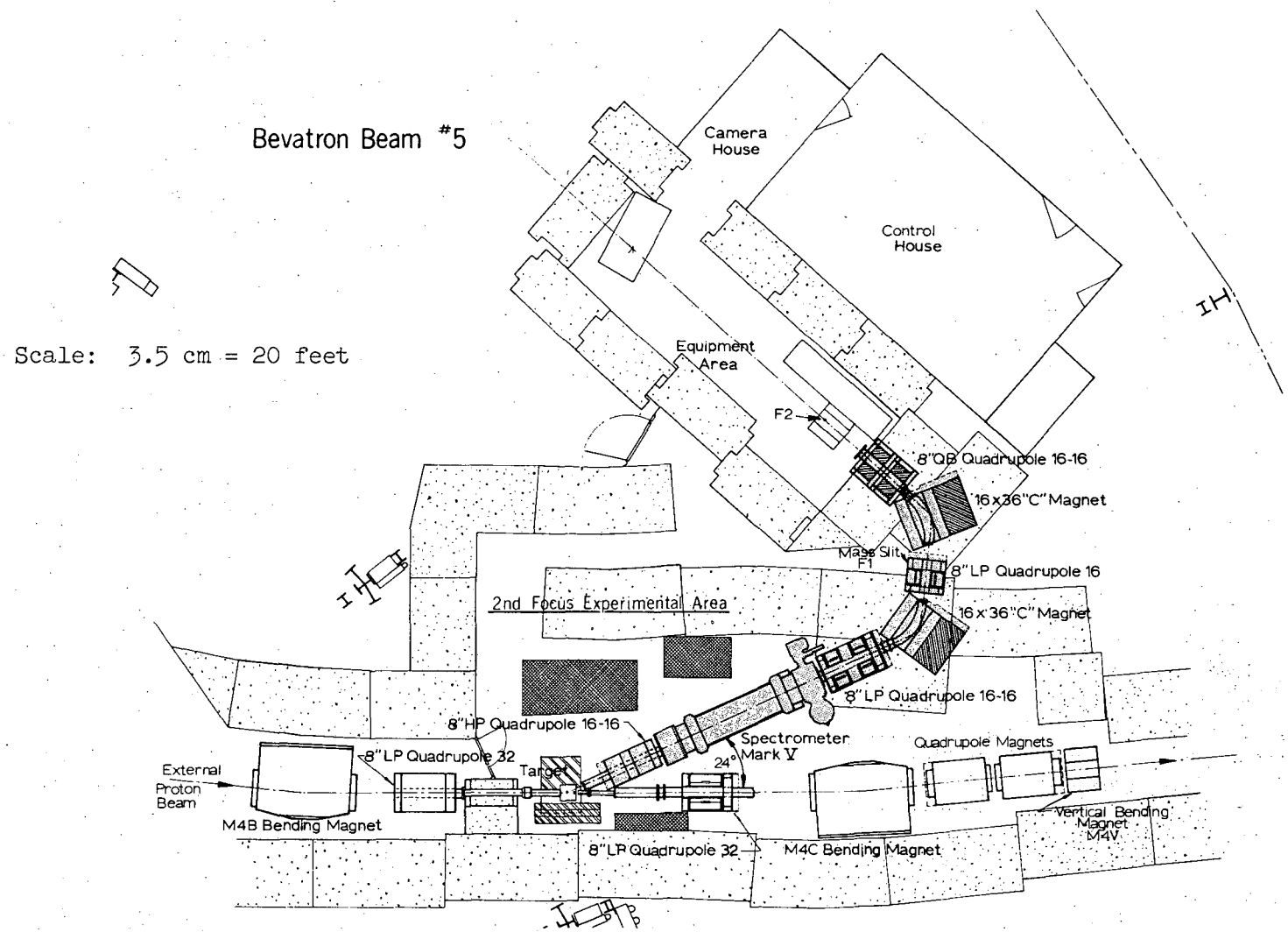

XBL 686-944

Fig. 2. Beam transport.

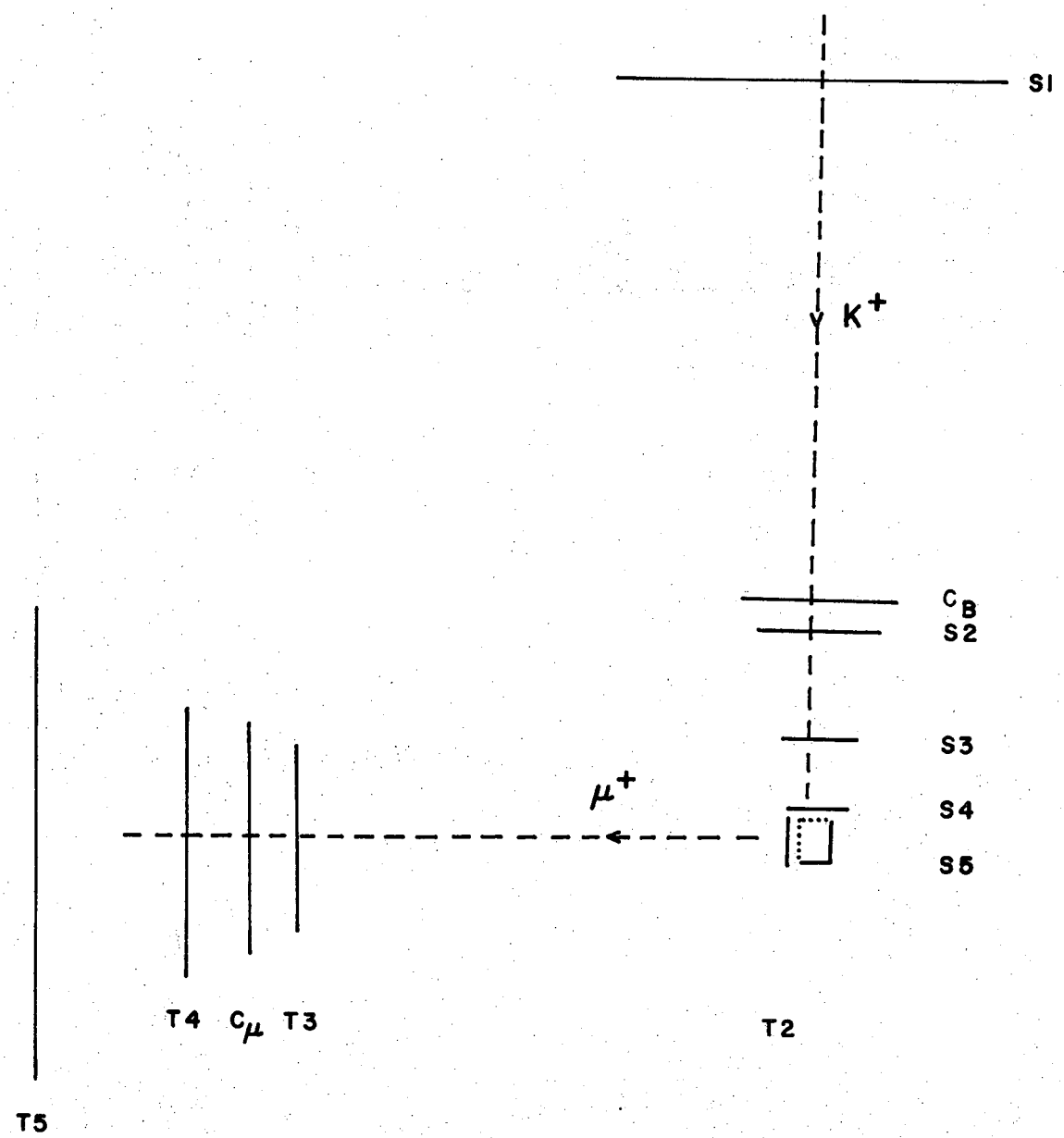

XBL 686-974

Fig. 3. Counter telescopes.

$(K^+ \rightarrow \pi^+\pi^o\pi^o)$. T_5 vetoes energetic charged particles from $K_{\pi 2}$ $(K^+ \rightarrow \pi^+\pi^o)$ and $K_{\mu 2}$ $(K^+ \rightarrow \mu^+\nu)$ decays.

The position of the incoming kaon was defined by two 2-gap spark chambers located between S_3 and S_4. Figure 4 gives a more detailed view of the μ^+ section in Fig. 3. The incident kaon comes out of the page. The position of the muon is defined by three 4-gap spark chambers SC1, SC2, and SC3. The muon is slowed down by a 1" aluminum degrader and passes through a water Cerenkov counter and T_3 into an aluminum range chamber. There are 28 gaps of total thickness 9.9 g/cm^2 between T_4 and T_5. T_4 limits the muons to a solid angle of 2.9%. T_4 and T_5 put an upper and lower limit on the muon energy. Eighteen percent of the $K_{\mu 3}$ events survive this energy cut.

The γ rays from π^o decay are converted into showers in aluminum-lead sandwich spark chambers. Each of the three chambers has 36 gaps. Individual plates are made from 0.8mm lead plates between 0.3mm Aℓ sheets. The first two plates in each chamber facing the stopper are aluminum only. We require that no sparks are in these gaps to make sure the showers are caused by γ-rays. The active volume in the right-most chamber extends to a depth of 26 gaps. The other two chambers are limited to 13 gaps because only 13 gaps of the indirect view are visible at the camera. Ninety percent of the γ-rays entering the right-hand chamber convert in the active volume; 55% of the γ-rays entering the upper or lower chambers convert in the active volume. With these efficiencies 41% of all $K_{\mu 3}$ events selected by our trigger have two converted γ-rays. However, the detection efficiency for the most energetic pions is five times that of pions with zero kinetic

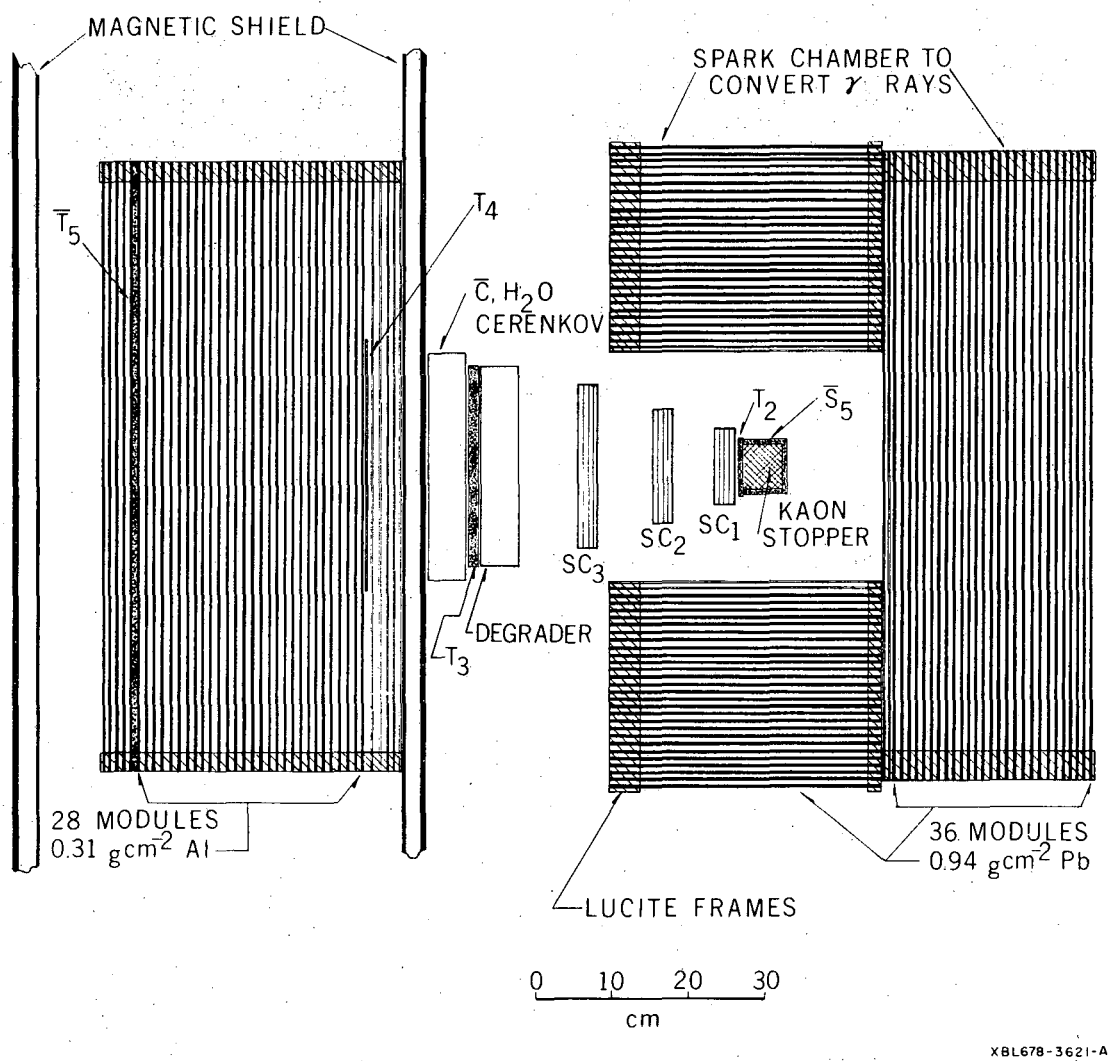

Fig. 4. Spark chambers and muon telescope. The K^+ beam comes out of the page. The μ^+ passes through T_2 and T_4 into the range chamber.

energy.

The signal $R_1 \cdot R_2$ triggers all spark chambers except the muon range chamber. The latter is triggered 3.5 microseconds later so that we can observe the decay $\mu^+ \rightarrow e^+\nu\bar{\nu}$. The views of the chambers, 18 in all, are projected onto film by mirrors and lenses. A picture of a typical event is reproduced in Fig. 2 of Part II. On the average we obtained one picture every six Bevatron pulses. The events we recorded were about evenly split between $K_{\pi 2}$ and $K_{\mu 3}$ decays. Other types of events such as K_{e3} and τ' were relatively few in number.

IV. ANALYSIS

A. Reconstruction of Events

Our spark chamber film was scanned by the automatic scanning system SPASS[11] at MIT. SPASS recorded the positions of the muon and kaon in their respective tracking chambers. In the shower chambers the conversion point of the γ-ray showers and the number of sparks in each shower was measured. SPASS did not scan the muon range chamber.

The position of the muon is measured at three points along its path. To make sure that we have a good track and measure $\hat{P}_\mu$ correctly, we calculate the cosine $\hat{P}_{\mu 1} \cdot \hat{P}_{\mu 2}$:

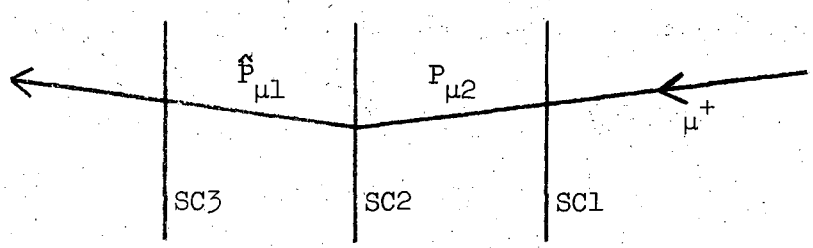

Figure 5 gives the distribution of $\delta_A = \hat{P}_{\mu 1} \cdot \hat{P}_{\mu 2}$. We make a cut at $\delta_A = 0.998$. The direction of the incident kaon ($\hat{P}_K$) is determined by two points along its path. We then take the stopping position of the kaon to be that point on the muon flight path which is closest to the line along the kaon direction. δ_D is the shortest distance between lines along the kaon and muon directions. δ_D is given by:

$$\delta_D = \left| (\vec{K}-\vec{\mu}) \cdot (\hat{P}_K \times \hat{P}_\mu) / |\hat{P}_K \times \hat{P}_\mu| \right|$$

$\vec{K}$ = position of kaon in spark chamber.

$\vec{\mu}$ = position of muon in spark chamber.

In the absence of scattering $\delta_D = 0$. Figure 6 shows the distribution

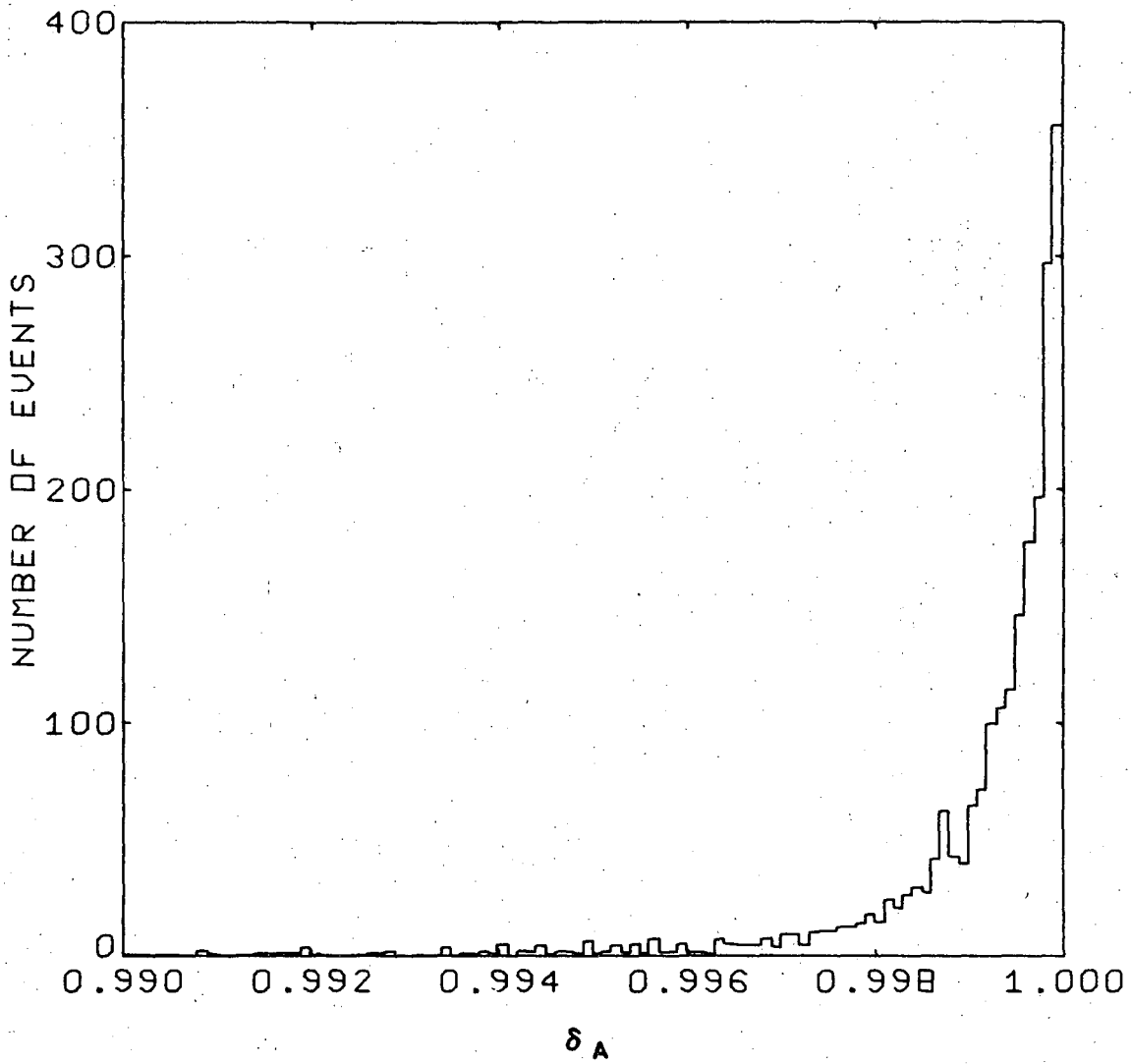

XBL 6812-6377

Fig. 5. δ_A is the cosine of the scattering angle of muons in the tracking chambers.

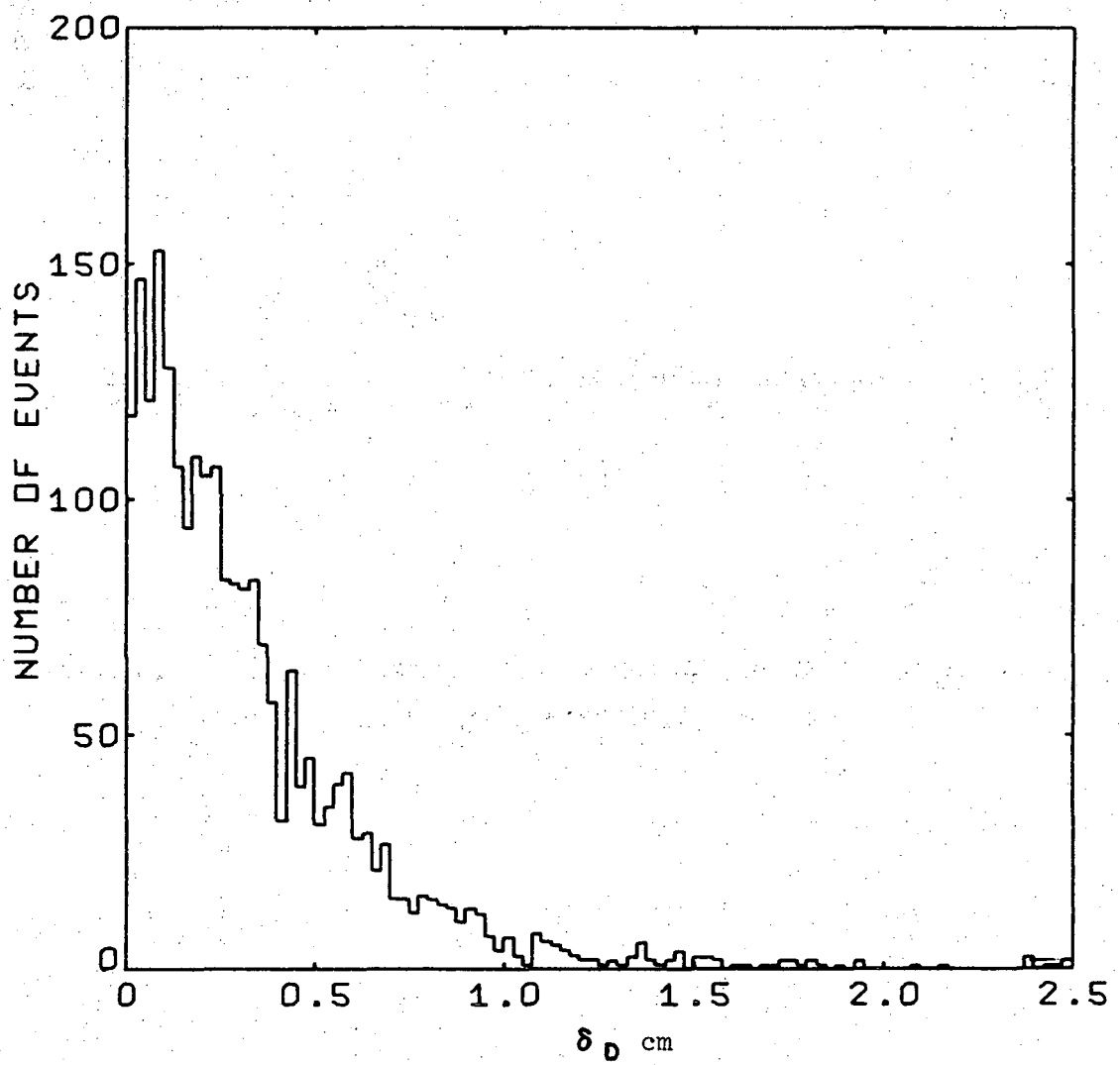

XBL 6812-6375

Fig. 6. δ_D is a measure of the amount of scattering of muons and kaons in our stopping material.

in δ_D. We eliminate all events with $\delta_D > 1$ cm. Eighty-four percent of our events were successfully scanned and reconstructed up to this point.

The directions of the γ-rays ($\hat{P}_i$) are defined by:

$$\hat{P}_i = \frac{\vec{CONV}_i - \vec{STOP}}{|\vec{CONV}_i - \vec{STOP}|}$$

CONV = conversion point of γ-ray.
STOP = stopping position of kaon.

The three vectors $\hat{P}_1$, $\hat{P}_2$, and $\hat{P}_\mu$ give us enough information to reject events of the type $K^+ \rightarrow \pi^+\pi^o$ ($K_{\pi 2}$). Appendix III gives a formula for the cosine of the angle between the two γ-rays in the center of mass of a π^o with $E_{\pi^o} = 110$ MeV and $\hat{P}_{\pi^o} = -\hat{P}_{\pi^+}(\delta_{cm} = \cos\theta_{cm})$. For $K_{\pi 2}$ events δ_{cm} should be equal -1. Figure 7 shows the distribution of events in the variable δ_{cm}. Figure 8 gives a more detailed view of the tail of the distribution. In our final analysis all events with $\delta_{cm} < -0.85$ were rejected.

All events which satisfy the following criteria are further measured on the manual system SCAMP at Berkeley:

a) $\delta_{cm} > -0.98$, $\delta_D < 1$ cm, $\delta_A > 0.998$.

b) Both γ-rays converted and were recognized by SPASS.

c) There is no charged particle except μ^+ associated with K^+ decay.

d) The angle between the two γ-ray directions is greater than 55°.

12381 of our original 99229 pictures survived the above cuts. They were further analyzed on SCAMP. On SCAMP we measured the direction of the muon in the range chamber (P'_μ), the stopping point of the muon ($\hat{\mu}'$), and the direction of the decay electron when visible. The scanner was also instructed to make sure that there were two good showers in the

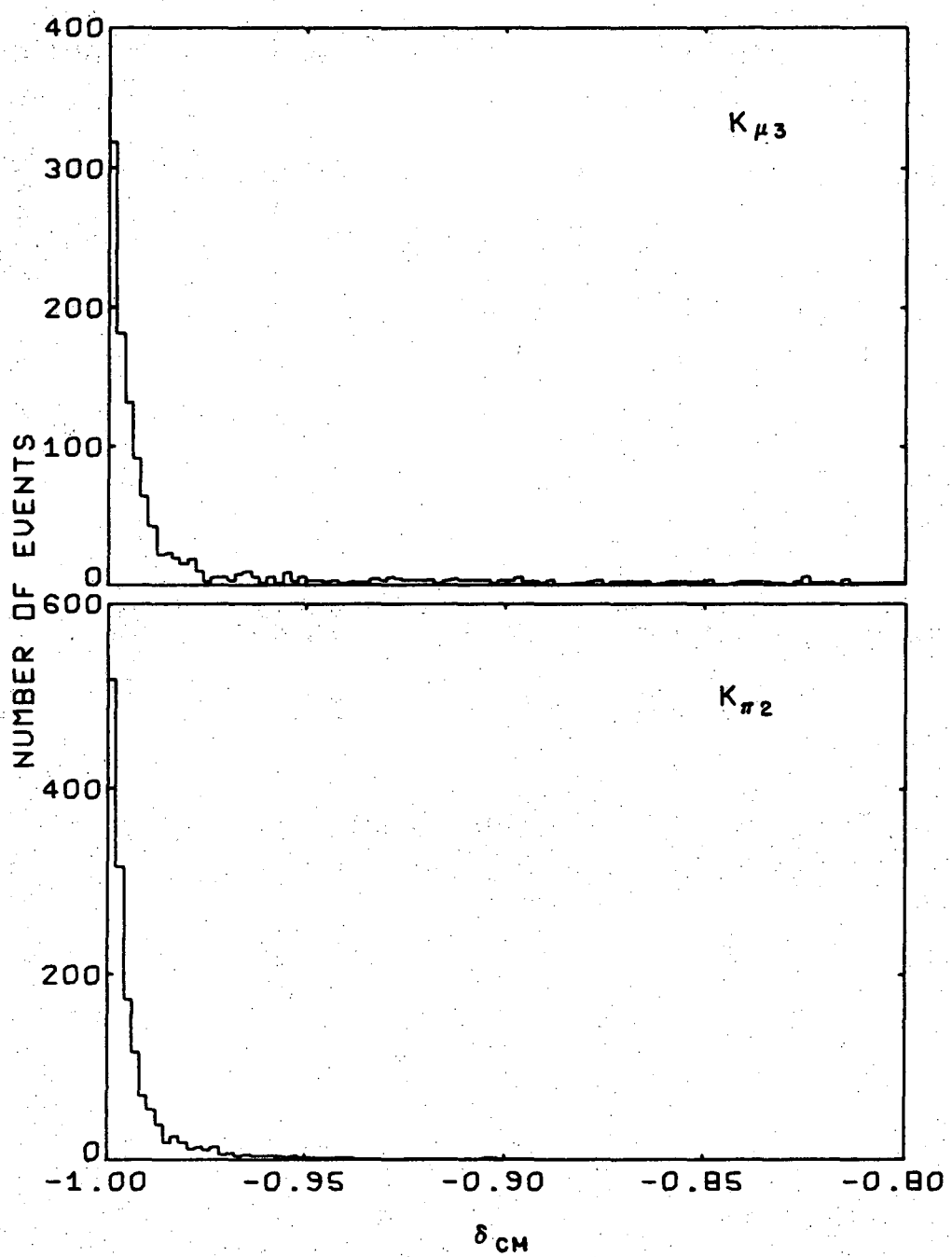

XBL 692-199

Fig. 7. δ_{cm} is the cosine of the angle between two γ-rays in the center of mass of a 110 MeV π^{o}.

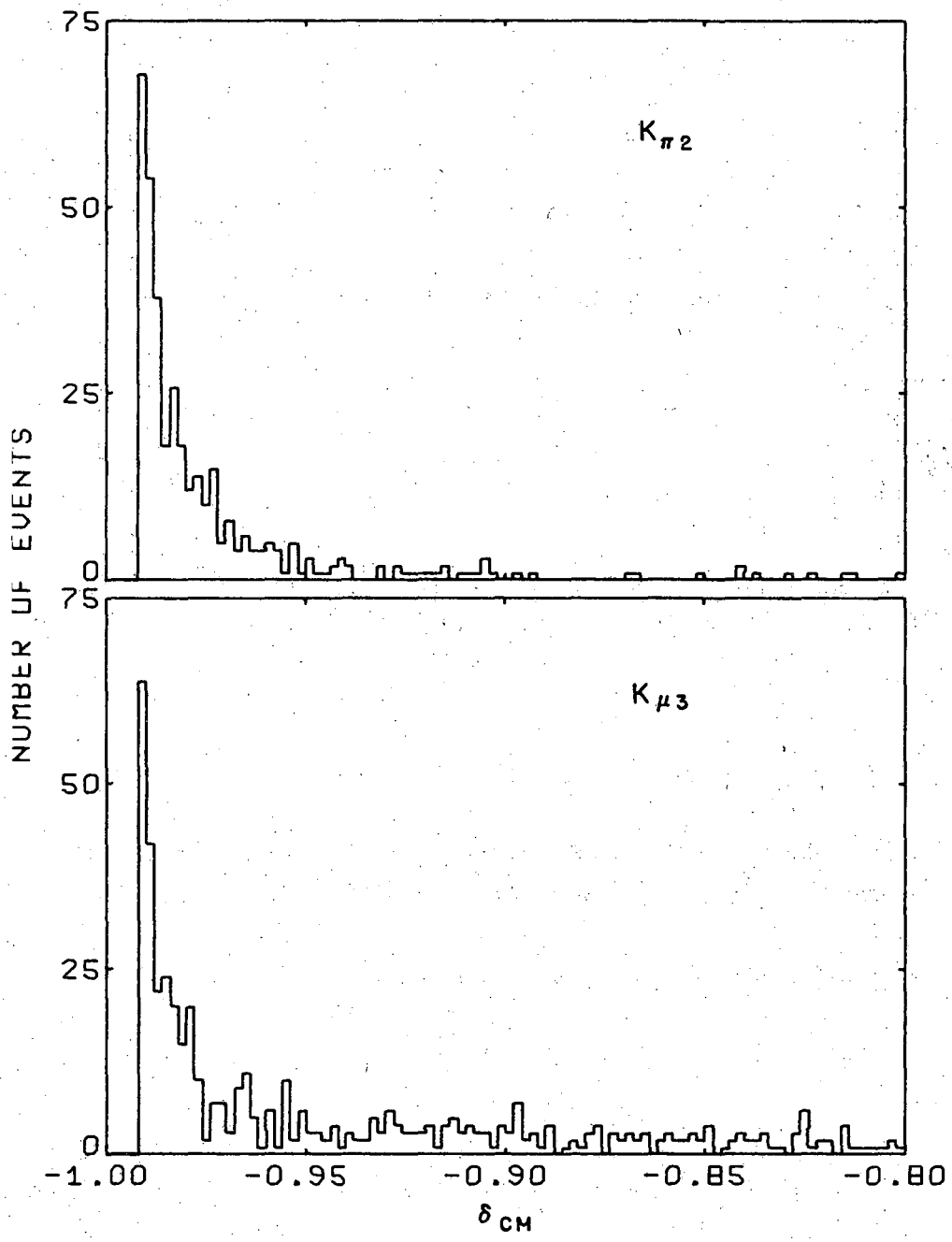

XBL 6812-6376

Fig. 8. δ_{cm} is the cosine of the angle between two γ-rays in the center of mass of a 110 MeV π^0. Events with $\delta_{cm} < -0.992$ are not plotted.

lead plate chambers.

Our sample was further reduced for the following reasons:

a) Showers must start in the third gap or later.

b) The resonstructed K-stop position must be within the stopping material.

c) The track in the muon range chamber must be measurable.

d) There must be two good showers.

e) Some events with no visible μ-e decay were not measured.

f) Events with showers close in one projected view were rejected. The reason for this is explained in the section on detection efficiency.

With these cuts we have left 5468 events to be kinematically reconstructed.

B. Kinematic Reconstruction

The kinematic quantities measured in our experiment are $\hat{P}_1$, $\hat{P}_2$, $\hat{P}_{\mu^+}$, and T_{μ^+}. The kinetic energy of the muon (T_{μ^+}) is found from the range of the muon. Positive pions from $K^+ \rightarrow \pi^+\pi^o$ are used to calibrate the energy scale. To stop muons from $K_{\mu 3}$ decay we had to decrease the amount of material degrading the muons. So we made an independent check of the μ^+ energy scale. We calculated the maximum possible μ^+ energy using all measured quantities except the μ^+ energy. We then plotted $T_\mu - T_\mu(\max)$. The result is shown in Fig. 9. If there were no measurement errors $T_\mu - T_\mu(\max)$ would never be larger than zero. Since we do have measurement errors, the histogram gradually decreases for $T_\mu - T_\mu(\max)$ greater than zero. A systematic error in the muon energy of say +10 MeV would shift the entire histogram to the right by 10 MeV. A Monte Carlo calculation is shown for comparison. Figure 10 gives our muon energy distribution.

The kinematic variable we are interested in for our analysis is the energy of the π^o. Appendix II gives T_{π^o} as a function of $\hat{P}_1$, $\hat{P}_2$, $\hat{P}_{\mu^+}$, T_{μ^+}. There are two possible solutions for T_{π^o}. To resolve this ambiguity we need a further piece of information. We have used an approximate measurment of the γ-ray energies to pick out the correct solution. The energies of the γ-rays can be crudely measured by counting the number of sparks made by the showers in our lead chambers. We can use the γ-rays from $K_{\pi 2}$ decay to find the average number of sparks expected for a given energy. We can then examine our $K_{\mu 3}$ events and compare the number of sparks in a shower to the number we expect from a particular solution. To make this comparison we calculate a χ^2 with

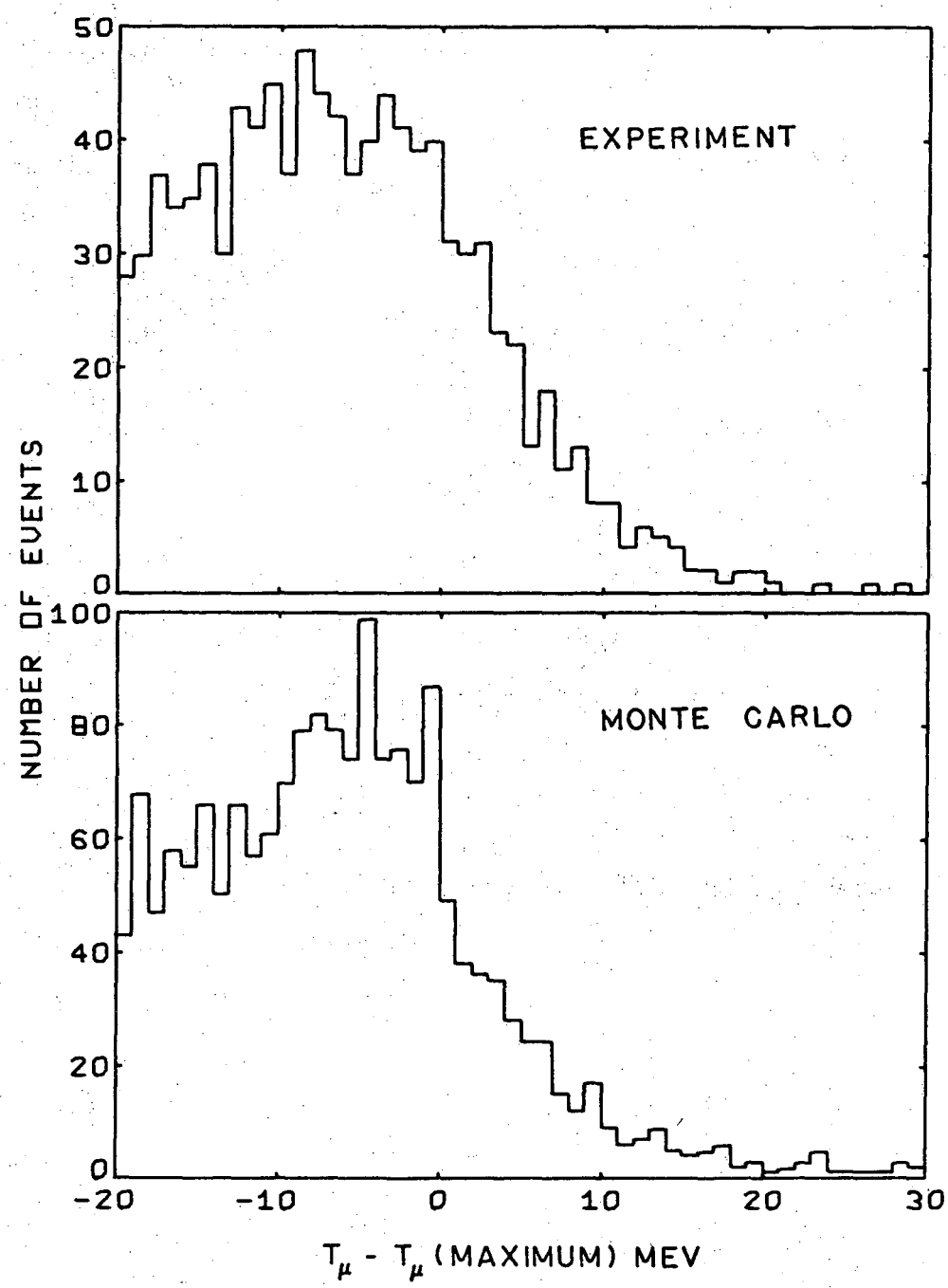

XBL 692-200

Fig. 9. T_μ-T_μ(maximum) is the difference between the measured energy and the maximum possible energy calculated from γ-ray information.

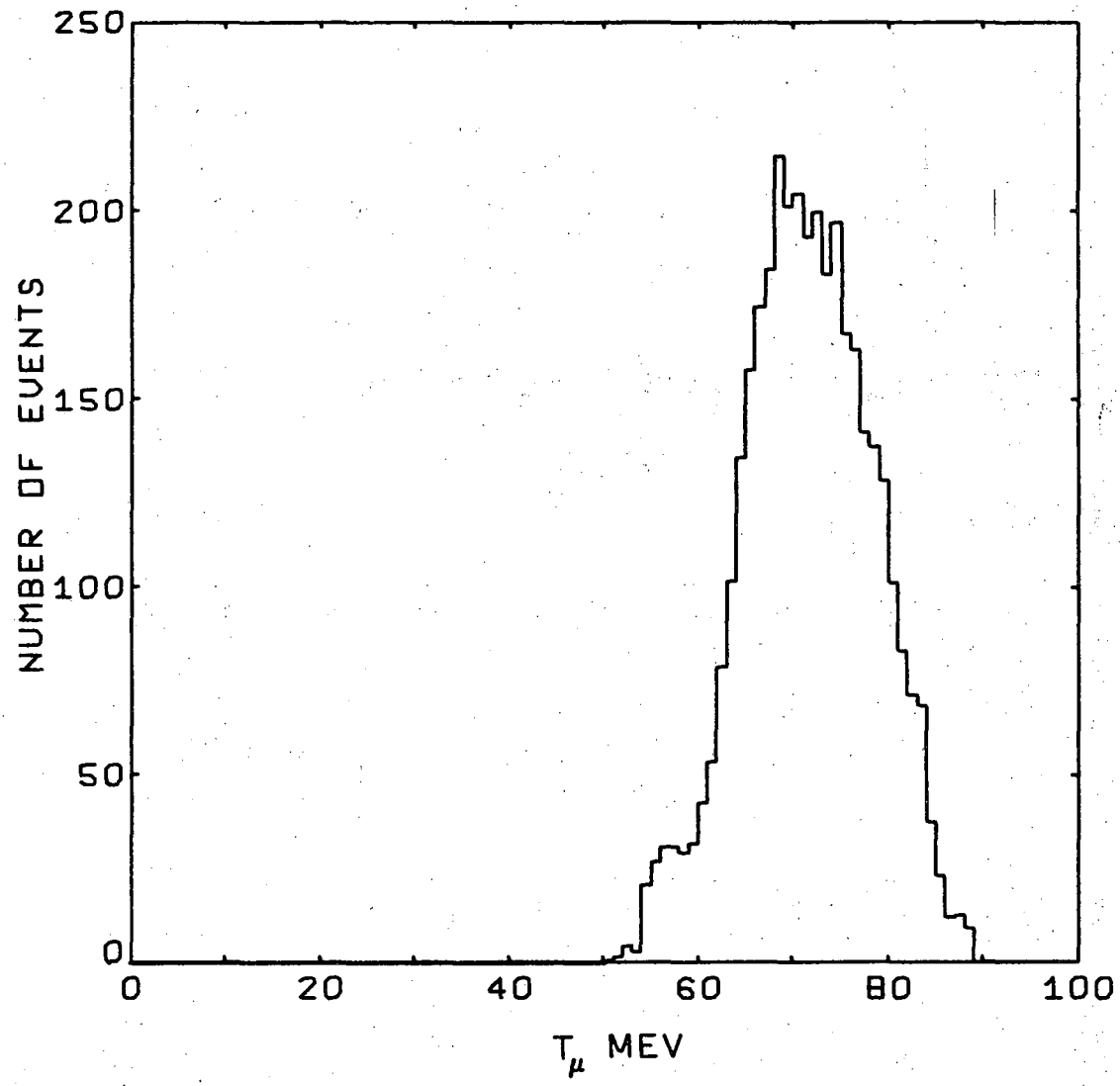

XBL 692-201

Fig. 10. Spectrum of muons accepted by our range chamber. Most of the data are taken with a 1" Aℓ degrader. The events in the region $T_\mu < 60$ MeV were obtained with a 3/4" Aℓ degrader.

two degrees of freedom:

$$({}^{i}\chi)^2 = \sum_{j=1}^{2} \left[\frac{N(E_j^{\,i}) - N_j}{\Delta N(E^i_{\,j})} \right]^2 \qquad \text{IV-1}$$

The correct solution is determined by the smaller of $({}^{1}\chi)^2$ and $({}^{2}\chi)^2$. In Eq. IV-1 i=1,2 corresponds to the two solutions. j=1,2 corresponds to the two γ-rays from π^o decay. N(E) is the number of sparks expected for a photon of energy E. N_j is the number of sparks actually observed. $\Delta N(E)$ is the standard error of N(E).

N(E) is found from photons of known energy. We have an ample supply of such photons from some 10,000 $K_{\pi 2}$ decays. We have used these events to find the dependence of N(E) on a number of geometrical factors peculiar to our experiment. Figure 11 shows the average number of sparks as a function of energy provided the following conditions are satisfied:

1) The direction of the photon is perpendicular to the spark chamber plates.
2) The photon converts in a gap far enough from the faces of the chamber so that the entire shower is contained in the chamber.
3) There is only one shower per chamber.

If these conditions are not satisfied corrections have to be applied to N(E). Figure 12 shows N(E) as a function of the angle between the photon and the normal to the spark chamber plates. A good fit to the points is provided by the following formula:

$$N(E,\cos\theta) = N(E,1)[1 + \epsilon(\cos\theta - 1)] \qquad \text{IV-2}$$

The straight line in Fig. 12 is drawn with ϵ=1.

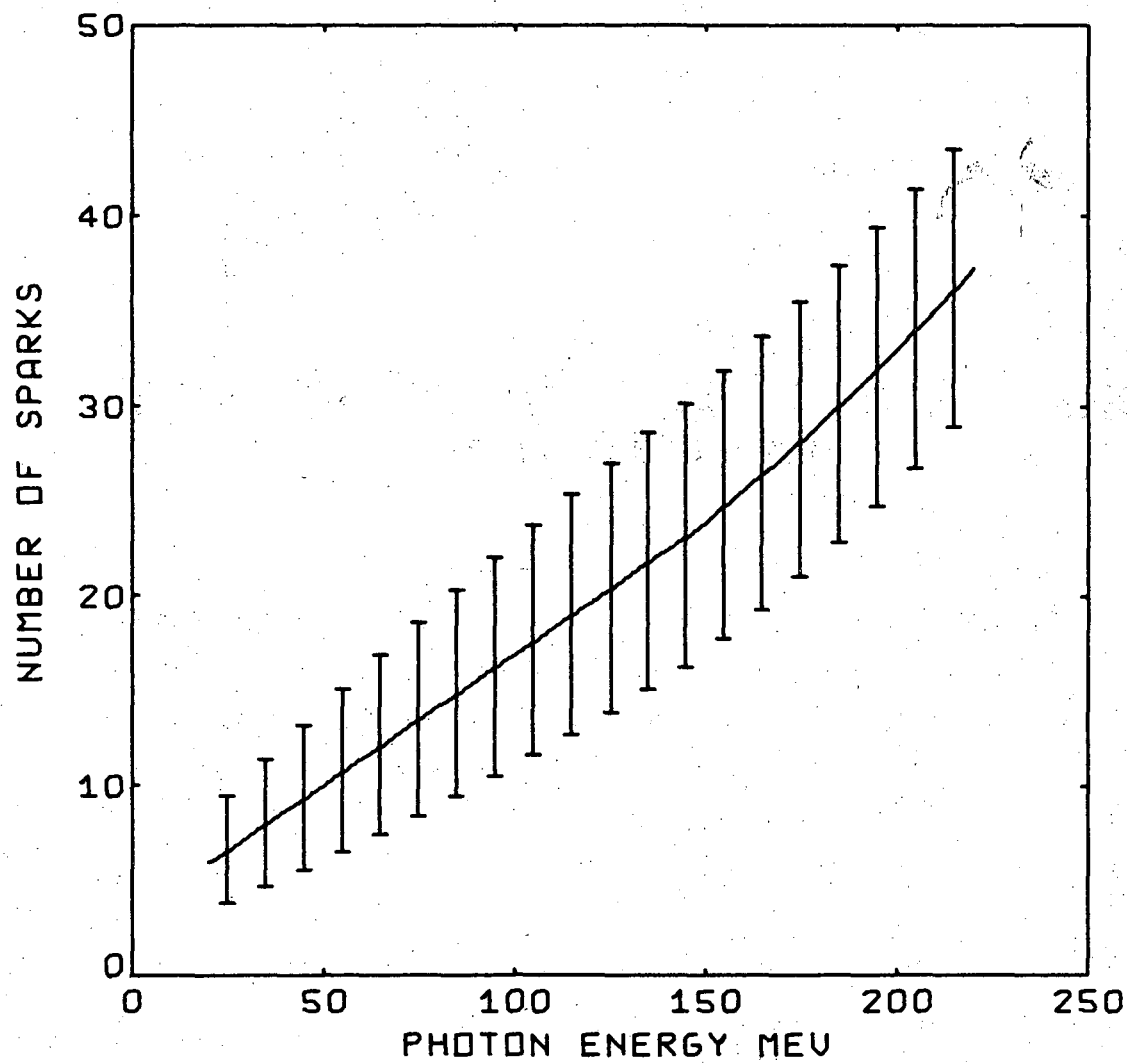

XBL 692-202

Fig. 11. The graph plots the average number of sparks N(E) versus photon energy. The error bars extend over the range N(E) ± ΔN(E) as calculated from Eq. IV-4. The graph is derived from smooth fits to our $K_{\pi 2}$ data.

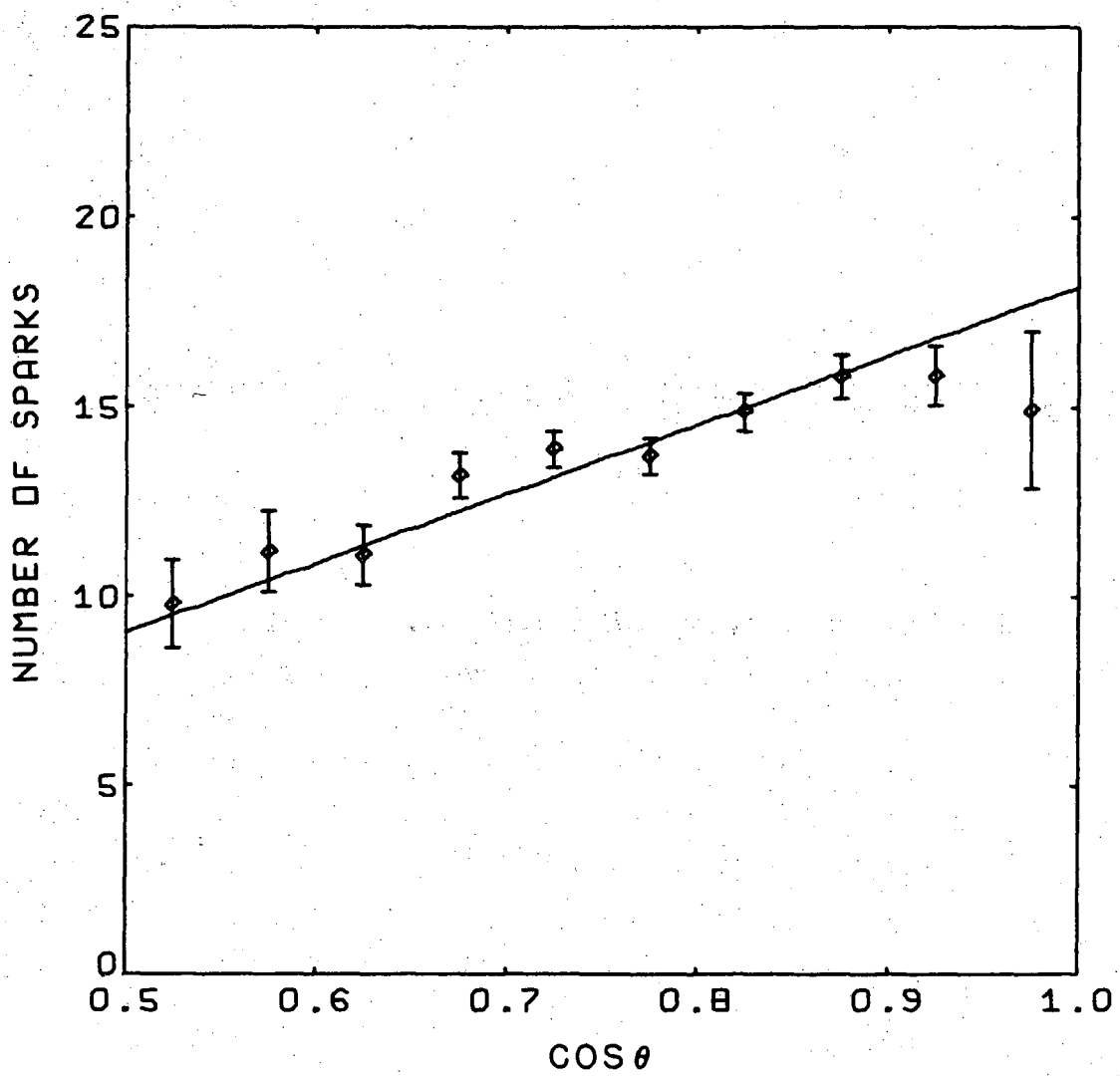

XBL 692-204

Fig. 12. θ is the angle between the normal of the spark chamber plane and the photon direction. The photon energy range extends from 100 MeV to 110 MeV.

To correct for the decrease in N(E) because part of a shower is not contained in the chamber we estimate what fraction of the shower has left the chamber. We measure the distance along the direction of the photon from the conversion point to the nearest edge of the chamber. N(E) is then multiplied by a factor which indicates what fraction of the shower remains in the chamber for that particular distance to the edge of the chamber. The fraction of the shower F_1 outside the chamber is found by calculating the area of the shaded region illustrated in the following drawing:

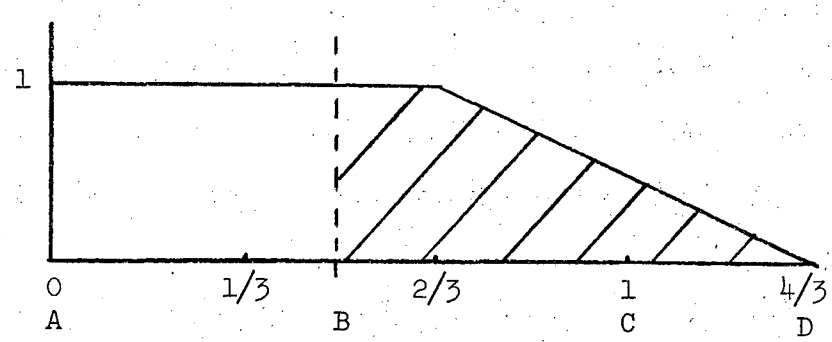

A - start of shower

B - edge of chamber

C - average length of shower for given energy.

All distances are measured in units of the average length of a shower and relative to the beginning of the shower. The decrease in the ordinate between 2/3 and 4/3 corresponds to the variation of 30% of the shower length about its average. If the edge of the shower is to the right of the point "D", the shower is fully contained in the chamber and F_1 is taken to be zero. We made a fit to our data with N(E) of the form:

$$N(E,F_1) = N(E,0)(1-\alpha F_1)$$

We find that $\alpha = 1$ provides a good fit for all energies. At a photon energy of 140 MeV about half of all showers have to be corrected for this effect. The most energetic showers (up to 220 MeV) may deposit as little as a third of their energy in the spark chambers. Figure 13 indicates how the average number of sparks changes with the fraction F_1.

Some showers have fewer sparks than expected because they have to share the charge in the spark chamber condensers with another shower. To correct for this effect we calculate a number F_2 which measures the fraction of a shower sharing its spark gaps with another shower. The average number of sparks is then fitted to:

$$N(E,F_2) = N(E,0)(1 - \alpha F_2)$$

All our data are corrected with α=0.1. This corresponds to a 10% decrease in the spark count if a shower shares all its gaps with another shower. Figure 14 illustrates the change in the average number of sparks per gap with F_2. Note we plot the number of sparks per gap rather than the number of sparks. The reason is that the effect we are looking for is masked by the following effect. Showers which fire fewer gaps than average have fewer sparks; they also share fewer gaps with other showers and hence have small values for F_2. Thus when the spark count should on the average be high it is in fact low. To compensate for this effect we divide the number of sparks by the number of gaps fired.

Including all three corrections discussed above we can write for N(E):

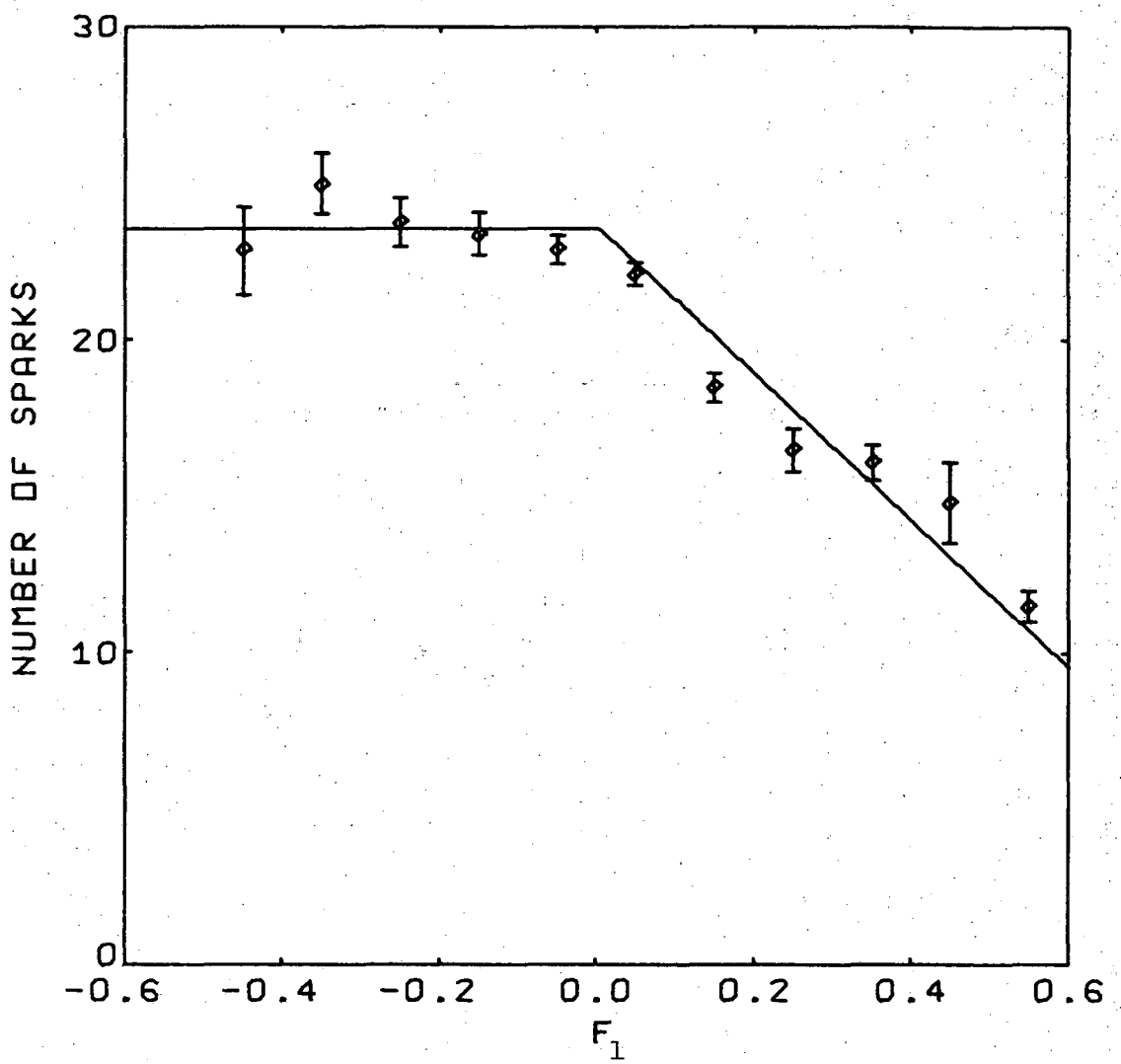

XBL 692-205

Fig. 13. F_1 is a measure of how close a shower is to the edge of the chamber. For $F_1 > 0$ at least part of the shower leaves the chamber. The photon energy range extends from 140 MeV to 150 MeV.

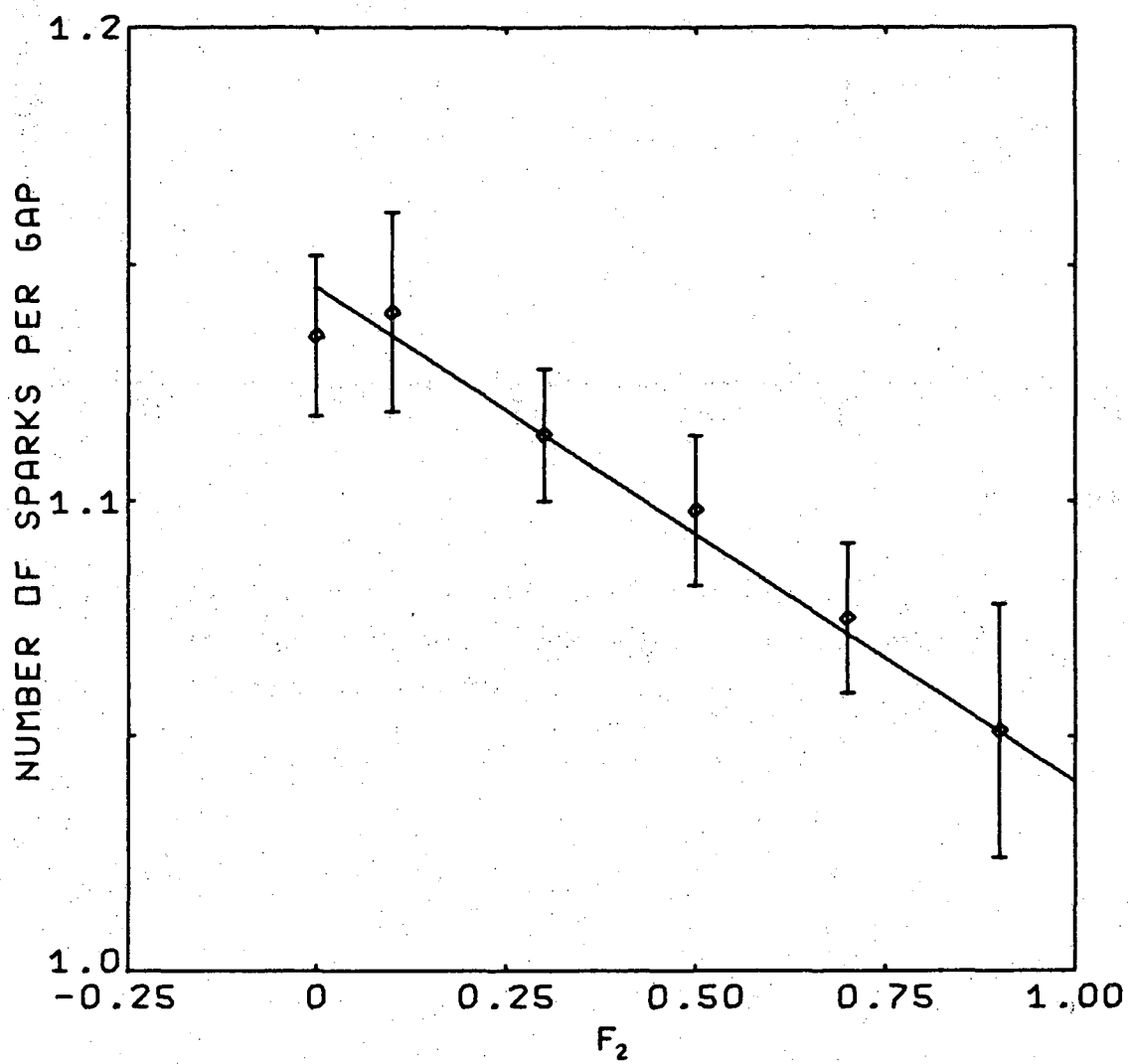

XBL 694-380

Fig. 14. F_2 is that fraction of a shower sharing its spark gaps with another shower. The photon energy is between 100 MeV and 110 MeV.

$$N(E,\cos\theta,F_1,F_2) = N(E,1,0,0)[1+\epsilon(\cos\theta-1)](1-F_1)(1-0.1\,F_2) \qquad \text{IV-3}$$

With the help of IV-3 we can now calculate the standard error $\Delta N(E)$:

$$[\Delta N(\bar{E})]^2 = \frac{1}{n}\sum_{j=1}^{n}(N(E_j) - N_j)^2 \qquad \text{IV-4}$$

N_j is the number of observed sparks in a given shower. The sum j is over all events in a given energy interval. We chose 10 MeV energy intervals to calculate the sum in IV-4. $\bar{E}$ is the average energy for the particular energy interval. The results of this calculation are graphically displayed in Fig. 11. The error bars extend over the range $N(E) \pm \Delta N(E)$.

As is evident from Fig. 11, the spark count may vary substantially for a given energy. With such large errors we will at times pick the incorrect value for T_{π^0}. To find out how often we make such an error we have performed a Monte Carlo calculation. We find that for 11% of all events T_{π^0} will be incorrect by more than 5 MeV. Figure 15 shows the resolution function for T_{π^0}. In calculating this histogram we considered measurement errors as well as incorrectly assigned solutions.

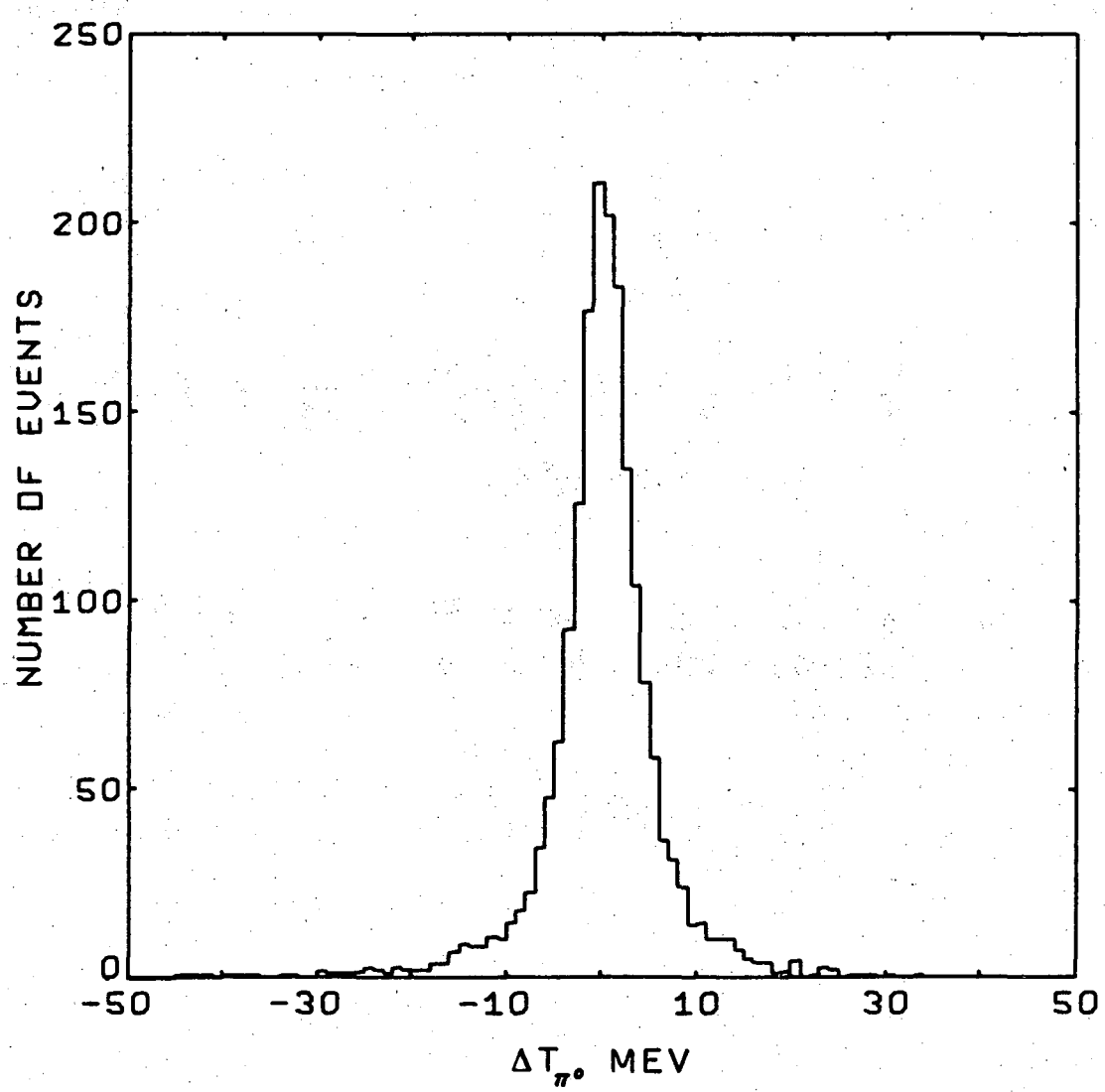

XBL 692-203

Fig. 15. ΔT_{π^0} is our error in measuring the π^0 energy. The histogram is obtained from a Monte Carlo calculation.

C. Detection Efficiency

To determine the shape of the π^o spectrum in $K^+ \rightarrow \pi^o\mu^+\nu$ we have to know how much the experimental spectrum has been distorted by the detection efficiency. The efficiency for detecting a π^o in our apparatus varies by about a factor of five between the highest and lowest π^o energies. An energetic π^o comes out of the stopper in a direction opposite to the μ^+. Referring to Fig. 4 we see that most of the γ-rays from such a π^o pass through the right-most conversion chamber. Since this chamber is sensitive to a depth of 26 gaps, or about 4 radiation lengths, the efficiency for detecting a π^o is high. As the energy of the π^o decreases, the π^o goes more nearly in the same direction as the μ^+. At least one of the γ-rays from such a π^o tends to come out in a direction not covered by a chamber, or passes through the upper or lower conversion chamber. The latter are only useful to a depth of 2 radiation lengths. Hence many soft pions escape being detected in our apparatus.

The efficiency for detecting a π^o from $K_{\mu 3}$ decay can be written as follows:

$$\mathrm{EFF}(E_{\pi^o},E_\mu) = \int \epsilon(\vec{P}_1)\epsilon(\vec{P}_2)\epsilon_{12}(\theta)\ N(\hat{P}_\mu,\vec{P}_1,E_{\pi^o},\ E_\mu)d^2\hat{P}_\mu d^3\vec{P}_1 \qquad \text{IV-5}$$

N is the probability that a $K_{\mu 3}$ event with pion energy equal E_{π^o} and muon energy equal E_μ produces a photon with momentum $\vec{P}_1$ and a muon with direction $\hat{P}_\mu$. The integral over $d^3\vec{P}_2$ has already been carried out. It is of the simple form:

$$1 = \frac{1}{(2\pi)^3}\int d^3(\vec{P}_2 - \vec{f}(\hat{P}_\mu,\vec{P}_1,E_{\pi^o},E_\mu))d^3\vec{P}_2$$

The function $\vec{f}$ can be calculated from energy and momentum conservation.

The integral over the five variables $\hat{P}_\mu$, $\vec{P}_1$ takes care of the independent variables left after E_{π^0} and E_μ have been specified. To put it another way, these five variables are equivalent to the orientation of the event in a fixed coordinate system (3 variables) and the random orientation of one of the photons in the rest system of the π^0 (2 variables).

$\epsilon(\vec{P})$ is the efficiency for detecting a photon with momentum $\vec{P}$. The principal variation of ϵ is with the direction $\hat{P}$. The dependence on energy is observable only for photons with energy less than 40 MeV. ϵ_{12} deviates from one when two showers are close in one projected view of a spark chamber. For showers closer than $\theta=25^\circ$ the automatic scanning system at times could not resolve the two showers. The resulting error in conversion point measurement was too large to reject $K_{\pi 2}$ background. Hence all events where the computer could not find two conversion points in each view were rejected. The efficiency ϵ_{12} increases from 0 to 1 between $\theta=0^\circ$ and $\theta=25^\circ$. There is no correction if θ is larger than 25° or the two showers convert in different chambers.

To find the functions ϵ and ϵ_{12} we have used $K_{\pi 2}$ events. They were scanned and reconstructed in the same way as our $K_{\mu 3}$ events. The same efficiency functions apply then to $K_{\mu 3}$ and $K_{\pi 2}$ events. For $K_{\pi 2}$ events, however, the spectra of the variables describing the decay are well known. Suppose $R(\vec{P})$ is the probability of observing a γ-ray from $K_{\pi 2}$ decay in our apparatus:

$$R(\vec{P}_1) = \epsilon(\vec{P}_1) \int \epsilon(\vec{P}_2)\epsilon_{12}(\theta)N'(\varphi,\vec{P}_1)d\varphi \qquad \text{IV-6}$$

φ is the only independent variable left after $\vec{P}_1$ has been fixed. φ

determines the azimuthal angle of the decay plane about the direction $\hat{P}_1$. $N'(\varphi,\vec{P}_1)$ is the probability of getting an event with azimuthal angle equal φ once $\vec{P}_1$ has been specified.

The integral Eq. IV-6 is solved for ϵ and ϵ_{12} by adjusting these functions until $R(\vec{P}_1)$ matches the γ-ray distributions actually observed. The integral is evaluated by a Monte Carlo technique. We pick a direction $\hat{P}_{\pi^+}$ according to the distribution actually observed. A π^0 is attached along the direction $-\hat{P}_{\pi^+}$. The π^0 then generates two photons with either one of them randomly distributed in the center of mass of the π^0. These steps correspond to calculating the function N'. The generated event is then given a weight according to $\epsilon(\vec{P}_2)\cdot\epsilon_{12}(\theta)$ and stored in a bin corresponding to two angles $(\hat{P}_1)$ and an energy $(|P_1|)$. A χ^2 method is used to compare this distribution with our experimental distribution. ϵ and ϵ_{12} are adjusted until all χ^2 values have a reasonable probability.

Of course $K_{\pi 2}$ events cannot provide us with a complete range of all variables. For example if we restrict $\hat{P}_1$ so that the photon appears in the upper or lower conversion chamber, then the energy $|P_1|$ has to be less than 70 MeV. To extend the calibration to higher energies we assume that the energy dependence of the efficiency is the same in all chambers.

Using our knowledge of ϵ and ϵ_{12} we can now evaluate the expression in Eq. IV-5. We use a Monte Carlo technique similar to the one described above for $K_{\pi 2}$ events. The result of this calculation is presented in Fig. 16 for two representative values of E_μ. The curves exhibit the strong dependence of the efficiency on the energy of the

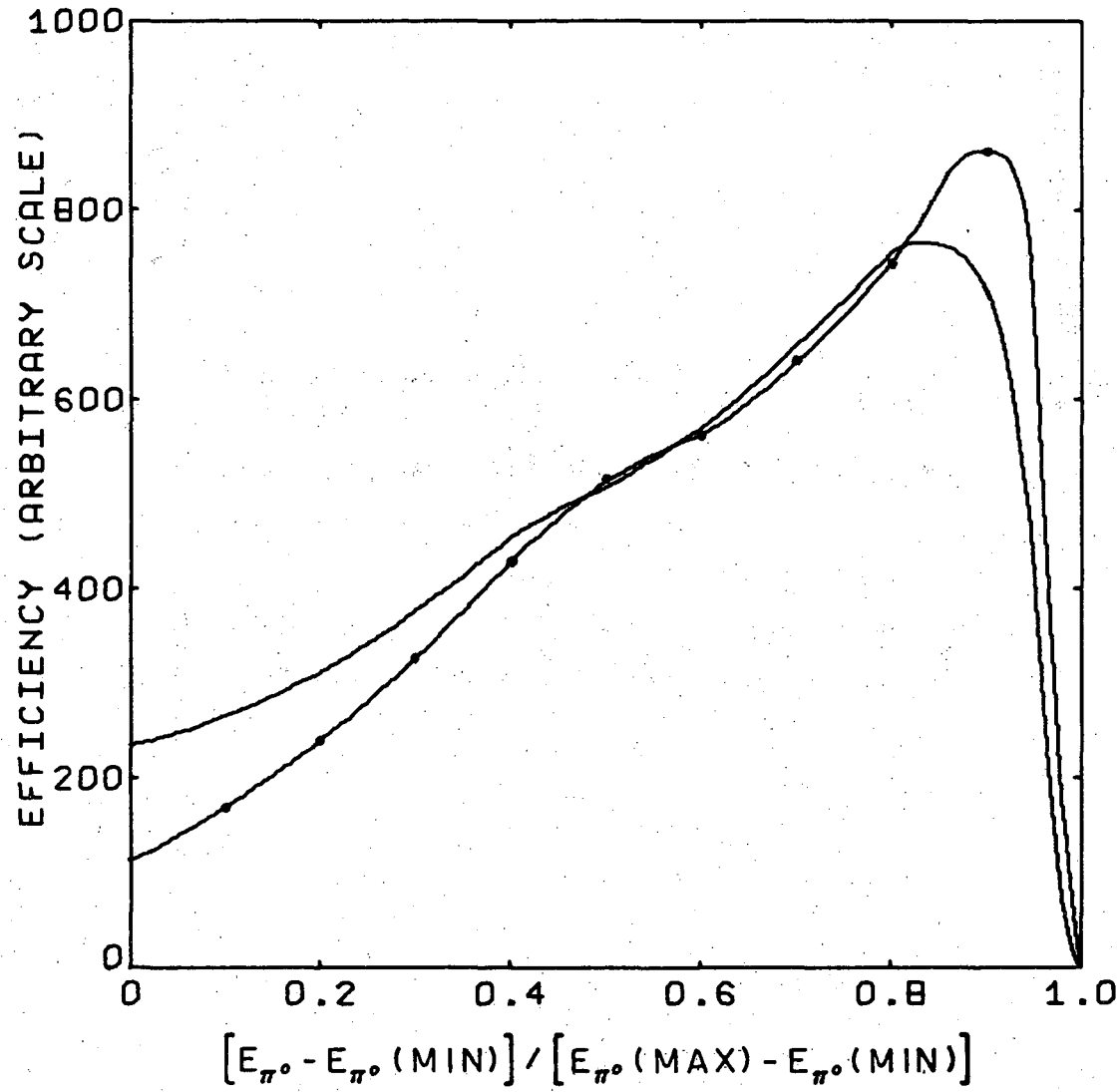

XBL 694-381

Fig. 16. Efficiency for detecting a π^0 in our apparatus. The curve with the dots is for T_μ = 60 MeV. The other curve is for T_μ = 80 MeV.

π^o. The decrease in efficiency at the upper end of the spectrum is caused by the cut on δ_{cm}.

To provide an internal check on our calculation we set up a relation similar to IV-6 but for $K_{\mu 3}$ events:

$$R(\vec{P}_1) = \epsilon(\vec{P}_1) \int \epsilon(\vec{P}_2)\epsilon_{12}(\theta) N(\hat{P}_\mu, \vec{P}_1, E_{\pi^o}, E_\mu) \frac{d\Gamma(K_{\mu 3})}{dE_{\pi^o} dE_\mu} dE_{\pi^o} dE_\mu d^2\hat{P}_\mu \qquad \text{IV-7}$$

To evaluate the integral we have to make some assumptions about the parameters determining $d\Gamma/dE_{\pi^o}dE_\mu$. However the detailed distributions of R as a function of $\vec{P}_1$ are relatively independent of such parameters. So IV-7 gives us a check on $\epsilon(\vec{P}_1)$ for those values of $\vec{P}_1$ which are not accessible to $K_{\pi 2}$ events. For this purpose we again used a χ^2 method to compare $R(\vec{P})$ calculated from IV-7 with $R(\vec{P})$ found from our sample of $K_{\mu 3}$ events.

D. Background

There are several decay modes of the K^+ which our analysis cannot distinguish from $K_{\mu 3}$ decay. We have used a combination of experimental information and Monte Carlo calculation to estimate the amount of backgound among our $K_{\mu 3}$ events. Table II presents a summary of the results we obtained.

One possible source of background is the decay $K^+ \rightarrow \pi^+\pi^o\pi^o$ (τ'). If only two of the four γ-rays convert in our chambers, the event looks like a $K_{\mu 3}$ decay. However, unless the π^+ decays in flight the event will be rejected by our trigger. The maximum energy of a π^+ from τ' decay is 53 MeV. The least energetic π^+ we detect has an energy of 56 MeV. To estimate the amount of τ' background we calculated the following ratio:

$$R = \frac{\iint \frac{d\Gamma(\tau')}{dE_{\pi^+}} G(E_\mu) F(E_{\pi^+}, E_\mu) dE_\mu dE_{\pi^+}}{\int \frac{d\Gamma(K_{\mu 3})}{dE_\mu} G(E_\mu) dE_\mu} = 0.0037 \qquad \text{IV-8}$$

$\frac{d\Gamma}{dE}$ is a decay rate. $G(E_\mu)$ is the probability of detecting a muon of energy E_μ in our apparatus. $F(E_{\pi^+}, E_\mu)$ is the probability that a π^+ with energy E_{π^+} produces a muon with energy E_μ. F was calculated by considering that the decay could take place anywhere between the K^+ stopper and T_4 (See Fig. 4). The ratio R in Eq. IV-8 is an upper limit for τ' background. Since in addition we require that only 2 photons be detected and the event be reconstructable as a $K_{\mu 3}$, the amount of τ' background is less than 0.4%.

There are two ways in which we reject events of the type $K^+ \rightarrow \pi^+\pi^0$ ($K_{\pi 2}$). First, we do not accept π^+ mesons with energies larger than 90 MeV. The π^+ from $K_{\pi 2}$ decay has an energy of 108 MeV. Second, we have to calculate the constraint δ_{cm} explained in Section IV-A. This quantity is cut very conservatively at $\delta_{cm} = -0.85$. The top frame in Fig. 8 shows that with this cut we are well beyond the tail of the δ_{cm} distribution.

There are several ways in which $K_{\pi 2}$ events can nevertheless be mistaken for $K_{\mu 3}$ events. A π^+ may end up with less than 108 MeV if it interacts with the material in the range chamber. We can find out how often this happens by simply counting the number of $K_{\pi 2}$ events among our $K_{\mu 3}$ events before we apply the cut on δ_{cm}. The ratio of the number of $K_{\pi 2}$ events to $K_{\mu 3}$ events is 0.57/0.43. δ_{cm} may be less than -0.85 because the event was improperly reconstructed or because the π^+ scatters in the K^+ stopper. We now look at the data we took with the degrader in the μ^+ telescope set to accept 108 MeV pions. We find that 3% of these events have $\delta_{cm} < -0.85$. 1.1% is expected from $K_{\mu 3}$ decay. The other 1.9% is from $K_{\pi 2}$ events. $K_{\pi 2}$'s can then contaminate our $K_{\mu 3}$ sample via a two step process. In the first step δ_{cm} is changed to some value less than -0.85; in the second step the π^+ energy is reduced to allow the π^+ to stop in the range chamber. The probability for this process is the product of the probabilities (0.57/0.43)(1.9%) = 2.5% derived above.

A $K_{\pi 2}$ may also look like a $K_{\mu 3}$ as the result of a single interaction. The π^+ can emit a γ ray while it is produced during the decay of the K^+. Only events with soft photons will occur with sufficient

frequency to contribute to the background. Such soft photons are not detected by our apparatus. They carry off enough energy to violate both $K_{\pi 2}$ constraints. We have performed a Monte Carlo calculation and find that our final sample of events should contain 1.6% events of the type $K^+ \rightarrow \pi^+\pi^0\gamma$. The π^+ can also scatter inelastically on a nucleus in the π^+ stopper. In this case δ_{cm} can be substantially different from -1 because the π^+ changes its direction before we have a chance to measure it. The π also stops in our chamber if an appropriate amount of energy is lost during the scatter. To estimate the amount of background from this source we Monte Carlo generated $K_{\pi 2}$ events and let the π^+ scatter inside the degrader. We assumed that $\sigma_{inelastic}$ = 100 mb and that $d\sigma/dE_{\pi^+}d\cos\theta$ is a constant. These assumptions roughly correspond to experimental data.[12] More complicated forms for $d\sigma/dE_{\pi}d\cos\theta$ do not substantially alter our analysis. The background from π^+ scattering turns out to be about 1%.

A final way in which $K_{\pi 2}$'s can contribute to the background is through decays in flight. To get a μ^+ from π^+ decay which stops in the range chamber, the angle between the μ^+ and π^+ has to be about 11°. Hence we mismeasure the π^+ direction anywhere between 0° and 11° depending on where the π^+ decays. Only very rarely will such a mismeasurement produce an event with $\delta_{cm} > -0.85$. Considering that the π^+ can decay at any point between the tracking chambers we find an upper limit on the background from decay in flight of 0.4%.

A further possible source of background is the decay $K^+ \rightarrow \pi^0 e^+ \nu$ (K_{e3}). To reject electrons we have a Cerenkov counter in the muon telescope. This counter has been measured to be 99.8% efficient.

Furthermore, it is unlikely that an electron passes through the degrader without substantially altering its direction. Since this scattering angle has an upper limit for acceptable events, electrons which do not trigger the Cerenkov counter will in many cases be eliminated by the cut on the scattering angle. Hence background from K_{e3} decays is negligible.

Finally we have to consider events where one of the photons comes from a source other than the K^+ decay which triggered our apparatus. We have recorded many events for which only one γ-ray converts in the spark chambers. If for such an event a shower appears during the resolving time of the chambers, the event will look like a $K_{\mu 3}$ event. However, in this case $\cos^{-1}(\hat{P}_1 \cdot \hat{P}_2)$ can be anywhere between 0° and 180°. For events where both showers originate from π^0 decay $\cos^{-1}(\hat{P}_1 \cdot \hat{P}_2)$ must be greater than 60°. Hence we look for background in the region $10^\circ \leq \cos^{-1}(\hat{P}_1 \cdot \hat{P}_2) \leq 60^\circ$ and extrapolate onto the $K_{\mu 3}$ Dalitz plot. We have scanned 30% of our data and found 22 acceptable events with $\cos^{-1}(\hat{P}_1 \cdot \hat{P}_2)$ between 10° and 60°. All our data should then contain 22/0.3=73 events. We now perform a Monte Carlo calculation and find the ratio:

$$R = \frac{\text{NUMBER OF ACCEPTABLE } K_{\mu 3} \text{ EVENTS}}{\text{NUMBER OF EVENTS IN THE INTERVAL } 10^\circ < \cos^{-1}(\hat{P}_1 \cdot \hat{P}_2) < 60^\circ} = 0.38$$

The Monte Carlo events are generated by taking our one shower events and attaching to them a photon randomly distributed in the fiducial volume. The amount of background we get then is:

$$73 \times R = 28 \text{ events} \qquad \text{or} \qquad 1.4\%$$

In Section IV F we will consider how the various types of background discussed above will affect our final result.

Table II. Summary of background calculations.

Event type	Percent Background*
$K^+ \to \pi^+\pi^o\pi^o$	< 0.4%
$K^+ \to \pi^+\pi^o$ short range π^+	2.5%
$K^+ \to \pi^+\pi^o$, π^+ interaction in stopper	1.0%
$K^+ \to \pi^+\pi^o$ decay in flight	< 0.4%
$K^+ \to \pi^+\pi^o\gamma$	1.6%
$K^+ \to \pi^o e^+\nu$	very small
$K^+ \to \pi^+\pi^o$ + random γ	1.4%
$\to \mu^+\nu\pi^o$ + random γ	

* Percent background means the percentage of events in our final sample of 2041 events that do not originate from the decay $K^+ \to \pi^o\mu^+\nu$.

E. Selection of Events

Of our 99229 pictures we have left 5468 events after scanning. In Section IV-A we explain how these events were selected. With the information obtained in the previous sections we can now proceed with the final selection of events relevant to our analysis. Table III shows how various cuts applied to our data reduce the number of events used for analysis to about 2000.

During the manual scan we looked at all events with $\delta_{cm} > 0.98$. However this cut fails to eliminate many $K_{\pi 2}$ events as was explained in the section on background. We rejected all events with $\delta_{cm} < -0.85$. A further attempt to eliminate background and incorrectly measured events was made by applying a cut to the quantity $\hat{P}_\mu \cdot \hat{P}'_\mu$ illustrated in the following drawing:

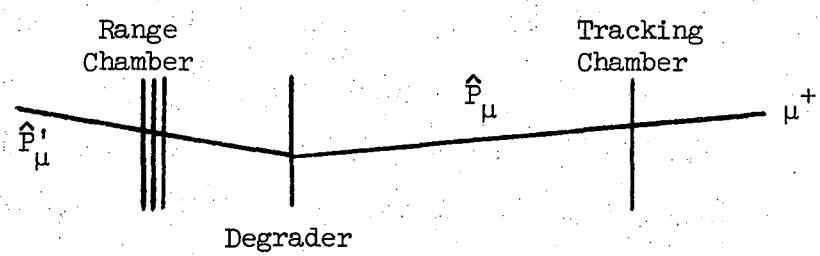

All events with $\hat{P}_\mu \cdot \hat{P}'_\mu$ less than 0.92 were eliminated.

We found that a class of events identified during the computer scan had unreliable spark count information. What happened during the scanning was that the computer could not decide whether it was looking at two showers or two parts of the same shower. We ascertained that this could happen with about equal probability for photons of all energies. All such events were rejected.

The largest block of events was thrown out when we applied a cut to our fiducial volume. The active volume of the counter chambers is

as illustrated:

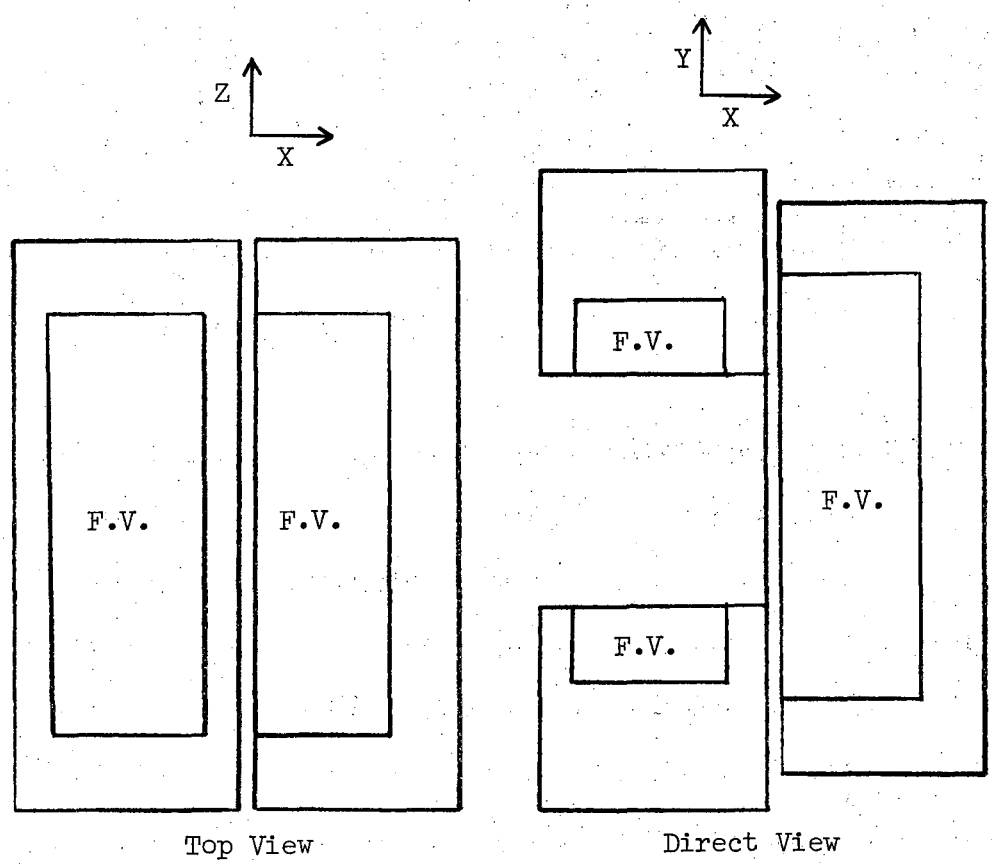

F.V. = Fiducial Volume

The reason for eliminating events close to the edge of the chamber is that the information in the spark count becomes very minimal. If a shower leaves the chamber after firing 10 gaps we simply cannot tell whether it was 50 MeV or 220 MeV. Of course there is a second shower which allows us to find the correct solution for E_{π^0}. However, our errors are simply too large to rely on a single shower to give us the information we need. The spark count analysis discussed in Section IV-B was done with events restricted to the above fiducial volume.

Finally we rejected events for which χ^2 as calculated from Eq. IV-1 was too large. Such events could either be from background or from large statistical fluctuations in the spark count. After this final cut we are left with 2041 events to be used in our subsequent analysis.

Table III. Number of events passing successive tests.

Number of pictures taken	99229
$K_{\mu 3}$ candidates left after computer scan	12381
$\delta_{cm} > -0.98$, $\delta_D < 1$ cm, $\delta_A > 0.998$	
Acceptable $K_{\mu 3}$ events left after manual scan	5468
Events left after rejection of events for which spark count uncertain	4734
Events left after rejection because $\delta_{cm} < -0.85$	3660
Events left after rejection because $\hat{P}_\mu \cdot \hat{P}'_\mu < 0.92$	3535
Events left after cut on fiducial volume	2131
Number of events which fit $K_{\mu 3}$ kinematics	2088
Events for which predicted shower energy matches actual shower energy $\chi^2 < 10$	2041
Final sample	2041

F. Calculation of Parameters

The purpose of this experiment is to extract information about $K_{\mu 3}$ decay from the π^o energy spectrum. In particular we want to find the form factors $f_+(q^2)$ and $f_-(q^2)$ describing the hadronic $\Delta S = 1$ current. Of course we cannot find f_+ and f_- in all generality. We parametrize f_+ and f_- as shown in Eq. I-6. There are then the three parameters $\xi(0)$, λ_+, λ_- to be calculated. Since we do not calculate an absolute rate, we cannot find $f_-(0)$ and $f_+(0)$ separately but only the ratio $\xi(0) = f_-(0)/f_+(0)$.

We have applied a likelihood method to compare theory with experiment. We divide the π^o spectrum into ten bins in the variable $[E_{\pi^o} - E_{\pi^o}(MIN)]/[E_{\pi^o}(MAX) - E_{\pi^o}(MIN)]$. The reason for choosing this variable is that its range from 0 to 1 is independent of the muon energy. Each bin contains N_i events. Since the numbers N_i are Poisson distributed, the likelihood function is:

$$\mathcal{L} = \sum_{i=1}^{10} \frac{(\bar{N}_i)^{N_i}}{N_i\,!}\, \ell^{-\bar{N}_i} \qquad \text{IV-9}$$

The numbers $\bar{N}_i$ are the number of events expected using the decay rate given in Appendix I and the efficiency function derived in Section IV-C. $\bar{N}_i$ are then numbers that depend on the parameters $\alpha = \xi, \lambda_+, \lambda_-$. Since we are interested only in the variation of the Dalitz plot with E_{π^o}, $\bar{N}_i$ is normalized in such a way that the variation with muon energy corresponds to the one actually observed:

$$\bar{N}_i = \sum_{j=1}^{N} \frac{\int_{E_{1i}}^{E_{2i}} \frac{d\Gamma(\alpha)}{dE_{\pi^o} dE_{\mu j}} \, EFF(E_{\pi^o}, E_{\mu j}) G(E_{\mu j}) dE_{\pi^o}}{\int_{E_{\pi^o}(MIN)}^{E_{\pi^o}(MAX)} \frac{d\Gamma(\alpha)}{dE_{\pi^o} dE_{\mu j}} \, EFF(E_{\pi^o}, E_{\mu j}) G(E_{\mu j}) dE_{\pi^o}} \qquad \text{IV-10}$$

E_{1i} and E_{2i} define the limits of the ith energy bin. $EFF(E_{\pi^o}, E_\mu)$ is the efficiency for detecting a π^o; $G(E_\mu)$ is the efficiency for detecting a μ^+. The sum j is over all events selected for analysis. If we take the logarithm of IV-9 and use IV-10 we get:

$$\log \mathcal{L} = \sum_{i=1}^{10} N_i \log \sum_{j=1}^{N} \frac{\int_{E_{1i}}^{E_{2i}} \frac{d\Gamma(\alpha)}{dE_{\pi^o} dE_{\mu j}} \, EFF(E_{\pi^o}, E_{\mu j}) dE_{\pi^o}}{\int_{E_{\pi^o}(MIN)}^{E_{\pi^o}(MAX)} \frac{d\Gamma(\alpha)}{dE_{\pi^o} dE_{\mu j}} \, EFF(E_{\pi^o}, E_{\mu j}) dE_{\pi^o}} + C \qquad \text{IV-11}$$

Note $G(E_{\mu j})$ cancels out. The constants C contain all terms which are independent of α. Our subsequent analysis is carried out with the help of IV-11. Our analysis essentially consists of maximizing $\log \mathcal{L}$ by varying the parameters $\alpha = \xi(0)$, λ_+, λ_-.

In principle the π^o spectrum contains enough information to pin down all three parameters. However, we are limited by statistics. The error in each one parameter would be very large if we varied all three of them simultaneously. We solve then several special cases with one or more of the parameters fixed at an assumed value.

The simplest analysis we can carry out is to assume that f_+ and f_- are independent of q^2. We maximize $\log \mathcal{L}$ as a function of $\xi(0)$ with $\lambda_+ = \lambda_- = 0$. As explained in the introduction this corresponds to finding the slope of the π^o energy spectrum. The result we obtain is:

$\xi = -0.3 \pm 0.3$ $\chi^2(8\text{D.F.}) = 12.2$

The errors correspond to the decrease in the likelihood function by a factor $\ell^{-1/2}$. We can make a similar analysis by taking $\lambda_+ = 0.023$, a value derived from theoretical arguments as well as experiment.[3] We get: $\xi = -0.9 \pm 0.3$ $\chi^2(8\text{D.F.}) = 12.8$

For a two parameter analysis we have drawn contours of constant likelihood. We have have used the variables $\xi(0)$, λ_+, $\lambda-\xi(0)$, with any one variable fixed for a two parameter fit. The reason for using $\lambda-\xi$ rather than λ_- is that λ_- appears in the decay rate only in the combination $\lambda_-\xi$. This means that near $\xi=0$ we are completely insensitive to λ_-. Figure 17 gives the result for ξ, λ_+ variable and $\lambda_-\xi=0$. From the fact that the error ellipse does not have its axes parallel to the coordinate axes, we see that ξ and λ_+ are correlated. Hence we cannot assign errors independently to ξ and λ_+. ξ and $\lambda_-\xi$ are even more strongly correlated than ξ and λ_+. However, we can define two numbers which do have independent errors:

$$\cos\theta\ \xi(0) + \sin\theta\ \Lambda = \gamma_1 \pm \Delta\gamma_1$$
$$-\sin\theta\ \xi(0) + \cos\theta\ \Lambda = \gamma_2 \pm \Delta\gamma_2$$
$$\Lambda = \lambda_+ \quad \text{or} \quad \lambda_-\xi$$

θ is the angle between the axes of the ellipse and the axes of the coordinates ξ and Λ. In Fig. 18 we plot contours of constant likelihood with γ_1 and γ_2 as axes and $\Lambda = \lambda_-\xi$. It is evident from the graph that γ_1 and γ_2 are not correlated. In Table IV we give the results for various possible two parameter fits.

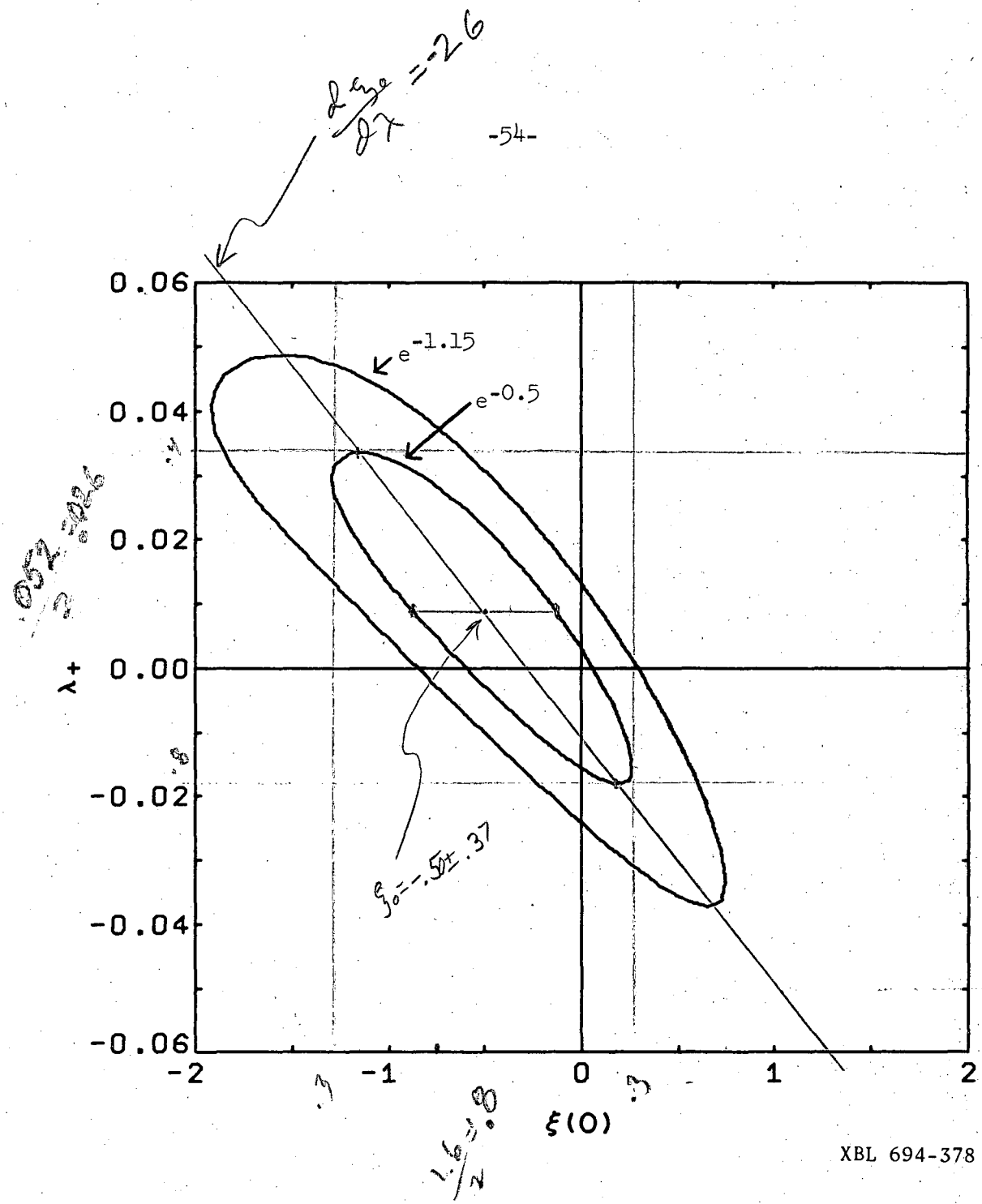

Fig. 17. Contours of constant likelihood. λ_- is taken equal zero.

$$\xi(0) = -0.5 \pm 0.8$$

$$\lambda_+ = 0.009 \pm 0.026$$

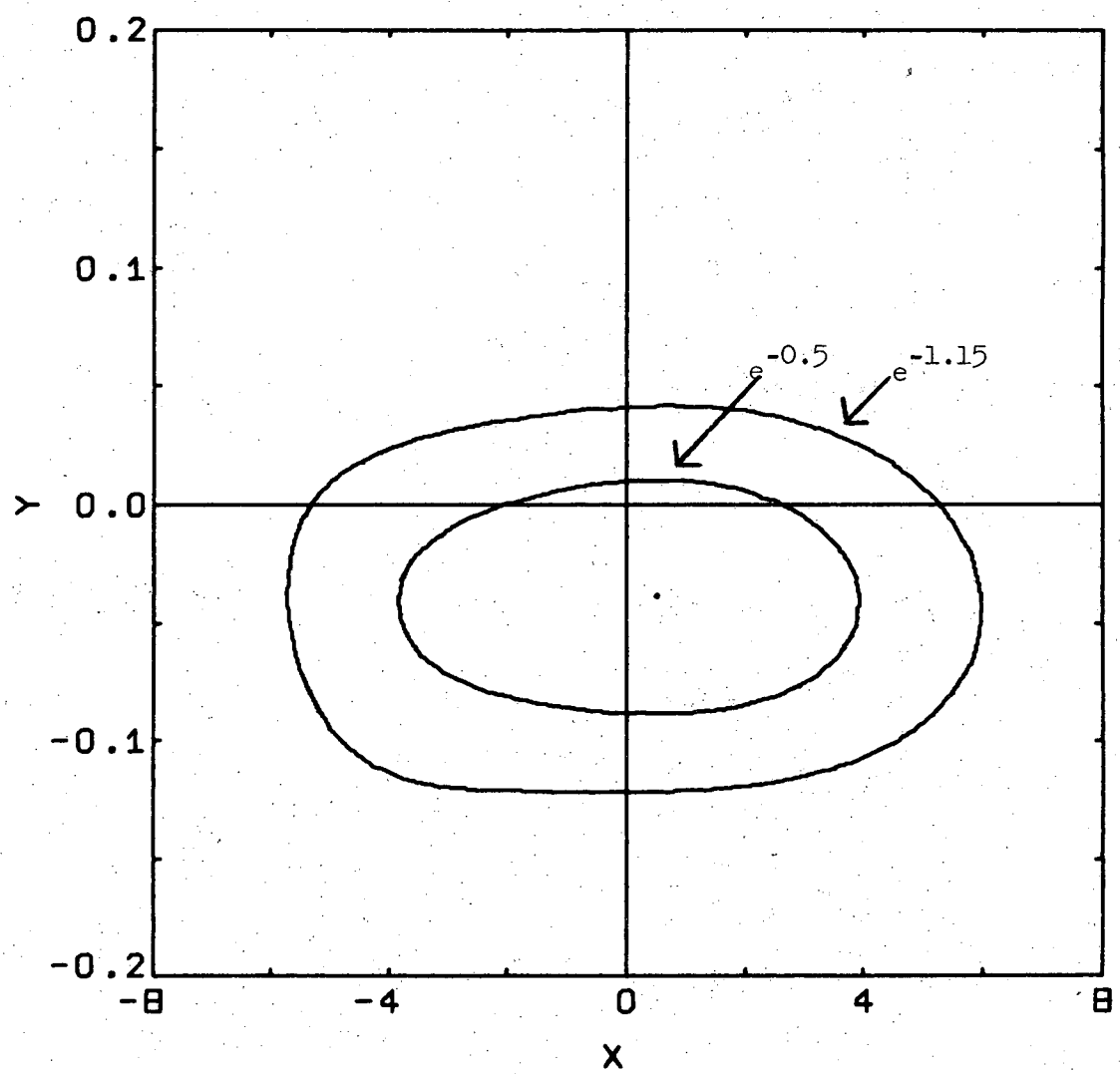

XBL 694-377

Fig. 18. Contours of constant likelihood for linear combinations of ξ and $\xi\lambda_-$:

$$x = \cos\theta\ \xi + \sin\theta\ \xi\lambda_-$$

$$y = -\sin\theta\ \xi + \cos\theta\ \xi\lambda_-$$

$$\theta = -8.1^{\circ} \qquad \lambda_+ = 0$$

Table IV. Results for two parameter fits.

$\gamma_1 \pm \Delta\gamma_1$	$\gamma_2 \pm \Delta\gamma_2$	θ	Parameters fitted	Parameter with assumed value	χ^2(7D.F.)
-0.5 ± 0.8	-0.006 ± 0.013	-1.65°	$\xi(0)$, λ_+	$\lambda_-\xi = 0$	12.0
$0.5\ ^{+3.4}_{-4.3}$	-0.04 ± 0.05	-8.1°	$\xi(0)$, $\lambda_-\xi(0)$	$\lambda_+ = 0$	12.1
$-0.9\ ^{+3.5}_{-2.9}$	-0.12 ± 0.06	-7.9°	$\xi(0)$, $\lambda_-\xi(0)$	$\lambda_+ = 0.023$	12.8

The meaning of the linear combinations defined above becomes somewhat more transparent if we rewrite them in a different form.[1] The q^2 dependence of f can be written as $\xi(q^2) = \xi(0)(1+\lambda_- q^2/m_\pi^2)$. Let us now evaluate ξ at two different points:

$$\xi(m_\pi^2 \tan\theta) = \gamma_1 \sec\theta$$
$$\xi(-m_\pi^2 \cot\theta) = -\gamma_2 \csc\theta$$

Substituting numbers from Table IV we find:

$$\xi(-0.14\ m_\pi^2) = 0.5\ ^{+3.4}_{-4.3} \qquad \xi(7.1\ m_\pi^2) = -0.3 \pm 0.4$$

So γ_1 and γ_2 are the values of $\xi(q^2)$ at two points on the q^2 axis.

All solutions presented above have a corresponding second solution. As explained in the introduction, this experiment measures the slope of the π^0 spectrum. There are two values of ξ which give the same slope. The particular solution we quote is the one selected by either branching ratio or polarization experiments.

So far all errors quoted are statistical. Now we will consider how background affects our final result. When we calculated the number of background events we also found how they were distributed as a function of π^0 energy. Suppose r is the fraction of events in the

lower half of the π^o spectrum. r is then a convenient measure of ξ. We also know r_i^B which is the fraction of events in the lower half of the π^o spectrum for some particular type of background. If we have several kinds of background each of which contibutes a fraction x_i to the $K_{\mu 3}$ spectrum, then the change in r due to background is:

$$\Delta r = r' - r = \frac{r + \sum r_i^B x_i}{1 + \sum x_i} - r$$

$$= \frac{\sum r_i^B x_i - r \Sigma x_i}{1 + \sum x_i} \qquad \text{IV-13}$$

The sum i is over all types of background. The error in ξ is $\Delta\xi = \Delta r d\xi/dr$. Putting in numbers from Monte Carlo calculations and Table II we get:

random γ	$x_1 = 0.014$	$r_1^B = 0.323$
$K \to \pi\pi\gamma$	$x_2 = 0.016$	$r_2^B = 0.034$
$K \to \pi^+\pi^o$	$x_3 = 0.035$	$r_3^B = 0.101$

$$\Delta\xi = \Delta r / \frac{dr}{d\xi} = -0.00346/0.028 = -0.12$$

So the systematic error in $\Delta\xi$ is somewhat smaller than the statistical error.

V. SUMMARY AND CONCLUSIONS

We have made a measurement of the parameters describing the strangeness changing hadron current. The method we employed is an analysis of the π^0 spectrum resulting from the decay $K^+ \rightarrow \pi^0\mu^+\nu$. To a first approximation this spectrum can be described by a straight line. The slope of the spectrum is a direct measure of the ratio $\xi = f_-(0)/f_+(0)$, where f_+ and f_- are the form factors of the strangeness changing hadron current. A best fit to our data gives $\xi = -0.3 \pm 0.3$.

In the case that form factors depend on the momentum transfer to the lepton pair we can expand f_+ and f_- as in equation I-6. We have made a two parameter analysis with $\xi(0)$ and λ_+ as variables and $\lambda_- = 0$. In Fig. 17 we plot the contours of constant likelihood for ξ and λ_+. The best fit occurs when $\xi(0) = -0.50$; $\lambda_+ = 0.009$. (Fig. 19) This result is in reasonable agreement with the polarization result $\xi(0) = -0.95 \pm 0.3$, a value which is relatively independent of λ_+.

There are two other types of experiments which limit the values of ξ and λ_+. From K_{e3} decay we get $\lambda_+ = 0.023 \pm 0.08$ [3] and $\Gamma(K_{\mu 3})/\Gamma(K_{e3}) = 0.6 \pm 0.02$.[6] To see how well these results agree with our analysis we have displayed them graphically in Fig. 20. In the middle graph we plot the contours for ξ and λ_+ with $\xi\lambda_- = 0$. It is evident from the figure that all four different types of experiments are in reasonable agreement. A value for $\xi(0)$ between -0.5 and -0.9 is well within the errors of all experiments. Note that we have used the value of Eichten et al. for $\Gamma(K_{\mu 3})/\Gamma(K_{e3})$. The reason for using this value is that it agrees with other types of experiments. Whether

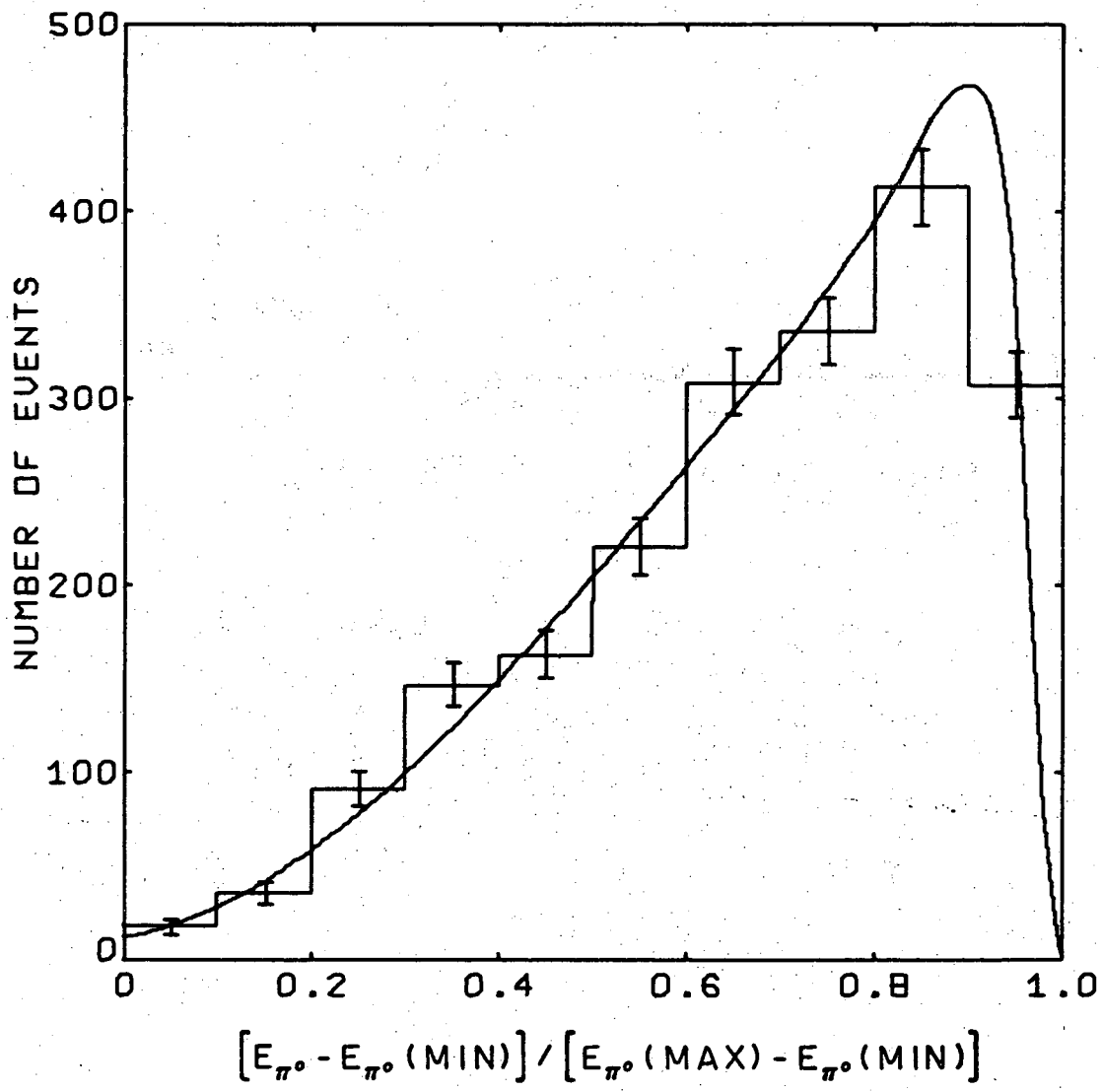

XBL 694-379

Fig. 19. The histogram gives the experimental π^0 energy spectrum. The smooth curve is the product of the theoretical spectrum for $\xi(0) = -0.5$, $\lambda_+ = 0.009$ and the efficiency for detecting $K^+ \rightarrow \pi^0\mu^+\nu$ in our apparatus.

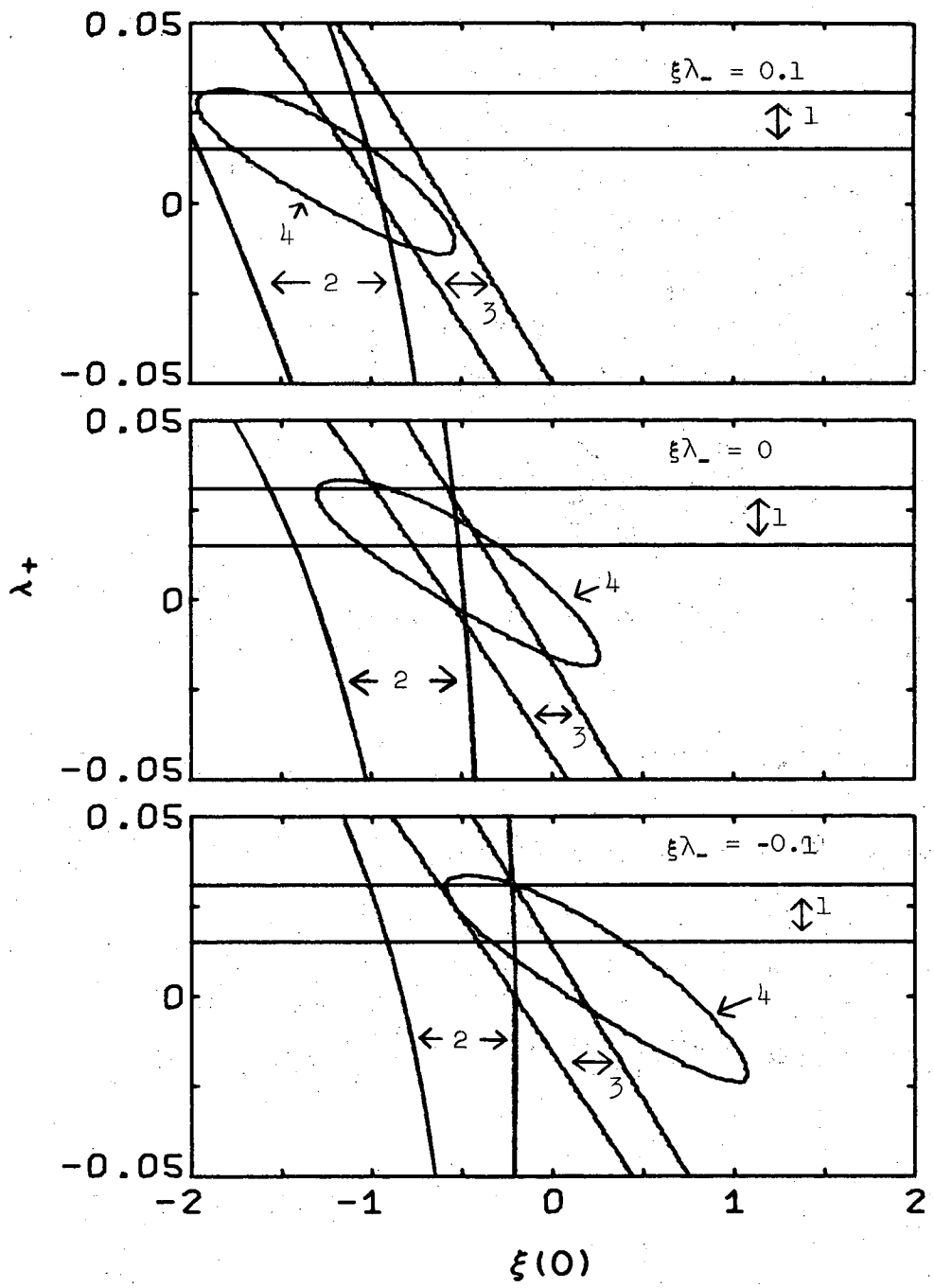

XBL 694-376

Fig. 20. One standard deviation boundaries for various experiments:

1. $\lambda_+ = 0.023 \pm 0.08$
2. D. Cutts polarization experiment
3. $\Gamma(K_{\mu 3})/\Gamma(K_{e3}) = 0.60 \pm 0.02$
4. This experiment

Top graph is for $\xi\lambda_- = 0.1$; the middle graph is for $\xi\lambda_- = 0$; the bottom graph is for $\xi\lambda_- = -0.1$.

to use instead the world average of $\Gamma(K_{\mu 3})/\Gamma(K_{e3}) = 0.68 \pm 0.02$ is open to speculation. If this latter value of 0.68 is correct then an agreement of all experiments becomes highly unlikely, and one would have to revise the present theoretical formulae for $K_{\mu 3}$ decay. As pointed out in the introduction this could be done by abandoning μ-e universality.

The statistical accuracy of our experiment does not warrant a three parameter fit for $\xi(0)$, λ_+ and λ_-. Also ξ and $\xi\lambda_-$ are strongly correlated. This simply means that we can fit our data to a wide range of $\xi\lambda_-$ values if we make a corresponding change in ξ. In Fig. 20 we have plotted contours of ξ and λ_+ for two nonzero values of $\xi\lambda_-$. The point to be made here is that unless all experiments are done to much greater precision even a combination of all experiments cannot put a good limit on $\xi\lambda_-$. Agreement among different experiments does not improve as $\xi\lambda_-$ changes by an amount $\xi\lambda_- = \pm 0.1$. On the other hand, agreement does not get sufficiently worse to limit the value of $\xi\lambda_-$. Values for $\xi\lambda_-$ much larger than 0.1 are not justified since then the linear expansions for f_- and f_+ no longer hold.

In conclusion we can say that at present there is no indication that the theory describing strangeness changing weak decays is incorrect. The ratio $\Gamma(K_{\mu 3})/\Gamma(K_{e3})$ cannot be used to point to an inconsistency before the disagreement among different measurements is straightened out. Certainly our spectrum analysis agrees well with polarization experiments.

APPENDICES

I. DECAY RATE $K^+ \to \pi^o \mu^+ \nu$

The differential decay rate $K^+ \to \pi^o \mu^+ \nu$ is given by:

$$\frac{d\Gamma}{dE_\pi dE_\mu} = \frac{G^2 m_\mu^2}{4\pi^3 m_k^2} \left\{ |f_+(q^2)|^2 \left[\left(\frac{2m_k E_\mu}{m_\mu^2} - 1 \right) E_1 - \left(\frac{m_k^2}{m_\mu^2} - \frac{1}{4} \right) E_2 \right] \right.$$

$$\left. + \operatorname{Re} f_-(q^2) f_+^*(q^2) (E_1 - \frac{1}{2} E_2) + |f_-(q^2)|^2 \frac{1}{4} E_2 \right\}$$

The variables are defined by:

$$E_1 = m_k - E_\pi - E_\mu$$

$$E_2 = \frac{m_k^2 + m_\pi^2 - m_\mu^2}{2m_k} - E_\pi$$

$$q^2 = m_\pi^2 + m_k(m_k - 2E_\pi)$$

$E_\pi = \pi^o$ TOTAL ENERGY

$E_\mu = \mu^+$ TOTAL ENERGY

G is the weak interaction coupling constant.

$f_+(q^2)$, $f_-(q^2)$ are the form factors of the hadronic current as discussed in the Introduction.

II. KINEMATICS FOR $K^+ \rightarrow \pi^o \mu^+ \nu$

In our experiment we have measured the muon energy and the unit vectors defining the directions of the $\mu^+(\hat{p}_\mu)$ and the γ-rays $(\hat{p}_i)$. Using these quantities we can calculate two possible solutions for the π^o energy:

Solution (1): $p_1 = \frac{X+T}{A}$ $p_2 = \frac{X-T}{B}$ $E_\pi = p_1+p_2$

Solution (2): $p_1 = \frac{X-T}{A}$ $p_2 = \frac{X+T}{B}$ $E_\pi = p_1+p_2$

X, T, A, B are given by:

$$X = m_k^2 + m_\pi^2 + m_\mu^2 - 2m_k E_\mu$$

$$A = 4(m_k - E_\mu + \vec{p}_\mu \cdot \hat{p}_1)$$

$$B = 4(m_k - E_\mu + \vec{p}_\mu \cdot \hat{p}_2)$$

$$T = \sqrt{X^2 - \frac{m_\pi^2 A B}{2(1-\hat{p}_1 \cdot \hat{p}_2)}}$$

If T is nearly zero, then measurement errors can result in $T^2 < 0$. As long as $|T^2|$ is small enough we find E_π by setting T=0. Events with $|T^2|$ much larger than can be explained by measurement errors cannot be interpreted as $K^+ \rightarrow \pi^o \mu^+ \nu$.

III. KINEMATICS FOR $K^+ \rightarrow \pi^+\pi^o$

The energies of the γ-rays resulting from π^o decay are:

$$p_1 = \frac{m_{\pi^o}^2}{2(E_{\pi^o}+p_{\pi^o}\hat{p}_{\pi^+}\cdot\hat{p}_1)}$$

$$p_2 = \frac{m_{\pi^o}^2}{2(E_{\pi^o}+p_{\pi^o}\hat{p}_{\pi^+}\cdot\hat{p}_2)}$$

The energy (E_{π^o}) and momentum (p_{π^o}) of the π^o is:

$$E_{\pi^o} = \frac{m_k^2+m_{\pi^o}^2-m_{\pi^+}^2}{2m_k} = 245.6 \text{ MeV}$$

$$p_{\pi^o} = \sqrt{E_{\pi^o}^2-m_{\pi^o}^2} = 205.2 \text{ MeV/c} .$$

If we make a Lorentz transformation to the center of mass of the π^o with $\beta = \frac{p_{\pi^o}}{E_{\pi^o}}$, $\gamma = \frac{E_{\pi^o}}{m_{\pi^o}}$; we can find the center of mass angle between the two γ-rays:

$$\cos(\theta_{c.m.}) = D = B_1B_2 + A\sqrt{(1-B_1^2)(1-B_2^2)}$$

where A, B_i are defined by:

$$A = \frac{\hat{p}_{\pi^+} \times \hat{p}_1}{|\hat{p}_{\pi^+} \times \hat{p}_1|} \cdot \frac{\hat{p}_{\pi^+} \times \hat{p}_2}{|\hat{p}_{\pi^+} \times \hat{p}_2|}$$

$$B_i = \frac{-C\,\hat{p}_{\pi^+}\cdot\hat{p}_i - \sqrt{C^2-1}}{\sqrt{1-(\hat{p}_{\pi^+}\cdot\hat{p}_i)^2 + (C\,\hat{p}_{\pi^+}\cdot\hat{p}_i + \sqrt{C^2-1})^2}}$$

$$C = \frac{m_k^2 + m_{\pi^o}^2 - m_{\pi^+}^2}{2m_{\pi^o}\,m_k}$$

For the decay mode $K^+ \rightarrow \pi^+\pi^o$ $\cos(\theta_{c.m.})$ should be -1.

REFERENCES

1. J. Bettels et al., Nuovo Cimento 56A, 1106(1968).

2. David Cutts (Ph.D. Thesis) UCRL-18143.

3. Proc. Heidelberg Int. Conf. on Elementary Particles (North-Holland Publ. Co., Amsterdam, 1967).

4. R. L. Imlay et al., Phys. Rev. 160, 1203 (1967).
R. T. Eschstruth et al., Phys. Rev. 165, 1487 (1968).

5. Rosenfeld et al., Review of Particle Properties, UCRL-8030 (Aug. 1968).

6. T. Eichten et al., Phys. Letters 27B, 586 (1968).
Botterill et al., Phys. Rev. Letters 21, 766 (1968).

7. Callahan et al., Phys. Rev. 150, 1153 (1966).

8. Eisler et al., Phys. Rev. 169, 1090 (1968).

9. C. G. Callan, S. B. Treiman, Phys. Rev. Letters 16, 153 (1966).

10. V. S. Mathur, L. K. Pandit, R. E. Marshak, Phys. Rev. Letters 16, 947 (1966)
T. Das, Phys. Rev. Letters 17, 671 (1966)
J. Iliopoulos, R. P. Van Royen, Physics Letters 25B, 146 (1967)
S. N. Biswas, J. Smith, Nuovo Cimento 51A, 214 (1967)
B. D'Espagnat, M. K. Gaillard, Physics Letters 25B, 346 (1967)
A. K. Mann, H. Primakoff, Phys. Rev. Letters 20, 32 (1968)
M. Fitelson, E. Kazes, Phys. Rev. Letters 20, 304 (1968)
B. W. Lee, Phys. Rev. Letters 20, 617 (1968)
D. P. Majumdar, Phys. Rev. Letters 20, 971 (1968)
Jong-Ping Hsu, University of Rochester UR-875-238, 1968

S. Matsuda, S. Oneda, Phys. Rev. 169, 1172 (1968)

Brian G. Kenny, Phys. Rev. Letters 20, 1217 (1968)

S. M. Berman, P. Roy, Physics Letters 27B, 88 (1968)

R. Arnowitt, M. H. Friedman, P. Nath, Northeastern University (June 1968)

S. P. De Alwis, Cambridge University, England, DAMTP 68-19, DAMTP 68-22, DAMTP 68-27, 1968

N. H. Fuchs, Phys. Rev. 170, 1310 (1968)

Lay Nam Chang, Y. C. Leung, Phys. Rev. Letters 21, 122 (1968)

H. T. Nieh, Phys. Rev. Letters 21, 116 (1968)

Riazuddin, A. Sarker, Phys. Rev. 173, 1752 (1968)

Kyungsig Kang, Phys. Rev. Letters 21, 857 (1968)

J. C. Pati, K. J. Sebastian, Phys. Rev. 174, 2033 (1968)

P. P. Srivastava, Nuclear Physics B7, 220 (1968)

H. D. Dahmen, K. D. Rothe, L. Schülke, Nuclear Physics B7, 472 (1968)

R. W. Griffith, B. Renner, Physics Letters 27B, 650 (1968)

S. M. Berman, P. Roy, Physics Letters 28B, 326 (1968).

11. H. Rudloe, M. Deutsch, T. Marill, Commun. Assoc. Computing Machinery 6, 332 (1963).

12. A. Meshkovskii, Y. Shalamov, JETP 10, 697 (1960)

J. Kessler, L. Lederman, Phys. Rev. 94, 689 (1954).

13. Jay Orear, Notes on Statistics for Physicists, UCRL-8417 (1958).

I. INTRODUCTION

The decay $K^+ \rightarrow \pi^+\pi^o\gamma$ is the radiative counter part of the easily observable decay $K^+ \rightarrow \pi^+\pi^o$. The existence of the radiative decay can be predicted on the basis of some very elementary considerations. We know for example that an accelerated electron can emit a photon. Similarly, any charged particle can emit a photon as it is accelerated outward from its point of production in a decay. We can put this idea in terms of the following Feynman diagram:

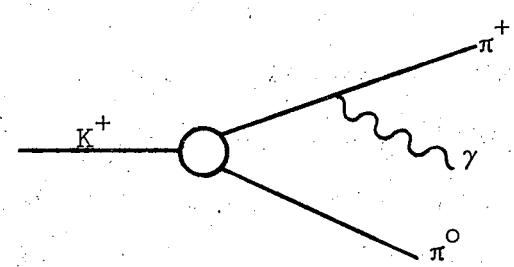

The K^+ decays into a real π^o and a virtual π^+, the virtual π^+ then radiates with the emission of a real pion and a photon. Assuming now that the coupling constant at the $K\pi\pi$ vertex is the same as the one derived from the decay $K^+ \rightarrow \pi^+\pi^o$, we can calculate an absolute decay rate for the radiative mode.

The above process is commonly referred to as inner bremsstrahlung. However, there is another way we can obtain a radiative decay. The photon can be emitted directly by the $K\pi\pi$ vertex. This type of radiation is usually called direct radiation. In terms of a Feynman diagram we have:

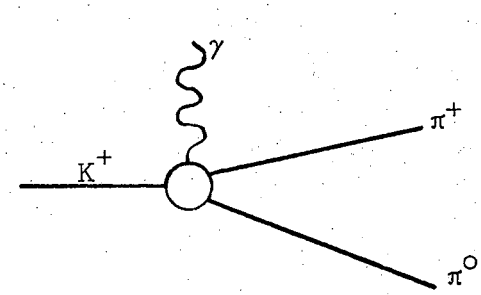

By this diagram we simply mean that any number of intermediate particles can emit a photon. Of course we do not know how to calculate the contribution from such diagrams. We consider only the lowest order of direct radiation which in our case are electric and magnetic dipole transitions. If they are the dominant contributions to the matrix element for the decay $K^+ \rightarrow \pi^+\pi^o\gamma$, we can write:[1]

$$\frac{d\Gamma}{dT_{\pi^+}d\cos\theta} = |X_B g + X_E \, \ell^{i(\delta_1-\delta_0)} h|^2 + |X_M|^2 \, h^2 \qquad \text{I-1}$$

X_B, X_E, X_M are constants describing the contributions of inner bremsstrahlung, electric dipole radiation, and magnetic dipole radiation respectively. g and h are functions of T_{π^+} and $\cos\theta$. $\cos\theta = \hat{\pi}^+\cdot\hat{\gamma}$. δ_1, δ_0 are ℓ=0,1 $\pi\pi$ phase shifts. A complete formula giving the functions g and h is written out in Appendix I.

It is the purpose of this experiment to look for direct radiation. To see how we propose to look for direct radiation consider how the parameters affect the decay distribution in the variable $\hat{\pi}^+\cdot\hat{\gamma}$. Figure 1 shows the contributions to the spectrum of direct radiation, inner bremsstrahlung, and the interference between electric dipole radiation and inner bremsstrahlung. Without direct radiation few events would appear in the region $\hat{\pi}^+\cdot\hat{\gamma} < -0.5$. On the other hand, many events in this region could be evidence for direct radiation.

We have found 27 events of the type $K^+ \rightarrow \pi^+\pi^o\gamma$. There is no evidence for direct radiation. We have fitted the spectrum in the variable $\hat{\pi}^+\cdot\hat{\gamma}$ to the decay rate as given in I-1. The fit was made with two sets of parameters:

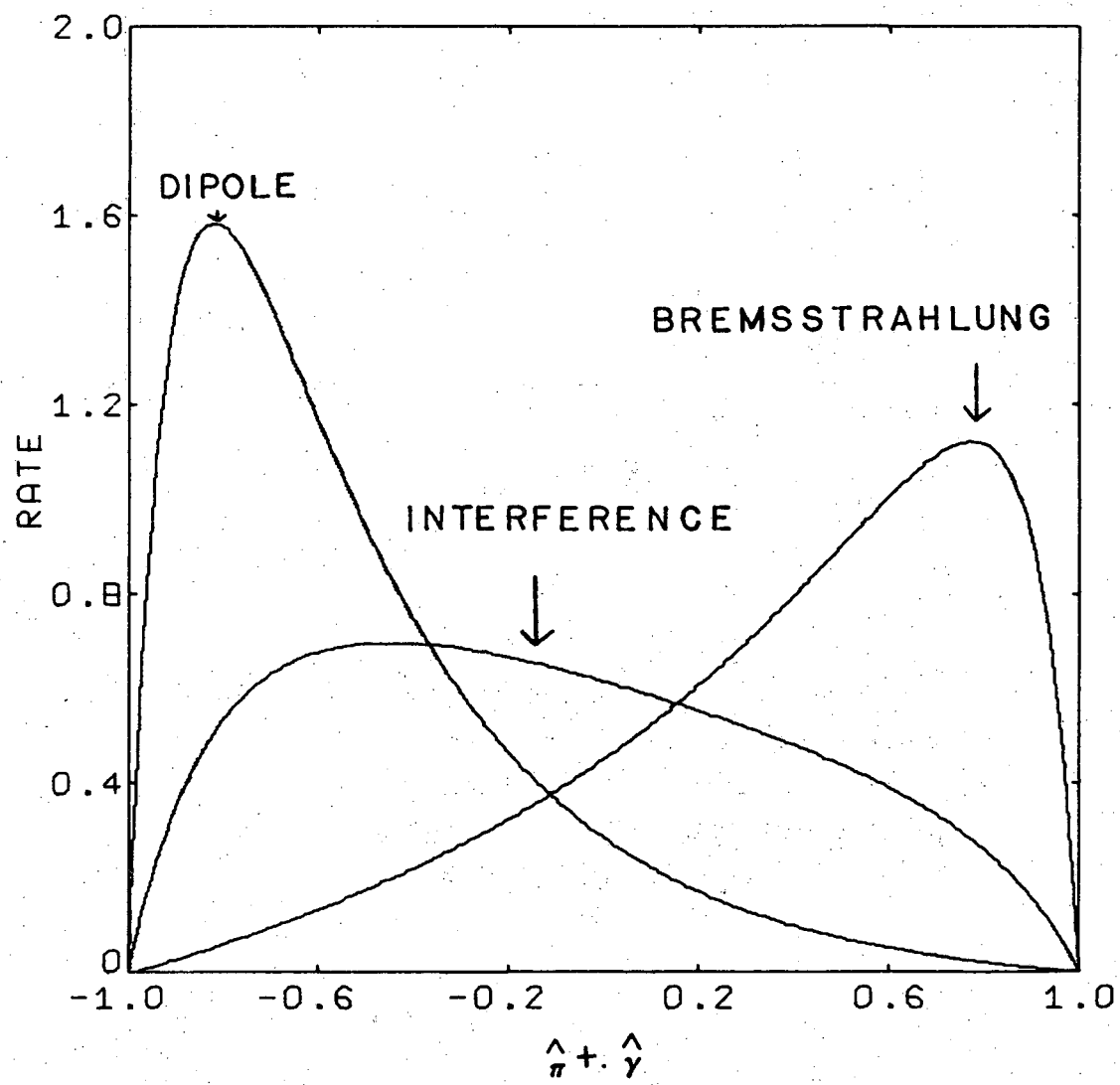

XBL 6812-6378

Fig. 1. Relative decay rate for $K^+ \to \pi^+\pi^0\gamma$. Curves are from inner bremsstrahlung, electric and magnetic dipole radiation, and interference between electric dipole radiation and inner bremsstrahlung.

case 1	X_E variable	$\mathrm{Im}\, X_E = 0 \quad X_M = 0$	$\delta_1 - \delta_0 = 0$
case 2	X_M variable	$X_E = 0$	$\delta_1 - \delta_0 = 0$

The answers are given in terms of maximum likelihood plots (Figs. 8,9). We can use the best values for X_E or X_M to calculate the contribution of direct radiation to the total delay rate. We find (rates are 95% conf.):

case 1	$X_E = 0.8^{1.2}_{-0.9}$	$-4.2\cdot 10^{-5} \leq R_D(E1) \leq 3.2\cdot 10^{-4}$
case 2	$X_M = 2.1 \pm 1.5$	$R_D(M1) \leq 1.7\cdot 10^{-4}$

We define R_D by expanding equation I-1:

$$\frac{\iint \frac{d\Gamma}{dT_{\pi^+} d\cos\theta}(K^+ \to \pi^+\pi^0\gamma)}{\Gamma(K^+ \to \mathrm{ALL})} \qquad \text{I-2}$$

$$= |X_B|^2 \frac{1}{\Gamma}\iint g^2 + 2\mathrm{Re}\, X_B X_E^* \, \ell^{-i(\delta_1-\delta_0)} \frac{1}{\Gamma}\iint g\, h + |X_E|^2 \frac{1}{\Gamma}\iint h^2$$

$$+ |X_M|^2 \frac{1}{\Gamma}\iint h^2$$

$$R_B = |X_B|^2 \frac{1}{\Gamma}\iint g^2$$

$$R_D(E1) = 2\mathrm{Re}\, X_B X_E^* \, \ell^{-i(\delta_1-\delta_0)} \frac{1}{\Gamma}\iint g\, h + |X_E|^2 \frac{1}{\Gamma}\iint h^2$$

$$R_D(M1) = |X_M|^2 \frac{1}{\Gamma}\iint h^2$$

$$R_D = R_D(E1) + R_D(M1)$$

The integral extends over all phase space. If only bremsstrahlung contributes to the decay we have $R_B > 0$, $R_D = 0$. If direct radiation is present then $R_D(E_1)$ will be greater than zero in the case of

constructive interference and less than zero in the case of destructive interference. $R_D(M1)$ is always greater than zero.

II. THEORY

Several models have been constructed to estimate the contribution of direct radiation to the decay rate $K^+ \to \pi^+\pi^o\gamma$. For example, Pepper and Ueda[2] have studied a model which can be described by the following diagram:

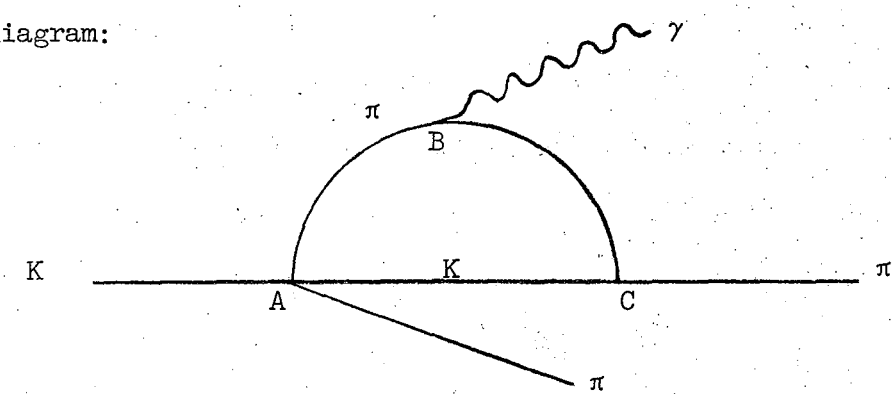

The vertices are determined by the following types of interactions:

A strong interaction

B electromagnetic interaction contributing a factor $\alpha = 1/137$

C strangeness changing, $|\Delta T| = 1/2$ weak interaction

Note that in contrast to the non-radiative decay $K^+ \to \pi^+\pi^o$, this decay is not suppressed by the $|\Delta T| = 1/2$ selection rule. Considering the uncertainty in coupling constants, Pepper and Ueda find:

$$-10^{-4} < R_D' < 10^{-4}$$

R_D' is defined as in equation I-2 of the previous section except that for R_D' the integration is restricted to the interval 55 MeV $\leq T_{\pi^+} \leq$ 80 MeV. Recall that R_D is calculated such that the total branching ratio $K^+ \to \pi^+\pi^o\gamma$ is $R_B + R_D > 0$ with R_B the branching ratio in the absence of direct radiation.

Pepper and Ueda have also considered a boson pole model with diagrams of the type:

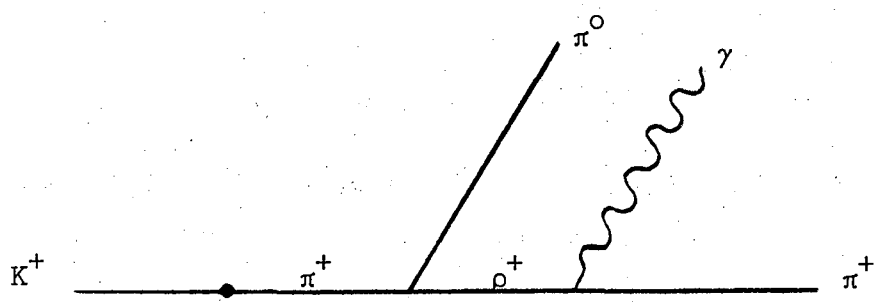

The weak coupling at the $K\pi$ vertex is estimated using a model for the K_1, K_2 mass difference. This way they find a relation of the form:

$$\Delta m = f^2_{K\pi} \cdot \text{constant}$$

the above diagram contributes to the M1 decay rate:

$$R'_D\ (M1) = 2.4 \cdot 10^{-4}$$

A diagram similar to the above, but replacing the π^+ with a ρ^+:

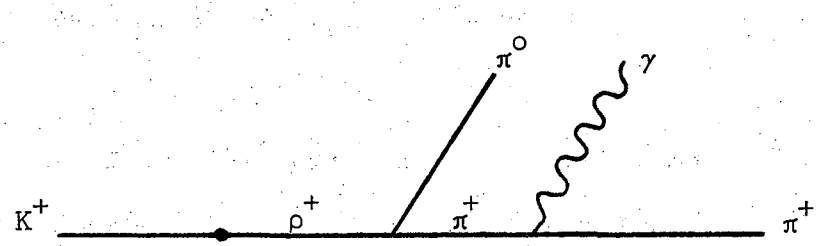

The contribution to the decay rate is:

$R'_D = 2.9 \cdot 10^{-5}$ constructive interference

$R'_D = -2.3 \cdot 10^{-5}$ destructive interference

Oneda, Kim, and Korff[3] also use a boson pole model. They neglect the last mentioned diagram but include K^+ intermediate states as well as ω-φ mixing. The M1 decay rate they get is:

$$R'_D(M1) = 1.2 \cdot 10^{-6}$$

Several authors[4] have studied how information about CP invariance can be extracted from the decay rates $K^\pm \to \pi^\pm \pi^o \gamma$. If CP invariance is to be valid then we must have $\text{Im}\ X_E = 0$. An experimental number

proportional to Im X_E can be found by considering the rate given in I-1 plus a similar one for $K^- \to \pi^-\pi^0\gamma$:

$$\frac{d\Gamma(K^- \to \pi^-\pi^0\gamma)}{dT_{\pi^+}d\cos\theta} = |X_B\, g + X_E^{\,*}\, \ell^{i(\delta_1-\delta_0)} h|^2 + |X_M|^2\, h^2 \qquad \text{I-3}$$

Subtracting I-3 from I-1:

$$\frac{d}{dT_{\pi^+}d\cos\theta}\ \Gamma(K^+ \to \pi^+\pi^0\gamma) - \Gamma(K^- \to \pi^-\pi^0\gamma) \qquad \text{I-4}$$

$$= -4\, g\, h\, \mathrm{Im}\, X_E \sin(\delta_1-\delta_0)$$

The smaller $\sin(\delta_1-\delta_0)$ the more difficult it becomes to measure Im X_E. If the difference between $\Gamma(K^+ \to \pi^+\pi^0\gamma) - \Gamma(K^- \to \pi^-\pi^0\gamma)$ is significant a lower limit on Im X_E can be found by simply setting $\sin(\delta_1-\delta_0) = 1$.

III. SCANNING AND SELECTION OF EVENTS

The events for this analysis were obtained by searching through our $K_{\mu 3}$ film for decays with three converted γ-rays. We examined all those events which the SPASS sutomatic scanning system considered 3-shower candidates. Before rescanning these events we applied cuts similar to those applied to our $K_{\mu 3}$ events:

a) $\delta_D < 1$ cm, $\delta_A > 0.998$ (see Section IV A of previous experiment)

b) To eliminate $K_{\pi 2}$ events all three possible pairs of γ-rays were fitted to $K_{\pi 2}$ kinematics. The $K_{\pi 2}$ constraint is $\delta_{cm} = -1$ as explained in Appendix III of the previous experiment. We required that for each pair of γ-rays $\delta_{cm} > -0.97$.

c) There is no charged particle except π^+ associated with K^+ decay.

d) The reconstructed K-stop position must be within the stopping material.

e) The showers have to convert in the third gap or later in the lead spark chambers.

The remaining 1115 events were rescanned manually by the author. At this point we rejected all those tracks in the lead chambers which obviously were not showers. The majority of the events fell into one of three categories. First, one of the showers was identified as being part of another large shower. Second, one of the showers was a straight track making a large angle with respect to the direction from the stopper. Third, several large sparks from a breakdown in the chamber looked to the computer like a shower. After rejecting all these types of events we were left with 100 events.

To reduce the amount of background in our sample we applied further cuts:

a) During the rescan all shower coordinates were remeasured. We again calculated δ_{cm} and dropped all events with $\delta_{cm} < -0.97$. There were 8 such events all with $\delta_{cm} < -0.99$.

b) We required that the π^+ coming out of the stopper connect with the π^+ in the range chamber. (See Fig. 4 of the previous experiment) The two tracks have to come within 5 cm of each other inside the degrader.

c) During our manual rescan we measured the angle between the γ-ray and the shower appearing in the lead chambers:

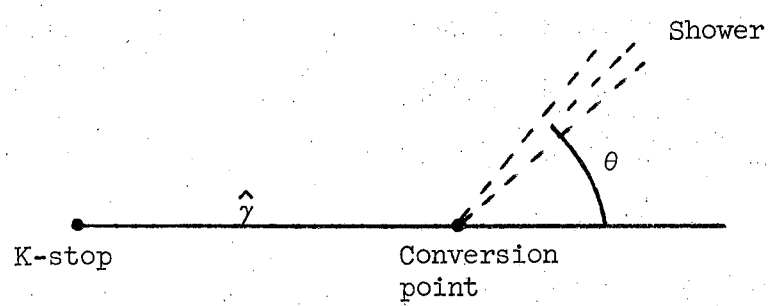

The angle of the shower is measured by estimating the average direction of the first three or four sparks of the shower. No events with $\theta \geq 30^\circ$ were accepted. This eliminated most showers not originating in the K-stopper.

d) All events with two charged particles entering the range chamber are not accepted. The reason is that the two particles could have come from two different kaons each of which produced two γ-rays.

e) An acceptable shower has to have at least four sparks.

f) No shower can convert in the first two gaps facing the

stopping material.

Of the original 100 events 57 survived the above cuts. The effect of the above cuts is illustrated by the fact that of the 100 events 36 satisfy the kinematic constraints explained below while 64 do not. Of the reduced sample of 57 events 30 fit the kinematic constraints while 27 do not.

A typical spark chamber photograph is shown in Fig. 2. A shower appears in each one of the three conversion chambers. The sparks near the center of the photograph labelled π^+ are from the tracking chamber. The left most track labelled π^+ is the π^+ stopping in the range chamber.

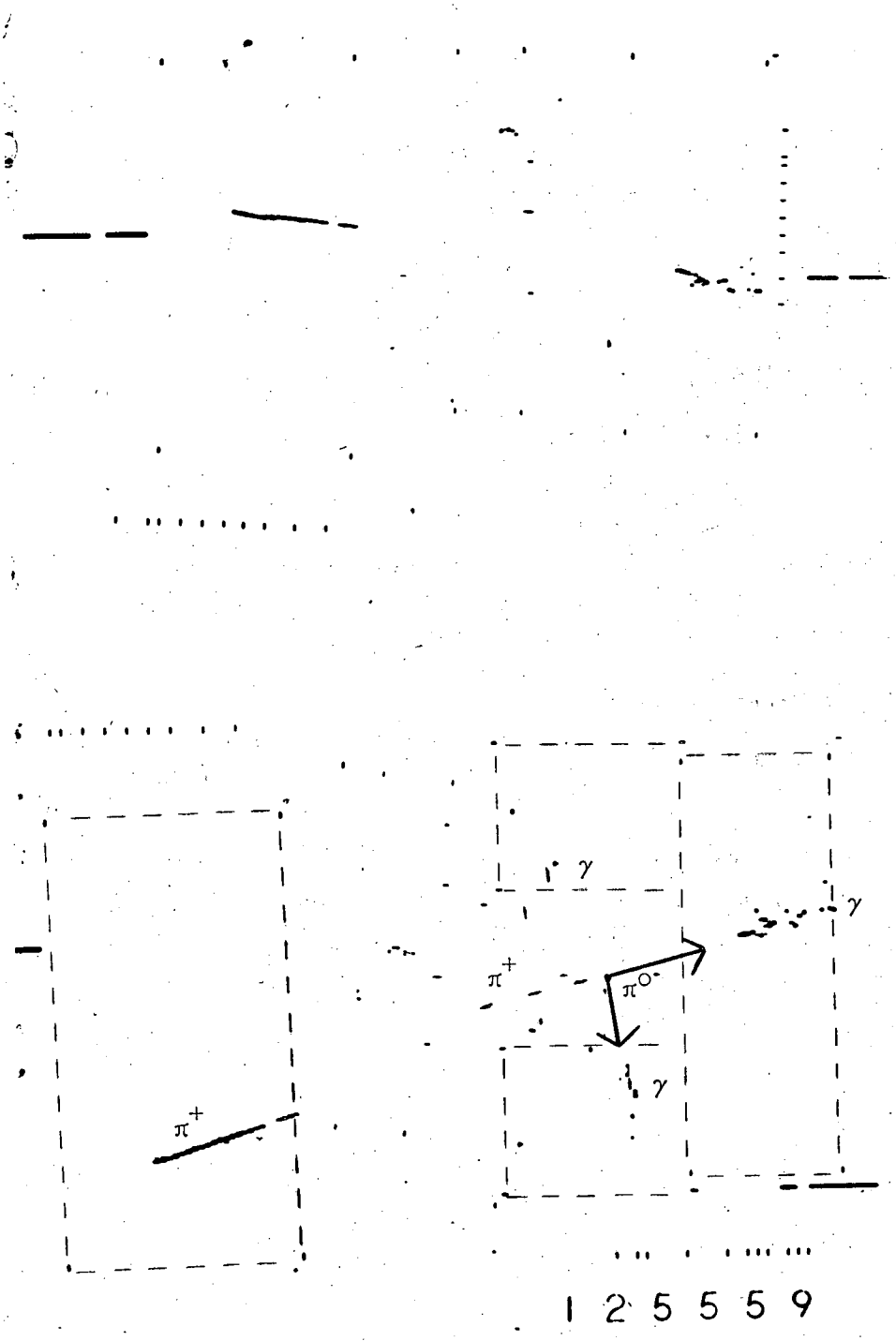

Fig. 2. Spark chamber picture of a 3 shower event from the decay $K^+ \rightarrow \pi^+\pi^0\gamma$. Dashed lines are outlines of direct view of spark chambers. Refer to Fig. 4 of Part I for comparison.

Table I. Selection of events $K^+ \rightarrow \pi^+\pi^o\gamma$.

Total number of pictures taken	99500
Candidates for 3 shower events selected by computer scan. Cuts on δ_D, δ_A, δ_{cm} are applied.	1115
Number of 3 shower events found during manual rescan of 1115 events.	100
Events passed on to be reconstructed kinematically. Cuts on quantities measured during manual scan are made.	57
Number of events which fit kinematics for $K^+ \rightarrow \pi^+\pi^o\gamma$ ($\chi^2 < 4$).	30
Events for which shower energy predicted matches actual shower energy ($\chi^2 < 6$).	27
Final sample	27

IV. ANALYSIS

A. Kinematical Reconstruction

There are two constraints which help us select the event type $K^+ \rightarrow \pi^+\pi^o\gamma$ from our sample of 3 shower events. To see how this comes about let $\vec{P}_{\pi^+}$, $\vec{P}_1$, $\vec{P}_2$, $\vec{P}_3$ be the momenta of the π^+ and γ-rays respectively. We measure $\vec{P}_{\pi^+}$ and the directions of the γ-rays. This leaves us with three undetermined quantities, namely the energies of the three γ-rays. However, we have five equations; 4 equations from energy and momentum conservation, and a fifth equation from the fact that two of the γ-rays come from a π^o. Hence we have five equations with three unknowns.

A simple way to express these constraints is shown in Appendix II. Here energy and momentum conservation is used to calculate P_{π^+}, P_1, P_2, P_3. The measured value of P_{π^+} is not used as an input. Also all three γ-rays enter the calculation of $P_{\pi^o}{}^2$, where P_{π^o} is the pion four momentum. This means that even if 2 γ-rays come from a π^o, with the third γ a background shower, $P_{\pi^o}{}^2$ is not necessarily equal $m_{\pi^o}{}^2$. The two constraints are then:

$$\Delta T_{\pi^+} = T_{\pi^+}(\hat{P}_1,\hat{P}_2,\hat{P}_3) - T_{\pi^+}(\text{MEASURED}) = 0 \qquad \text{IV-1}$$

$$\Delta m_{\pi^o} = m_{\pi^o} - \sqrt{2\, P_i P_j (1-\hat{P}_i \cdot \hat{P}_j)} = 0 \qquad \text{IV-2}$$

$$i,j = 1,2 \quad \text{or} \quad 2,3 \quad \text{or} \quad 1,3$$

We do not know which of the three possible pairs of γ-rays comes from π^o decay. So constraint IV-2 has to be calculated for three cases. If there were no measurement errors, only one combination of γ-rays would satisfy IV-2 exactly. This would tell us which γ-rays come from the π^o. Figure 3 is a plot illustrating the second constraint. We plot

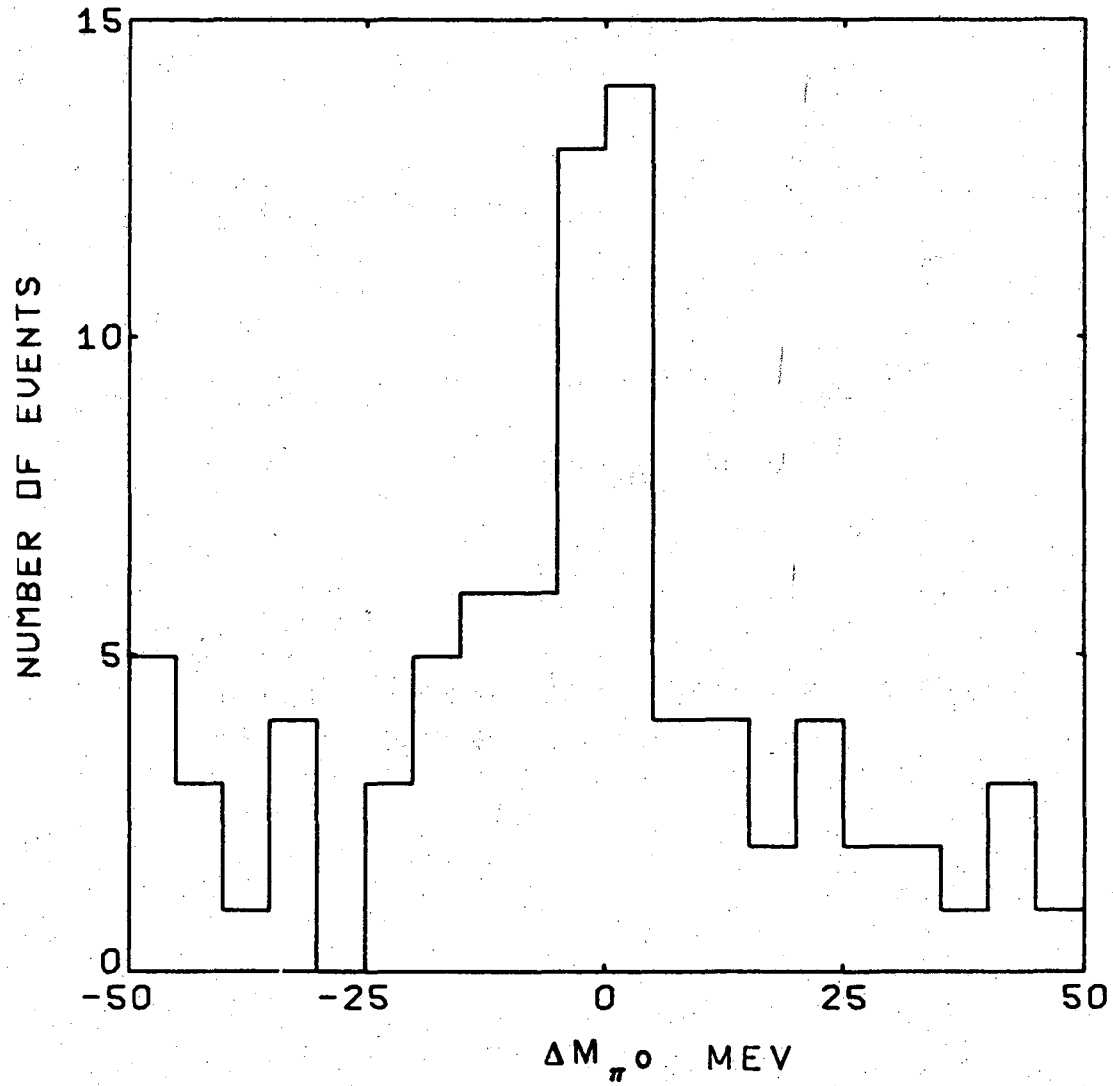

XBL 6812-6379

Fig. 3. Histogram of the constraint given in Eq. IV-2 of the text. For good events $\Delta m_{\pi^o} = 0$.

the number of events versus Δm_{π^o} with $|\Delta T_{\pi^+}| < 8$ MeV. All three cases of constraint IV-2 are plotted. Each event of the type $K^+ \rightarrow \pi^+\pi^o\gamma$ should have one point near zero corresponding to the correct pair of γ-rays assigned to the π^o. Other points come from background events, or the incorrect assignment of γ-rays to the π^o.

One problem of analyzing our events with the above method is that small measurement errors can cause large violations of the constraints. So we have chosen a χ^2 method to make a fit of our events to $K^+ \rightarrow \pi^+\pi^o\gamma$ kinematics. Since χ^2 depends only on measurement errors, this method allows us to select good events without bias against certain geometrical configurations.

Our χ^2 calculation is set up by constructing an event which resembles our actual event, but satisfies the constraints of $K \rightarrow \pi\pi\gamma$ kinematics exactly. The constructed event is described by vectors $\vec{P}_1'$, $\vec{P}_2'$, $\vec{P}_3'$, $\vec{P}_{\pi^+}'$ which satisfy the equations:

$$T_{\pi^+}(\hat{P}_1', \hat{P}_2', \hat{P}_3') - T_{\pi^+}' = 0$$

$$m_{\pi^o} - \sqrt{P_i' P_j'(1-\hat{P}_i' \cdot \hat{P}_j')} = 0 \qquad i,j = 1,2 \text{ or } 2,3 \text{ or } 1,3 \qquad \text{IV-3}$$

The χ^2 is then

$$\chi^2 = \sum_{i=1}^{3} \frac{|\hat{P}_i \times \hat{P}_i'|^2}{\Delta\theta_i^2} + \frac{|\hat{P}_{\pi^+} \times \hat{P}_{\pi^+}'|^2}{\Delta\theta_{\pi^+}^2} + \frac{(T_{\pi^+} - T_{\pi^+}')^2}{\Delta T_{\pi^+}^2} \qquad \text{IV-4}$$

$\Delta\theta$ is the angular measurement error in $\hat{P}_i$ or $\hat{P}_{\pi^+}$. In our case $\Delta\theta$=0.02 radians. The measurement error of the π^+ energy is 4 MeV. The P's and T' are adjusted subject to Eq. IV-3 until χ^2 attains a minimum value. For each event there are three possible values for χ^2 depending on the assignment of γ-rays to the π^o. In Fig. 4 we plot the smallest of

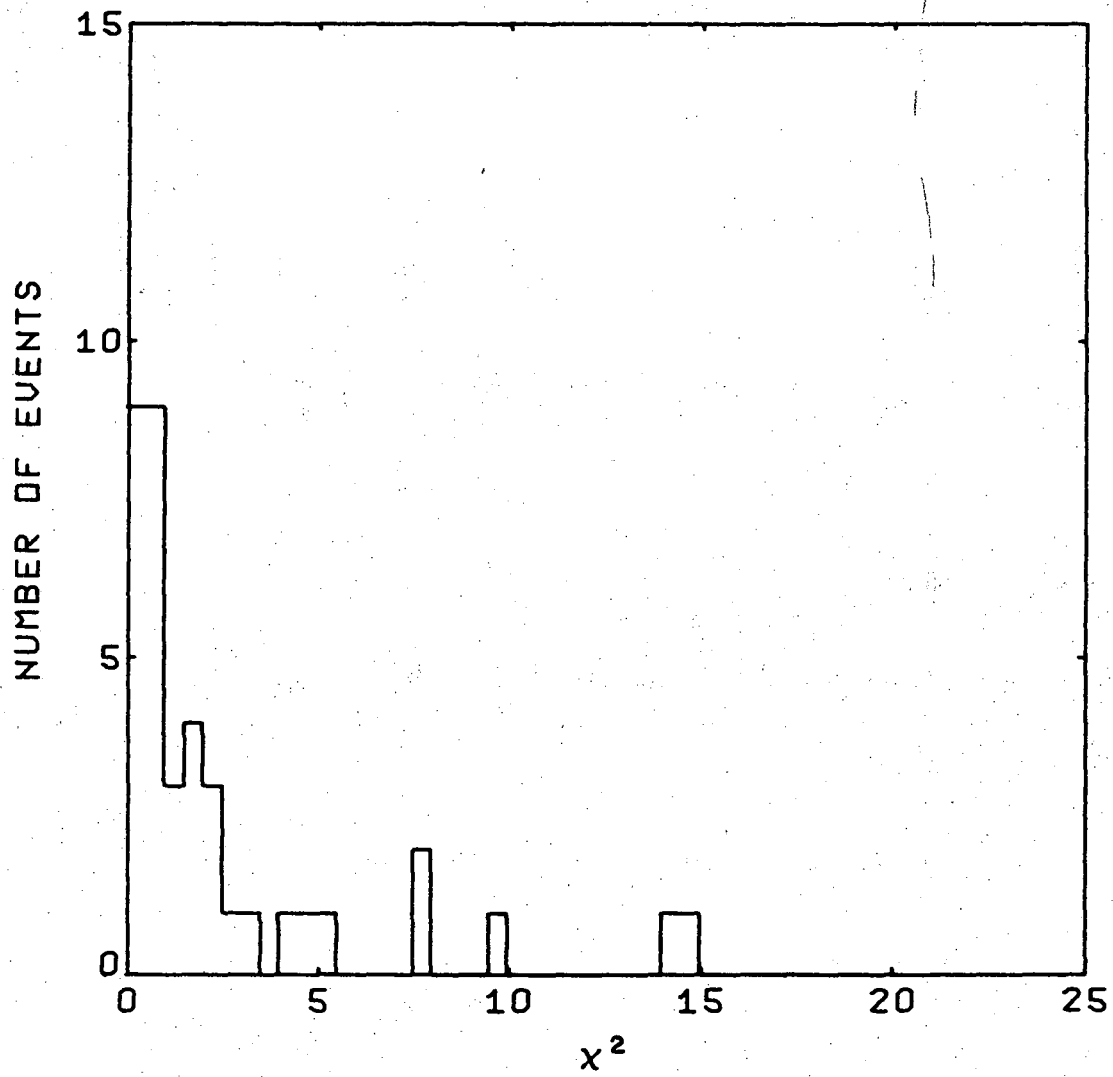

XBL 6812-6370

Fig. 4. χ^2 fit for $K^+ \rightarrow \pi^+\pi^0\gamma$ kinematics. 38 events are plotted. There are 19 events with $\chi^2 > 25$.

the three χ^2 values. We throw away all events with $\chi^2 > 4$. Since the χ^2 is calculated for two degrees of freedom, this cut should reduce the number of good events by about 14%. On the other hand, most of the background events should not pass this cut. Thirty of our 57 events satisfy $\chi^2 < 4$.

To find information about the decay $K^+ \rightarrow \pi^+\pi^0\gamma$ we are interested in the variable $\hat{\pi}^+ \cdot \hat{\gamma}$. $\hat{\gamma}$ is the one of the three vectors $\hat{P}_i$ which is not assigned to the decay $\pi^0 \rightarrow 2\gamma$. So it is essential that the solution picked by the smallest χ^2 is indeed the correct one. For some of our events the smallest χ^2 is not very different from the next larger one. To find how often we find the incorrect value for $\hat{\pi}^+ \cdot \hat{\gamma}$ we have generated events by a Monte Carlo technique and washed them out with our measurement errors. We then subjected them to the same analysis as our real events. Out of 107 Monte Carlo generated events 16 solutions were incorrectly assigned. So our final sample of 27 events contains about $16/107 \cdot 27 = 4$ events with $\hat{\pi}^+ \cdot \hat{\gamma}$ incorrect.

We have another constraint we can apply to our events. From the spark count of our showers we have an approximate idea of the energies of the γ-rays. We apply the same technique as explained in Section IVB of the previous experiment. Since we have three γ-rays, we can calculate a χ^2 fit to the energiés with three degrees of freedom. We cut χ^2 at 6 and this way reduce our 30 events to 27. This is our final sample used for further analysis. Figure 5 shows how these 27 events are distributed in the variable $\hat{\pi}^+ \cdot \hat{\gamma}$.

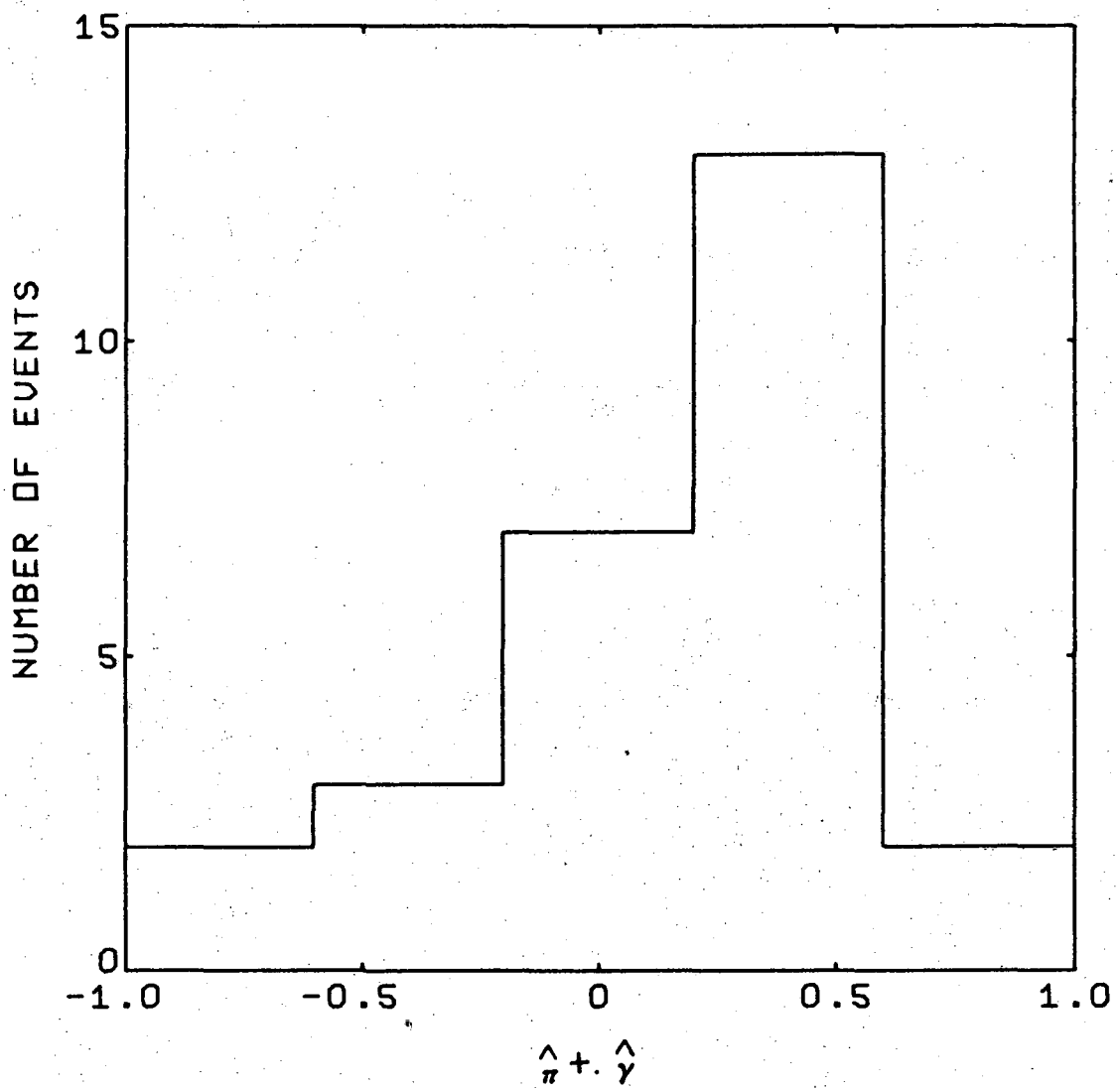

XBL 6812-6368

Fig. 5. Distribution in the variable $\hat{\pi}^+ \cdot \hat{\gamma}$ for our final sample of 27 events.

B. Background

A potential source of background events are K^+ decays of the type $K^+ \rightarrow \pi^o\pi^o\pi^+(\tau')$. Our π^+ energy range is adjusted to exclude these events unless the π^+ decays in flight. If this happens and three of the four γ-rays from π^o decay convert in our lead chambers, the event looks like $K^+ \rightarrow \pi^+\pi^o\gamma$. To find out whether there is any evidence for τ' events in our data we have generated τ' decays by a Monte Carlo method. We require that three γ-rays convert in the lead chambers according to our detection efficiency. We then fit them to the kinematic constraints of $K^+ \rightarrow \pi^+\pi^o\gamma$ with $\chi^2 < 4$, and plot them as a function of $\hat{\pi}^+ \cdot \gamma$. Figure 6 gives the result. If we now compare Fig. 6 with our data in Fig. 5, we can show that our data contains at most one or two τ' events. Half of the τ' events should fall in the interval $-1 \leq \hat{\pi}^+ \cdot \hat{\gamma} \leq -0.9$. Since our data contains only one event in this interval, there is no indication of τ' decays in our sample.

A second source of background comes from either $K^+ \rightarrow \pi^+\pi^o$ + background shower or $K^+ \rightarrow \mu^+\pi^o\nu$ + background shower. Some of the background γ-rays were eliminated by applying the cuts described in Section III. Any background event which involves $K^+ \rightarrow \pi^+\pi^o$ is rejected by the cut $\delta_{cm} < -0.97$. This leaves us with background events contributed by the decay $K^+ \rightarrow \mu^+\pi^o\nu$. To estimate the amount of background in our sample from this source we took good events from the previous experiment and attached to them a γ-ray randomly distributed in our fiducial volume. We analyzed them as if they were $K^+ \rightarrow \pi^+\pi^o\gamma$ and found the ratio of the number with $\chi^2 < 4$ to those with $\chi^2 > 4$. This ratio was found to be $r=6/179$. We now assume that all 30 events rejected

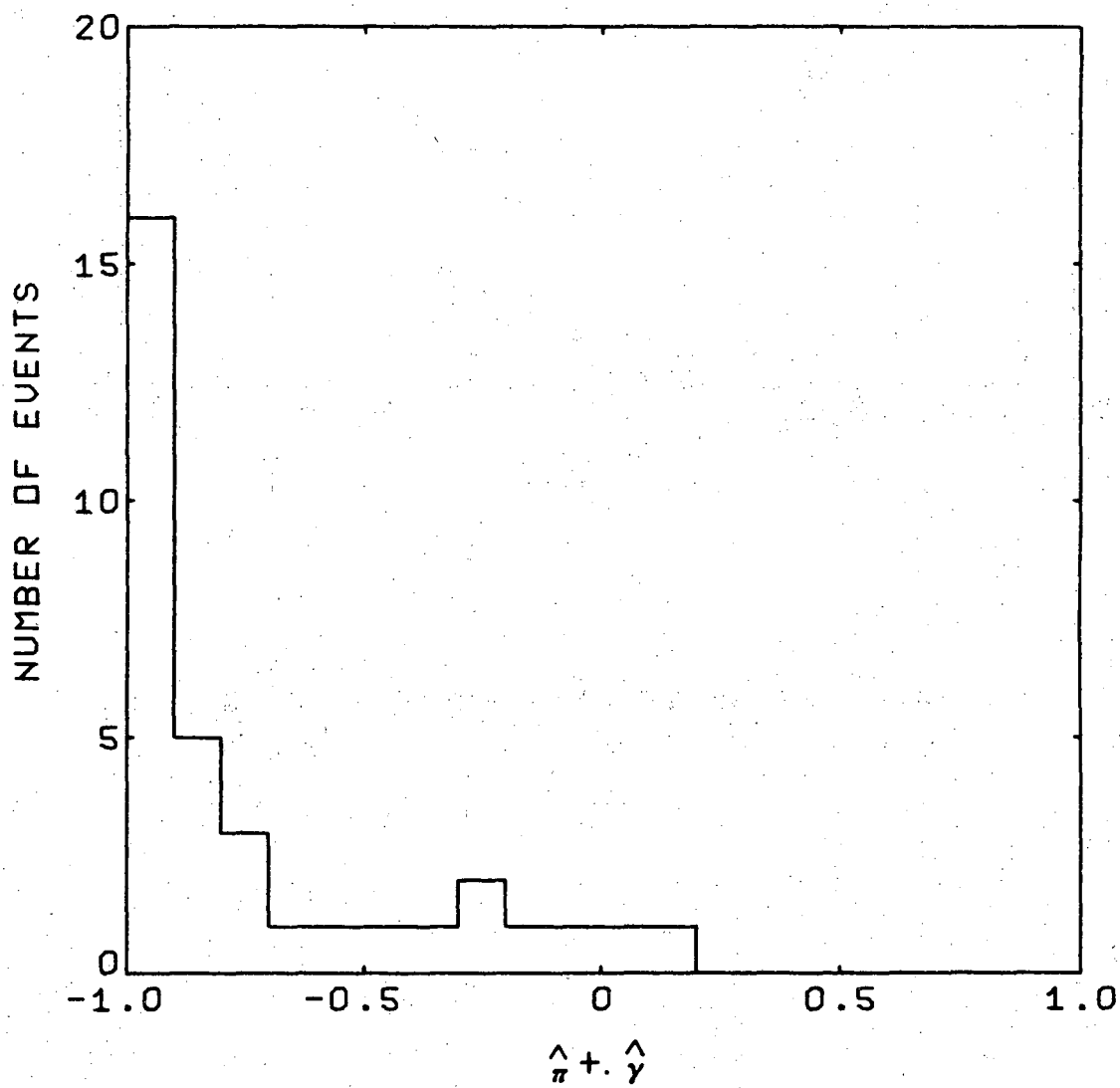

XBL 6812-6371

Fig. 6. Events of the type $K^+ \to \pi^+\pi^o\pi^o$ are reconstructed as $K^+ \to \pi^+\pi^o\gamma$. χ^2 fit is cut at 4.

solely on the basis of kinematic constraints are of the above type. The amount of background should then be $30 \cdot 6/179 = 1$ event.

C. Calculation of Parameters

We have made a Monte Carlo calculation to find the efficiency for detecting $K^+ \rightarrow \pi^+\pi^0\gamma$ events. Events are generated with the variable $\hat{\pi}^+ \cdot \hat{\gamma}$ randomly distributed. T_{π^+} is fixed at several energies between 70 MeV and 90 MeV. All three γ-rays are required to convert within the fiducial volume of our lead spark chambers. They are assigned a weight according to their conversion probability. All events for which $\delta_{cm} < -0.97$ are rejected. Figure 7 shows a plot for the relative detection efficiency as a function of $\hat{\pi}^+ \cdot \hat{\gamma}$ with $T_{\pi^+} = 80$ MeV. This energy is in the middle of our energy range. The efficiency drops off rapidly to zero as the γ-ray becomes more collinear with the positive pion. The reason for this is that the lead chambers do not cover the region facing the pion range chamber. In any case events in this region are primarily from inner bremsstrahlung with soft γ-rays. The detection efficiency is reasonably constant over a region which includes events from direct radiation as well as inner bremsstrahlung.

With this information the histogram in Figure 5 is easily explainable. The lack of events in the region $\hat{\pi}^+ > 0.6$ is due to our detection efficiency. Comparing the histrogram with Fig. 1 in the region $\hat{\pi}^+ \cdot \hat{\gamma} < 0.6$ we see that its shape essentially follows that of inner bremsstrahlung. There is no increase in the number of events toward $\hat{\pi}^+ \cdot \hat{\gamma} = -1$ as would be expected if direct radiation were present.

To state the above more precisely we have used a maximum likelihood method. The likelihood function is defined by a product of probabilities:

$$\mathcal{L} = \prod_{i=1}^{N} f(\cos\theta_i, E_{\pi^+ i}) \qquad \text{IV-5}$$

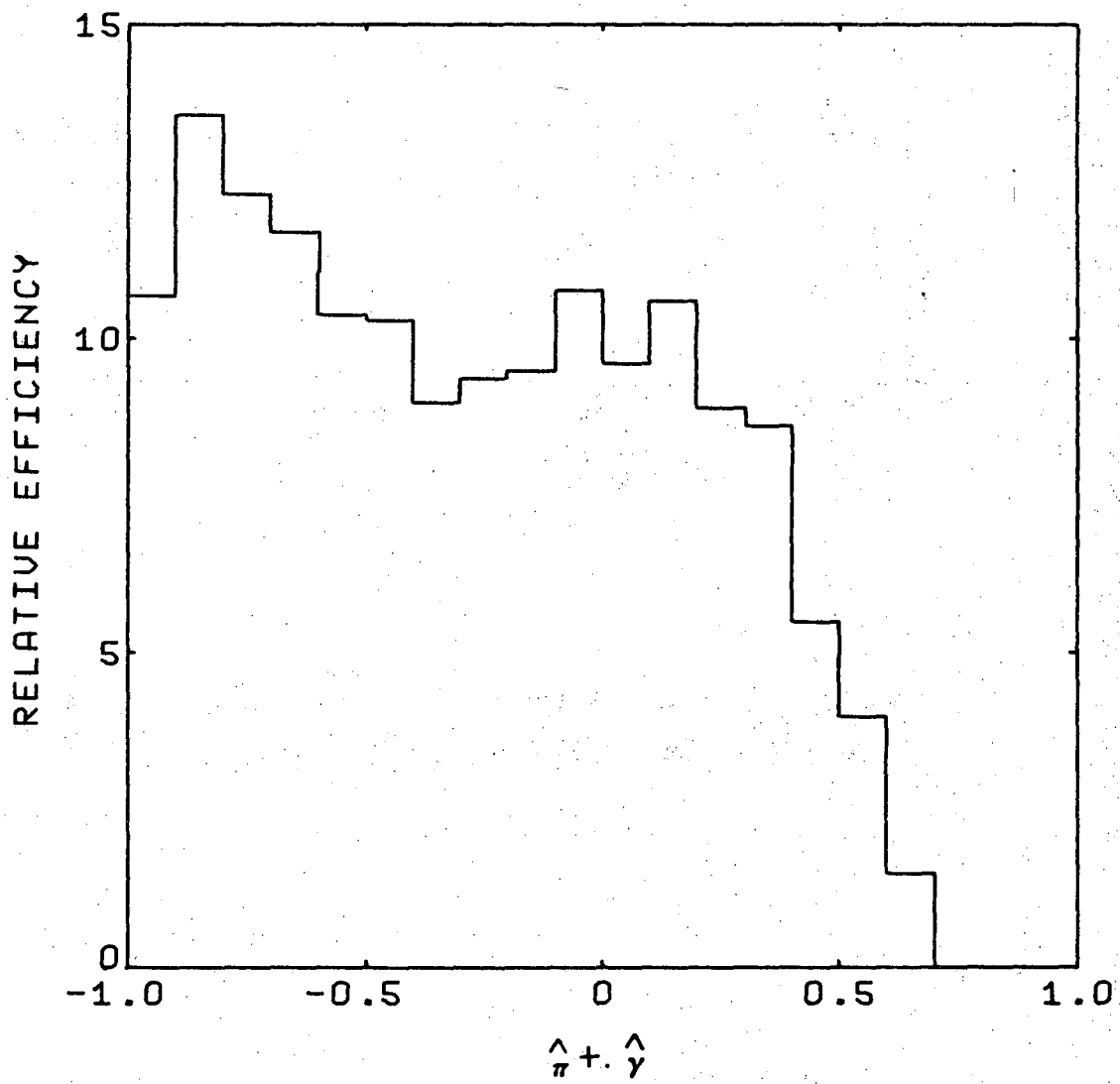

XBL 6812-6369

Fig. 7. Relative efficiency for detecting $K^+ \rightarrow \pi^+\pi^o\gamma$. The energy of the π^+ is fixed at $T_{\pi^+} = 80$ MeV.

The product is over all events in our sample. $E_{\pi^+ i}$ and $\cos\theta_i = \hat{\pi}^+ \cdot \hat{\gamma}_i$ are the kinematical variables of the ith event. $f(\cos\theta, E_{\pi^+})$ is the probability of getting an event at the point $(E_{\pi^+}, \cos\theta)$. α is the parameter we are trying to measure. For the decay $K^+ \to \pi^+\pi^0\gamma$ we have:

$$f(\cos\theta, E_{\pi^+}) = \frac{d\Gamma(\cos\theta, E_{\pi^+},)}{d\cos\theta\, dE_{\pi^+}} EFF(\cos\theta, E_{\pi^+})\, G(E_{\pi^+}) \qquad \text{IV-6}$$

$$\int EFF(\cos\theta, E_{\pi^+})d\cos\theta = 1$$

$\frac{d\Gamma}{d\cos\theta\, dE_{\pi^+}}$ is the decay rate given in Appendix I. $EFF(\cos\theta, E_{\pi^+})$ is the efficiency for detecting a π^0 as a function of $\cos\theta$ and E_{π^+}. $G(E_{\pi^+})$ is the efficiency for detecting a π^+ as a function of the energy E_{π^+}. Since in our experiment the energy range of the π^+ is rather small and the dependence of f on E_{π^+} is almost exclusively determined by G, we have normalized f in such a way as to make a knowledge of G unnecessary:

$$f(\cos\theta, E_{\pi^+}) = \frac{d\Gamma/(d\cos\theta\, dE_{\pi^+})EFF(\cos\theta, E_{\pi^+})G(E_{\pi^+})}{\int d\Gamma/(d\cos\theta\, dE_{\pi^+})EFF(\cos\theta, E_{\pi^+})G(E_{\pi^+})d\cos\theta} \qquad \text{IV-7}$$

$$= \frac{d\Gamma/(d\cos\theta\, dE_{\pi^+})EFF(\cos\theta, E_{\pi^+})}{\int d\Gamma/(d\cos\theta\, dE_{\pi^+})EFF(\cos\theta, E_{\pi^+})d\cos\theta}$$

Substituting IV-7 into IV-5 and taking the logarithm of the result we get

$$\log \mathcal{L} = \sum_{i=1}^{N} \log \frac{d\Gamma(\cos\theta_i, E_{\pi^+ i}, \alpha)/(d\cos\theta\, dE_{\pi^+})\ EFF(\cos\theta_i, E_{\pi^+ i})}{\int d\Gamma/(d\cos\theta\, dE_{\pi^+ i})EFF(\cos\theta, E_{\pi^+ i})d\cos\theta} \qquad \text{IV-8}$$

We have considered two cases in calculating IV-8. Figure 8 shows a plot of log $\mathcal{L}$ with $\alpha = X_E$ and $X_M = 0$. The maximum occurs at $X_E = 0.8^{+1.2}_{-0.9}$. The errors are found by reading of X_E at those points where $\mathcal{L}$ has decreased by a factor of $\ell^{-1/2}$. There is a second maximum at $X_E = -2$. However at this point the likelihood function was decreased by a factor of ℓ^{-3} making this a very unlikely solution. A similar analysis for $\alpha = X_M$, $X_E = 0$ yields the result $X_M = 2.1 \pm 1.5$.

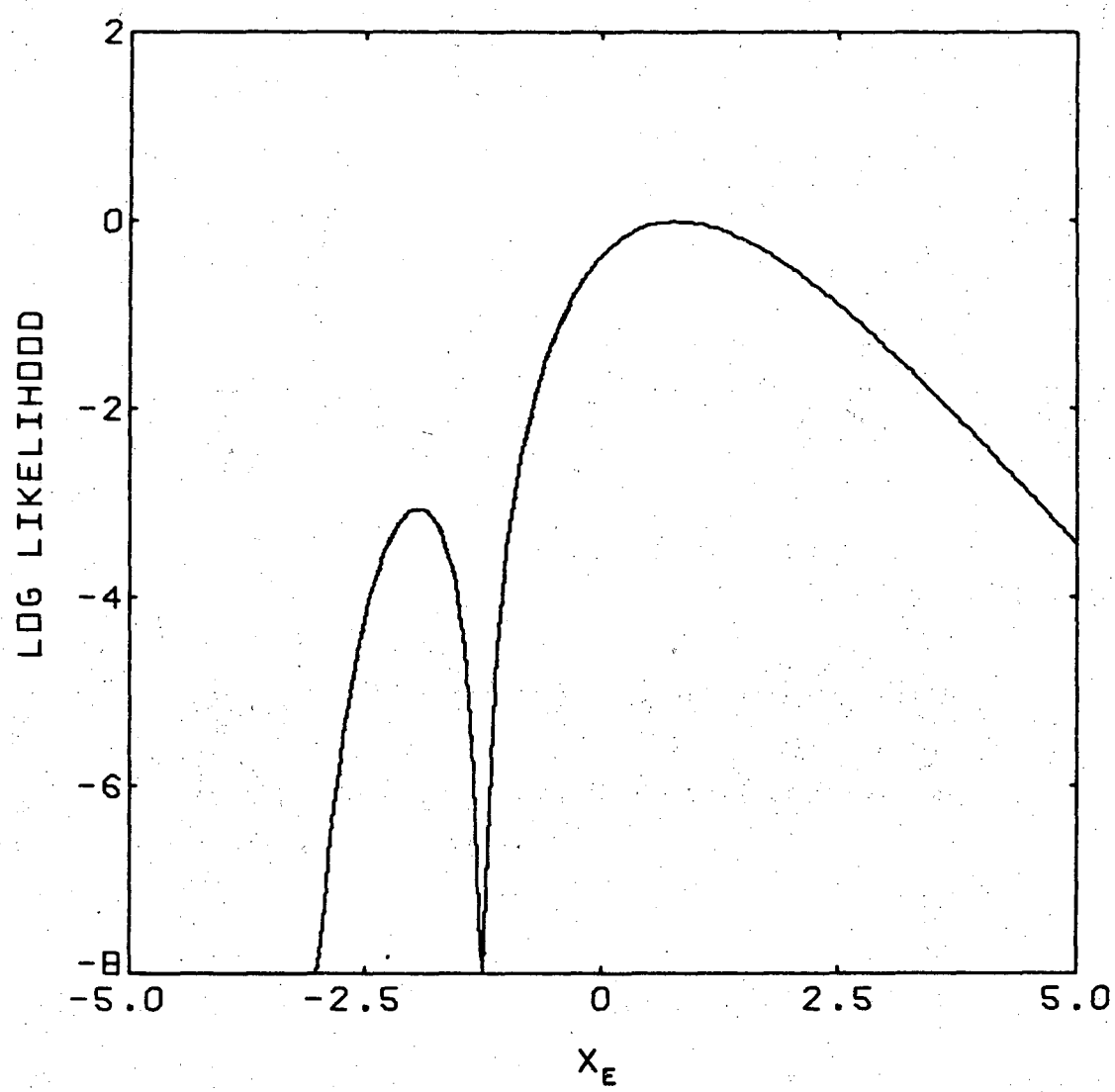

XBL 6812-6373

Fig. 8. X_E is the form factor for electric dipole radiation. X_M is set equal zero. A positive value for X_E indicates constructive interference; a negative value indicates destructive interference.

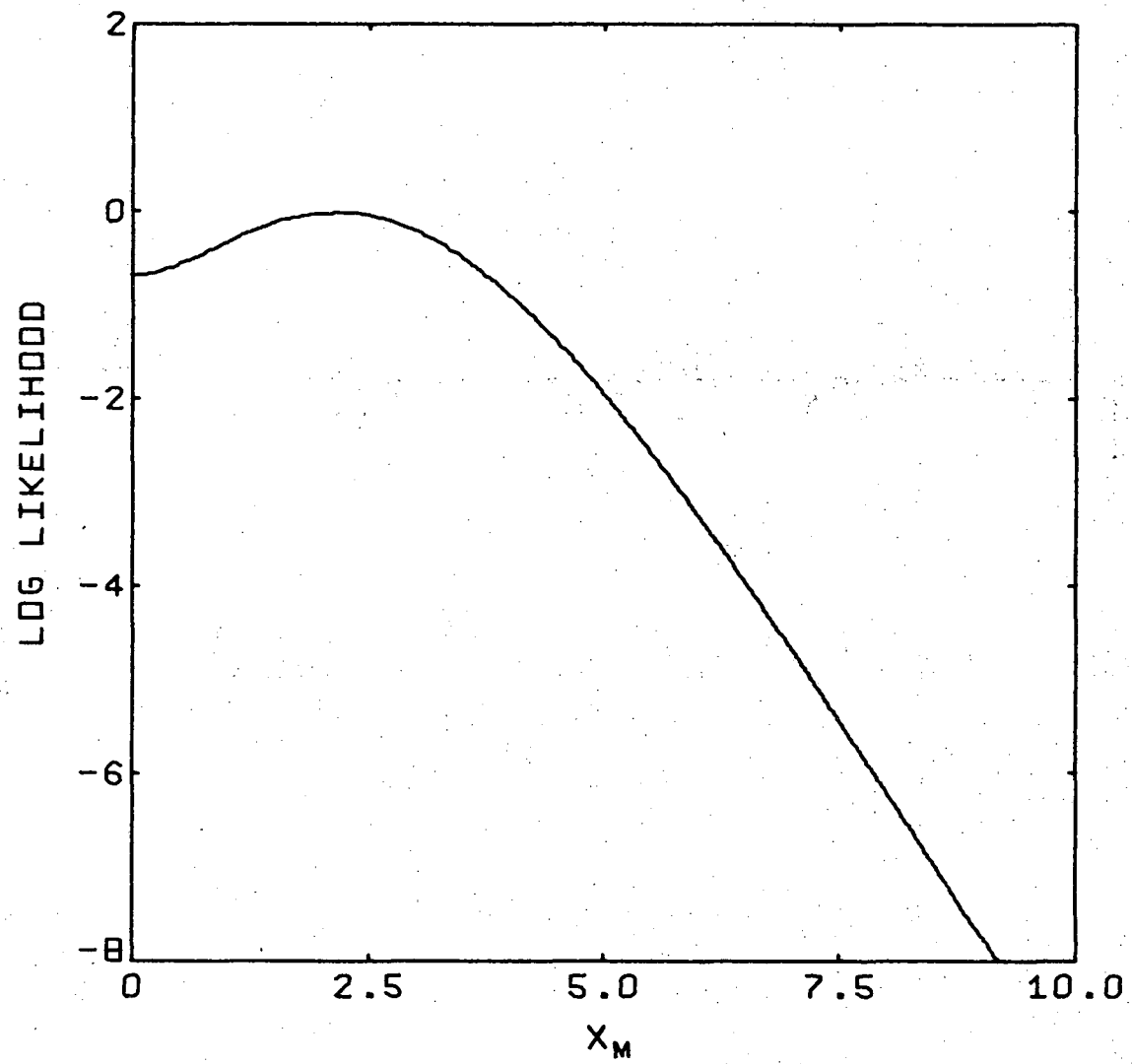

XBL 6812-6372

Fig. 9. X_M is the form factor for magnetic dipole radiation. The electric dipole form factor is taken to be zero.

V. SUMMARY AND CONCLUSIONS

To the limit of accuracy dictated by our experiment we have not been able to observe direct radiation in the process $K^+ \rightarrow \pi^+\pi^o\gamma$. The spectrum of gamma rays we observe agrees well with what would be expected from inner bremsstrahlung alone. We can place a sufficiently low limit on the direct decay rate to question the model of Pepper and Ueda. Our experimental numbers corresponding to their result are:

	Their Result	Our Result (95% Conf.)
M1	$R_D' = 2.4 \cdot 10^{-4}$	$R_D' < 6.5 \cdot 10^{-5}$
E1	$10^{-4} < R_D' < 10^{-4}$	$-1.6 \cdot 10^{-5} < R_D' < 1.2 \cdot 10^{-4}$

To make this comparison we have recalculated our branching ratio for the interval 55 MeV $\leq$ 80 MeV. The branching ratio of Kim and Korff on the other hand is much lower than our upper limit.

There are several experiments which also have looked for the decay $K^+ \rightarrow \pi^+\pi^o\gamma$.[5] Wolff and Aubert[5] have observed 14 events with three converted γ-rays in a bubble chamber. They quote the contribution of electric dipole radiation as $\gamma = 0.5 \begin{smallmatrix}+0.3\\-0.25\end{smallmatrix}$. γ is related to our X_E:

$$X_E = \frac{G}{g}\left(\frac{m_K}{m_{\pi^+}}\right)^4 \gamma = 10.1\,\gamma$$

In terms of γ our result is $\gamma = 0.08 \begin{smallmatrix}+0.12\\-0.09\end{smallmatrix}$. Cline et al.[5] have studied the π^+ spectrum for the decay $K^+ \rightarrow \pi^+\pi^o\gamma$. However they did not observe any γ-rays. They give the result $\gamma = -0.6 \begin{smallmatrix}+0.4\\-0.15\end{smallmatrix}$. So they observe a small amount of destructive interference.

We can also compare our result with the decay rate of $K_L^o \rightarrow \pi^+\pi^-\gamma$ if we assume the $\Delta I=1/2$ selection rule. In this case we have:

$$\Gamma(K^+ \to \pi^+\pi^o\gamma,\ M1) = \Gamma(K_L^o \to \pi^+\pi^-\gamma,\ M1)$$

From the experiment of Thatcher[6] we find $R_D(M1) < 9 \cdot 10^{-5}$. This upper limit compares with our limit $R_D(M1) < 1.7 \cdot 10^{-4}$ (95% conf.). Their experiment is different from ours in that the rate from inner bremsstrahlung is an order of magnitude lower than their upper limit. So their upper limit corresponds to observing no radiative decays at all.

The possibility of observing CP violating effects in $K^+ \to \pi^+\pi^o\gamma$ will be severely limited by the fact that the amount of direct radiation is significantly lower than the contribution from inner bremsstrahlung. At first it was thought that direct radiation dominates inner bremsstrahlung since direct radiation is not suppressed by the $\Delta I=1/2$ selection rule. As this is not the case the decays $K^\pm \to \pi^\pm\pi^o\gamma$ do not look very promising as a source of information about CP violation.

APPENDICES

I. Decay Rate $K^+ \to \pi^+\pi^o\gamma$

The decay rate for $K^+ \to \pi^+\pi^o\gamma$ is:

$$\frac{d\Gamma}{dE_{\pi^+}dE_{\pi^o}}(K^+ \to \pi^+\pi^o\gamma) = \Gamma(K^+ \to \pi^+\pi^o)$$

$$\times \frac{\alpha}{\pi}\left[\left(1 + \left(\frac{m_{\pi^+}}{m_k}\right)^2 - \left(\frac{m_{\pi^o}}{m_k}\right)^2\right)^2 - 4\left(\frac{m_{\pi^+}}{m_k}\right)^2\right]^{-1/2}$$

$$\times\left[\left(\frac{K}{K\cdot\gamma} - \frac{P}{P\cdot\gamma}\right)^2\right.$$

$$+ 2\mathrm{Re}\, X_E e^{i(\delta_1-\delta_0)}\frac{g}{G}\frac{1}{M^4}\left(\frac{K}{K\cdot\gamma} - \frac{P}{P\cdot\gamma}\right)\left((P\cdot\gamma)Q-(Q\cdot\gamma)P\right)$$

$$\left.+ \left(\frac{g}{G}\right)^2\left(X_E^{\,2} + X_M^{\,2}\right)\left((P\cdot\gamma)Q-(Q\cdot\gamma)P\right)^2\frac{1}{M^8}\right]$$

The variables are defined by:

K 4-momentum of K^+

P 4-momentum of π^+

Q 4-momentum of π^o

γ 4-momentum γ-ray

X_E coupling constant for electric dipole

X_M coupling constant for magnetic dipole

$\alpha = \frac{1}{137}$

M = arbitrary mass to make X_E, X_M dimensionless.

We have chosen $M = m_k$.

$$\left(\frac{g}{G}\right)^2 = \frac{.783\cdot 10^{10}}{2\cdot 16.96\cdot 10^6} = \frac{\Gamma(K_s^o\to\pi^+\pi^-)}{2\Gamma(K^+\to\pi^+\pi^o)} = 231$$

δ_1, δ_0 are the ℓ=0,1 π-π phase shifts.

II. KINEMATICS $K^+ \to \pi^+\pi^o\gamma$

Using the unit vectors along the direction of the $\pi^+(\hat{p}_{\pi^+})$ and along the directions of the three γ-rays $(\hat{p}_i)$ we can solve for the momentum of the π^+ and the energies of the γ-rays (p_i).

$$p_{\pi^+} = \frac{X\, m_k - \left[m_k^{\,2} + (X^2-1)m_{\pi^+}^{\,2}\right]^{1/2}}{(X^2 - 1)}$$

$$p_i = A_i p_{\pi^+} \qquad i = 1,2,3$$

X and A_i are:

$$A_1 = -\frac{\hat{p}_{\pi^+} \cdot (\hat{p}_2 \times \hat{p}_3)}{\hat{p}_1 \cdot (\hat{p}_2 \times \hat{p}_3)}$$

$$A_2 = -\frac{\hat{p}_1 \cdot (\hat{p}_{\pi^+} \times \hat{p}_3)}{\hat{p}_1 \cdot (\hat{p}_2 \times \hat{p}_3)}$$

$$A_3 = -\frac{\hat{p}_1 \cdot (\hat{p}_2 \times \hat{p}_{\pi^+})}{\hat{p}_1 \cdot (\hat{p}_2 \cdot \hat{p}_3)}$$

$$X = A_1 + A_2 + A_3 \; .$$

Note that we have not used the fact that two of the γ-rays are on π^o mass shell. To see which of the two γ-rays come from the decay of the π^o we write:

$$m_{ij}^2 = 2\, p_i\, p_j (1 - \hat{p}_i \cdot \hat{p}_j) \qquad i,j = 1,2 \text{ or } 2,3 \text{ or } 3,1$$

If we do not have any measurement errors, then we get for only one combination i,j:

$$m_{ij}^2 = m_{\pi^o}^2 \; .$$

REFERENCES

1. J. D. Good, Phys. Rev. 113, 352 (1959).

2. S. V. Pepper, Y. Ueda, Nuovo Cimento 33, 1614 (1964).

3. S. Oneda, Y. S. Kim, D. Korff, Phys. Rev. 136, B 1064 (1964).

4. G. Costa, P. K. Kabir, Phys. Rev. Letters 18, 429 (1967);
   S. Barshay, Phys. Rev. Letters 18, 515 (1967).

5. B. Wolff, B. Aubert, Physics Letters 25B, 624 (1967);
   D. Cline, W. F. Fry, Phys. Rev. Letters 13, 101 (1964);
   D. Cline, Phys. Rev. Letters 16, 367 (1966).

6. R. C. Thatcher, Thesis COO-1195-113, University of Illinois.

ACKNOWLEDGMENTS

I like to express my indebtedness to Professor Emilio Segrè for his support and counsel throughout my graduate work. I am grateful to Dr. Rae Stiening under whose supervision this work was done. I like to thank Professor Martin Deutsch for the time and effort he devoted to the automatic scanning. I wish to express my gratitude to Dr. Clyde Wiegand who designed and supervised the building of the experimental apparatus. I also owe my thanks to Dr. Min Chen for many helpful discussions, and to Dr. David Cutts who set up and supervised the scanning of the $K_{\mu 3}$ experiment. I am deeply indebted to Rosemary Fowell for her patient attention to the preparation of this manuscript.

This work was performed under the auspices of the Atomic Energy Commission.

LEGAL NOTICE

This report was prepared as an account of Government sponsored work. Neither the United States, nor the Commission, nor any person acting on behalf of the Commission:

A. Makes any warranty or representation, expressed or implied, with respect to the accuracy, completeness, or usefulness of the information contained in this report, or that the use of any information, apparatus, method, or process disclosed in this report may not infringe privately owned rights; or

B. Assumes any liabilities with respect to the use of, or for damages resulting from the use of any information, apparatus, method, or process disclosed in this report.

As used in the above, "person acting on behalf of the Commission" includes any employee or contractor of the Commission, or employee of such contractor, to the extent that such employee or contractor of the Commission, or employee of such contractor prepares, disseminates, or provides access to, any information pursuant to his employment or contract with the Commission, or his employment with such contractor.

TECHNICAL INFORMATION DIVISION
LAWRENCE RADIATION LABORATORY
UNIVERSITY OF CALIFORNIA
BERKELEY, CALIFORNIA 94720